Homeostatic compensation and neuromodulation maintain synchronized motor neuron activity in the crustacean cardiac ganglion

---

A Dissertation

Presented to

The Faculty of the Graduate School

At the University of Missouri

In Partial Fulfillment

Of the Requirements for the Degree

Doctor of Philosophy

By

LANE, BRIAN J. (MU-STUDENT)

Dr. David J. Schulz, Dissertation Supervisor

December 2016

The undersigned, appointed by the dean of the Graduate School,

have examined the Dissertation entitled

HOMEOSTATIC COMPENSATION AND NEUROMODULATION MAINTAIN SYNCHRONIZED MOTOR NEURON ACTIVITY IN THE CRUSTACEAN CARDIAC GANGLION

Presented by Lane, Brian J. (MU-Student)

A candidate for the degree of

Doctor of Philosophy

And hereby certify that, in their opinion, it is worthy of acceptance.

Dr. David J. Schulz

Dr. Troy Zars

Dr. Lorin S. Milescu

Dr. Satish S. Nair

ACKNOWLEDGEMENTS

My Ph.D., and the work herein, is a product of the David Schulz lab at the University of Missouri-Columbia.

I would like to express my sincere gratitude to my advisor Dr. David Schulz for his continuous support, patience, and guidance throughout my doctoral training. His commitment to mentorship has been invaluable in clarifying my thinking and improving my approach to scientific questions. Being a member of the Schulz has been a wonderful experience and has been a positive influence in shaping my professional and personal experience at the University of Missouri in more ways than I can express.

The many current and former members of the Schulz lab throughout my time in the lab have been both colleagues and friends. I have had the fortune of overlapping with all of the Schulz lab's graduate students to date: Simone Temporal (PhD 2012), Joey Ransdell (PhD 2013), Kawasi Lett (PhD 2014), Cindy Kyi, Adam Northcutt, Jennifer Wekenborg, Daniel Kick, and Sherryl Henderson. Through this period of time, many undergraduates have been a part of the lab, and I especially wish to mention those with whom I worked most closely: Lupe Torres, Destiny Cobb, Ellen Fjellman, Gabby Dohmen, Sonia Dermer, Kelly Hiersche, Clare Diester, Zeina Ziade, and David Wilson (whose experiments contributed to Chapter 2). Finally, our talented lab technician Virginia (Ginny) Garcia, and postdocs: Dr. Aihua Dai and Dr. Michael Gray. All of these people have all been a joy to work with, and to simply have fun with outside the lab.

Next, I would like to thank my advisory committee: Dr. Lorin Milescu, Dr. Troy Zars, and Dr. Satish Nair. Their variety of perspectives and expertise has helped me to better frame the context and importance of my projects, and to improve the technical approaches used. Our collaboration with Dr. Nair's Lab, including the work of his student Pranit Samarth, have complemented our biological studies with computational modeling.

I would also like to thank Dr. Mark Hannink and Debbie Allen, who oversaw the NIH T32 molecular biology training grant that supported me and furthered my education for two of my years as a graduate student.

Finally, I wish to thank my family. First, my parents Paul and Debbie Lane. Without their continuous support and understanding this adventure would never have been possible. I would also like to thank my brother Michael and his wife Meg, and their amazing daughters Rachel and Erin. Finally, my brother Kevin and his fiancé Cassandra. I cherish the many trips to St. Louis and time spent with all of you during the years I have lived in Columbia.

TABLE OF CONTENTS

LIST OF FIGURES AND TABLES

ABSTRACT

Animals rely on the nervous system to produce appropriate behavior throughout their lives. In sending commands to the musculature for rhythmic motor behaviors such as breathing or walking, neural networks must be stable enough to send a reliable level of drive with the proper temporal coordination. Networks must also be flexible enough to meet changing environmental demands. A network's output ultimately arises from the intrinsic excitability of its constituent neurons and the synaptic connections between them. Interestingly, neurons and networks are able to produce highly conserved output from highly variable underlying intrinsic and synaptic properties.

To explore the consequences of this variability, we have used the crustacean cardiac ganglion (CG) which consists of 9 neurons: 4 pacemaker cells that give excitatory input to 5 Large Cell motor neurons (LCs) which are responsible for driving the simultaneous contraction of the musculature that makes up the walls of the animal's single-chambered heart (Alexandrowicz, 1934; Hartline, 1967; Anderson and Cooke, 1971). The intact network can be dissected from the animal in physiological saline and it continues to produce robust, reliable, and rhythmic output (Welsh and Maynard, 1951; Cooke, 2002). LCs have virtually identical synchronized activity, but their intrinsic ionic conductances can be highly variable (Ransdell et al., 2013a).

In Chapter 1, we exploit this variability by pharmacologically blocking a subset of their conductances to make LCs hyperexcitable and desynchronize their activity. We find that homeostatic compensation restores synchronized activity and excitability within

one hour. This happens via two synergistic mechanisms: the membrane properties of each cell are re-tuned to converge on similar voltage activity, and increased conductance of the gap junctions between the cells helps to buffer away differences in their voltage activity.

A separate but related study asked whether naturalistic perturbations of network activity would also result in desynchronization. Neuromodulation provides flexibility in the output of neural networks by altering a subset of their conductances. We hypothesized that this could also cause desynchronization. We found that modulation with serotonin and dopamine both increased the excitability of the CG. Interestingly, serotonin desynchronized the CG, but dopamine did not. We found that dopaminergic modulation directly increases gap junctional conductance. By co-applying these modulators, we found dopamine was able to prevent serotonin from desynchronizing the network without occluding its effects. It was also able to prevent the desynchronization caused by ion channel blockers.

Finally, to fully understand the output of LCs, we must recognize that their activity arises not only from their intrinsic properties, but also from their synaptic drive from pacemaker cells. To address how variable this can be from one animal to the next, we analyze the activity of 131 animals taken over the course of approximately 5 years. We use this to address the fundamental question of how variable networks underlying a particular behavior can be across animals. We recognize two distinct classes of pacemaker inputs to LCs, and characterize bursting patterns for both types of pacemaker

spike and LC output. We conclude that LCs from different animals receive different temporal patterns of pacemaker drive, which may have important functional implications. We also compare animals from winter and summer months, and find that temperature-independent seasonal effects may explain some of the variance in our data.

INTRODUCTION

The themes of neuronal variability and network synchrony are themes of central importance to the following chapters. Until relatively recently, it was thought that neurons or networks achieve a particular output by finding a singular "ideal" solution (Marder, 2011; Nowotny et al., 2007). It is now firmly established that a great deal of variability can exist in intrinsic conductances of cells and synapses underlying the same behavior across animals (Bucher et al., 2005; Calabrese et al., 2011; Goaillard et al., 2009; Marder and Goaillard, 2006; Roffman et al., 2012). To maintain appropriate cellular output, it is not necessary to tightly regulate each conductance, but rather it is relationships among conductances that produce conserved output (Ball et al., 2010; Doloc-Mihu and Calabrese, 2014; Marder and Goaillard, 2006). Even within the same animal, the same cell type can achieve conserved output from variable underlying conductances (Ransdell et al., 2013).

In the context of neuronal variability, this body of work focuses on how stable network output is maintained over the lifetime of an animal. Network output ultimately arises as a consequence of the properties of each of its constituent neurons and their interactions. Many different characteristics of network activity might be used as a benchmark, and a handful of studies have examined how neuronal variability affects characteristics such as post-inhibitory rebound, half-center oscillator activity, bursting phenotype, or network oscillations (Doloc-Mihu and Calabrese, 2016; Grashow et al., 2010, 2009; Marder et al., 2014). The following chapters focus in particular on how variable neurons are able to maintain appropriate excitability and reliable and robust

synchrony. Relatively little work has addressed whether variable neurons can maintain stable synchrony, and we find a striking vulnerability: perturbations that affect a subset of conductances across variable neurons can desynchronize their activity.

Synchronized activity is important for a wide variety of reasons across nervous systems. Shortly after the first discovery of electrical synapses in crayfish (Furshpan and Potter, 1957)(Furshpan and Potter, 1959), pioneering work by Akira Watanabe using the decapod crustacean cardiac ganglion (CG) firmly established the principle that electrotonic coupling can serve to synchronize activity across cells (Watanabe, 1958; Watanabe and Bullock, 1960; reviewed in Connors et al., 2010). To name only a few cases where gap-junction mediated synchrony is important: temporal coordination of escape reflexes in *D. melanogaster* (Card and Dickinson, 2008a, 2008b; Card, 2012), normal activity of the inferior olive (Marshall and Lang, 2004; Mathy et al., 2014) and inspiratory neurons of the mammalian breathing CPG (Bou-Flores and Berger, 2001), but also pathological states such as Parkinson's disease (Phookan et al., 2015; Schwab et al., 2013) and epilepsy (Bedner and Steinhäuser, 2013; Jin and Chen, 2011; Nakase and Naus, 2004; Popovych and Tass, 2014; Traub and Wong, 1982).

The CG of the crab *C. borealis* is a Central Pattern Generator (CPG) network responsible for driving the rhythmic contraction of the animal's single-chambered heart. The network is comprised of 4 small pacemaker interneurons that give excitatory input to 5 Large Cell (LC) motor neurons, which are responsible for the monophasic contraction of the heart musculature. These 5 LCs have nearly identical burst waveforms which

drive synchronized burst of action potentials which represent the output of the network. CPG networks make excellent model systems for the study of stable network output. Two fundamental features of network output across nervous systems are the level of spiking output and temporal coordination among the neurons that produce that output. The cardiac ganglion of the crab *C. borealis* provides an excellent model to study the level of excitatory drive produced by LCs and also the tightly regulated synchrony across these cells.

We find important roles for homeostatic compensation and neuromodulation of gap junction-mediated electrical coupling in maintaining reliable synchronization. Electrical synapses have long been considered little more than lowpass filters that help to provide synchrony or speed of synaptic transmission (Marder, 1998; Pereda et al., 2003; Bennett and Zukin, 2004). Only recently been recognized to play important roles in the mammalian central nervous system, and they are now recognized as dynamic (Curti et al., 2012; Pereda and Faber, 1996) and modifiable structures subject to modulation (Landisman and Connors, 2005; Lasater and Dowling, 1985; Pereda et al., 1992) and activity-dependent changes (Connors et al., 2010; Haas et al., 2011; O'Brien, 2014; Palacios-Prado and Chapuis, 2014; Pereda et al., 2007)

After the cardiac ganglion was first introduced as a preparation for the study of neurophysiology by Welsh and Maynard (Welsh and Maynard, 1951), many classic and pioneering studies in neurophysiology made use of this tractable system to address basic questions about neuronal properties and network function (reviewed in Cooke, 2002).

This small network is singularly dedicated to the task of driving the rhythmic contraction of the single-chambered crustacean heart (Anderson and Cooke, 1971; Cooke, 2002). Collectively, the body of work over the following decades characterized, the moment-to-moment organization of electrical activity, the functional morphology of the cells, and the interactions among the cells to understand the basis of rhythmic motor pattern generation, and how network output is influenced by neuromodulation (Cooke, 1966; Friesen, 1975; Hartline, 1979; Mayeri, 1973).

As a testament to both the complexity and usefulness of the preparation, Ian Cooke speculated in 1988 that "the 9-celled crustacean cardiac ganglion has possibly given rise to more Ph.D. theses per cell than any other neural network" (Cooke, 1988).

We have continued to repurpose the CG, and in the following chapters use it to explore neuronal and network variability, neuromodulation, and the homeostatic regulation of neuronal excitability and synchrony. After these data are presented, I discuss their implications and potential future directions of research along these lines.

REFERENCES

Anderson, M., Cooke, I.M., 1971. Neural activation of the heart of the lobster Homarus americanus. J. Exp. Biol. 55, 449–68.

Ball, J.M., Franklin, C.C., Tobin, A.-E., Schulz, D.J., Nair, S.S., 2010. Coregulation of ion channel conductances preserves output in a computational model of a crustacean cardiac motor neuron. J. Neurosci. 30, 8637–49.

Bedner, P., Steinhäuser, C., 2013. Altered Kir and gap junction channels in temporal lobe epilepsy. Neurochem. Int. 63, 682–687.

Bennett, M., Zukin, R., 2004. Electrical Coupling and Neuronal Synchronization in the Mammalian Brain. Neuron 41, 495–511.

Bou-Flores, C., Berger, A., 2001. Gap Junctions and Inhibitory Synapses Modulate Inspiratory Motoneuron Synchronization. J. Neurophysiol. 1543–1551.

Bucher, D., Prinz, A.A., Marder, E., 2005. Animal-to-animal variability in motor pattern production in adults and during growth. J. Neurosci. 25, 1611–9.

Calabrese, R.L., Norris, B.J., Wenning, A., Wright, T.M., 2011. Coping with variability in small neuronal networks. Integr. Comp. Biol. 51, 845–55.

Card, G., Dickinson, M.H., 2008a. Visually Mediated Motor Planning in the Escape Response of Drosophila. Curr. Biol. 18, 1300–1307.

Card, G., Dickinson, M.H., 2008b. Performance trade-offs in the flight initiation of Drosophila. J. Exp. Biol. 211, 341–353.

Card, G.M., 2012. Escape behaviors in insects. Curr. Opin. Neurobiol. 22, 180–6.

Connors, B.W., Long, M.A., 2004. Electrical synapses in the mammalian brain. Annu. Rev. Neurosci. 27, 393–418.

Connors, B.W., Zolnik, T.A., Lee, S.C., 2010. Enhanced Functions of Electrical Junctions. Neuron.

Cooke, I., 1966. The Sites of Action of Pericardial Organ Extract and 5-Hydroxytryptamine in the Decapod Crustacean Heart. Am. Zool 6, 107–121.

Cooke, I.M., 2002. Reliable, responsive pacemaking and pattern generation with minimal cell numbers: the crustacean cardiac ganglion. Biol. Bull. 202, 108–36.

Cooke, I.M., 1988. Studies on the crustacean cardiac ganglion. Comp. Biochem. Physiol. C. 91, 205–18.

Curti, S., Hoge, G., Nagy, J.I., Pereda, A.E., 2012. Synergy between electrical coupling and membrane properties promotes strong synchronization of neurons of the mesencephalic trigeminal nucleus. J. Neurosci. 32, 4341–59.

Doloc-Mihu, A., Calabrese, R.L., 2016. Analysis of Family Structures Reveals Robustness or Sensitivity of Bursting Activity to Parameter Variations in a Half-Center Oscillator (HCO) Model. eNeuro 3.

Doloc-Mihu, A., Calabrese, R.L., 2014. Identifying crucial parameter correlations maintaining bursting activity. PLoS Comput. Biol. 10, e1003678.

Friesen, W., 1975. Physiological anatomy and burst pattern in the cardiac ganglion of the spiny lobsterPanulirus interruptus. J. Comp. Physiol. 173–189.

Furshpan, E.J., Potter, D.D., 1959. Transmission At the Giant Motor Synapses of the Crayfish. J. Physiol. 45, 289–325.

FURSHPAN, E.J., POTTER, D.D., 1957. Mechanism of nerve-impulse transmission at a crayfish synapse. Nature 180, 342–3.

Goaillard, J., Taylor, A., Schulz, D., Marder, E., 2009. Functional consequences of

animal-to-animal variation in circuit parameters. Nat. Neurosci. 12, 1424–1430.

Grashow, R., Brookings, T., Marder, E., 2010. Compensation for variable intrinsic neuronal excitability by circuit-synaptic interactions. J. Neurosci. 30, 9145–56.

Grashow, R., Brookings, T., Marder, E., 2009. Reliable neuromodulation from circuits with variable underlying structure. Proc. Natl. Acad. Sci. U. S. A. 106, 11742–6.

Haas, J.S., Zavala, B., Landisman, C.E., 2011. Activity-dependent long-term depression of electrical synapses. Science 334, 389–93.

Hartline, D., 1979. Integrative neurophysiology of the lobster cardiac ganglion. Am. Zool. 19, 53–65.

Jin, M.M., Chen, Z., 2011. Role of gap junctions in epilepsy. Neurosci. Bull.

Landisman, C.E., Connors, B.W., 2005. Long-term modulation of electrical synapses in the mammalian thalamus. Science 310, 1809–13.

Lasater, E.M., Dowling, J.E., 1985. Dopamine decreases conductance of the electrical junctions between cultured retinal horizontal cells. Proc. Natl. Acad. Sci. U. S. A. 82, 3025–9.

Marder, E., 2011. Variability, compensation, and modulation in neurons and circuits. Proc. Natl. Acad. Sci. U. S. A. 108 Suppl , 15542–8.

Marder, E., 1998. Electrical synapses: beyond speed and synchrony to computation. Curr. Biol. 8, R795–7.

Marder, E., Goaillard, J.-M., 2006. Variability, compensation and homeostasis in neuron and network function. Nat. Rev. Neurosci. 7, 563–74.

Marder, E., O'Leary, T., Shruti, S., 2014. Neuromodulation of circuits with variable parameters: single neurons and small circuits reveal principles of state-dependent

and robust neuromodulation. Annu. Rev. Neurosci. 37, 329–46.

Marshall, S.P., Lang, E.J., 2004. Inferior olive oscillations gate transmission of motor cortical activity to the cerebellum. J. Neurosci. 24, 11356–67.

Mathy, A., Clark, B.A., H??usser, M., 2014. Synaptically induced long-term modulation of electrical coupling in the inferior olive. Neuron 81, 1290–1296.

Mayeri, E., 1973. Functional Organization of the Cardiac Ganglion of the Lobster, Homarus americanus. J. Gen. Physiol. 62, 448–72.

Nakase, T., Naus, C.C.G., 2004. Gap junctions and neurological disorders of the central nervous system. Biochim. Biophys. Acta 1662, 149–158.

Nowotny, T., Szücs, A., Levi, R., Selverston, A.I.A., 2007. Models Wagging the Dog: Are Circuits Constructed with Disparate Parameters? Neural Comput. 2003, 1985–2003.

O'Brien, J., 2014. The ever-changing electrical synapse. Curr. Opin. Neurobiol. 29, 64–72.

Palacios-Prado, N., Chapuis, S., 2014. Molecular determinants of magnesium-dependent synaptic plasticity at electrical synapses formed by connexin36. Nat. ….

Pereda, A., O'Brien, J., Nagy, J.I., Bukauskas, F., Davidson, K.G. V, Kamasawa, N., Yasumura, T., Rash, J.E., 2003. Connexin35 mediates electrical transmission at mixed synapses on Mauthner cells. J. Neurosci. 23, 7489–7503.

Pereda, A., O'Brien, J., Nagy, J.I., Smith, M., Bukauskas, F., Davidson, K.G. V, Kamasawa, N., Yasumura, T., Rash, J.E., 2007. Short-range functional interaction between connexin35 and neighboring chemical synapses. Cell Commun. Adhes. 10, 419–423.

Pereda, A., Triller, A., Korn, H., Faber, D.S., 1992. Dopamine enhances both electrotonic coupling and chemical excitatory postsynaptic potentials at mixed synapses. Proc. Natl. Acad. Sci. U. S. A. 89, 12088–92.

Pereda, A.E., Faber, D.S., 1996. Activity-dependent short-term enhancement of intercellular coupling. J. Neurosci. 16, 983–92.

Phookan, S., Sutton, A.C., Walling, I., Smith, A., Connor, K.A.O., 2015. Gap junction blockers attenuate beta oscillations and improve forelimb function in hemiparkinsonian rats. Exp. Neurol. 1–11.

Popovych, O. V., Tass, P.A., 2014. Control of abnormal synchronization in neurological disorders. Front. Neurol. 5, 17–22.

Ransdell, J.L., Nair, S.S., Schulz, D.J., 2013. Neurons within the Same Network Independently Achieve Conserved Output by Differentially Balancing Variable Conductance Magnitudes. J. Neurosci. 33, 9950–9956.

Roffman, R.C., Norris, B.J., Calabrese, R.L., 2012. Animal-to-animal variability of connection strength in the leech heartbeat central pattern generator. J. Neurophysiol. 107, 1681–93.

Schwab, B.C., Heida, T., Zhao, Y., Marani, E., van Gils, S. a, van Wezel, R.J. a, 2013. Synchrony in Parkinson's disease: importance of intrinsic properties of the external globus pallidus. Front. Syst. Neurosci. 7, 60.

Traub, R.D., Wong, R.K., 1982. Cellular mechanism of neuronal synchronization in epilepsy. Science 216, 745–747.

WATANABE, A., 1958. The interaction of electrical activity among neurons of lobster cardiac ganglion. Jpn. J. Physiol. 8, 305–18.

Watanabe, A., Bullock, T.H., 1960. Modulation of activity of one neuron by subthreshold slow potentials in another in lobster cardiac ganglion. J. Gen. Physiol. 43, 1031–45.

Welsh, J., Maynard, D., 1951. Electrical activity of a simple ganglion. Fed. ….

CHAPTER 1

Synergistic Plasticity of Intrinsic Conductance and Electrical Coupling Restores Synchrony in an Intact Motor Network

Brian J. Lane[1*], Pranit Samarth[2*], Joseph L. Ransdell[1], Satish S. Nair[2], and David J. Schulz[1]

[1]Division of Biological Sciences, University of Missouri-Columbia, Columbia, MO 65211 USA
[2] Department of Electrical and Computer Engineering, University of Missouri-Columbia, Columbia, MO 65211 USA

[*] indicates equal contribution of these two authors

Correspondence to:
Dr. David J. Schulz
University of Missouri
Department of Biological Sciences
Columbia, MO, 65211, USA
schulzd@missouri.edu

ABSTRACT

Motor neurons of the crustacean cardiac ganglion generate virtually identical, synchronized output despite the fact that each neuron uses distinct conductance magnitudes. As a result of this variability, manipulations that target ionic conductances have distinct effects on neurons within the same ganglion, disrupting synchronized motor neuron output that is necessary for proper cardiac function. We hypothesized that robustness in network output is accomplished via plasticity that counters such destabilizing influences. By blocking high-threshold K^+ conductances in motor neurons within the ongoing cardiac network, we discovered that compensation both resynchronized the network and helped restore excitability. Using model findings to guide experimentation, we determined that compensatory increases of both G_A and electrical coupling restored function in the network. This is one of the first direct demonstrations of physiological regulation of coupling conductance in a compensatory context, and of synergistic plasticity across cell- and network-level mechanisms in the restoration of output.

INTRODUCTION

The hallmarks of robust central pattern generator (CPG) output are appropriately tuned excitability of individual neurons combined with circuit-level interactions that maintain appropriate temporal coordination (i.e., phasing) of these neurons. Through both developmental and ongoing tuning processes, CPGs can maintain reliable network output for decades across the lifespan of an individual, despite constant feedback from the changing nature of both the organismal and natural environment. Yet underlying this constant reliability of network output exists a surprising amount of variability in the individual parameters necessary for producing activity. For instance, despite having nearly identical output across animals, networks can exhibit a five-fold or more range in intrinsic and synaptic conductance values (Marder and Goaillard, 2006; Marder, 2011a; Roffman et al., 2012; Schulz et al., 2006). Such variability in intrinsic conductances is not limited to CPGs, but has been documented in several cell types of the mammalian brain, including cerebellar Purkinje cells (Swensen and Bean, 2005), and globus pallidus neurons (Günay et al., 2008). Additionally, synaptic strengths among mammalian central neurons have been shown to vary in several brain regions (Maffei et al., 2012; Nelson and Turrigiano, 2008; Turrigiano, 2008).

The origins and implications of this variability are still an intense area of investigation (Ciarleglio et al., 2015; Krubitzer and Kahn, 2003; Turrigiano and Nelson, 2004). We hypothesize that this variability might be a result of ongoing compensatory changes required to maintain reliable output over time. This compensation, termed homeostatic plasticity, has been well documented both for plasticity of intrinsic excitability via changing ionic conductances (Turrigiano et al., 1994), as well as for changes in chemical synaptic strength (Desai, 2004; Turrigiano, 2012). Variability in conductances may also be an adaptive trait in and of itself:

variable solutions that produce convergent circuit output may provide a selective advantage, or perhaps be a substrate for adaptation and evolution (Grashow et al., 2009; Marder and Goaillard, 2006).

Regardless of whether such variability is the result of homeostatic compensation, differential tuning across networks, or a combination of these and other heretofore undiscovered causes, a potential cost to such variability has recently been identified. In the cardiac ganglion (CG) of the Jonah crab (*Cancer borealis*), five Large Cell motor neurons (LCs) generate completely synchronous output, as a result of pacemaker inputs within the network, to drive simultaneous heart muscle contraction in the crab (Tazaki, 1972). Despite completely uniform and synchronous activity within the network, LCs show highly variable underlying maximal conductances (Ransdell et al., 2012a). These variable conductances render the neurons susceptible to perturbations that target a subset of ionic conductances: when high-threshold K^+ currents were blocked with tetraethylammonium (TEA), the motor neurons lost coordinated output and became divergent in their patterns of firing (Ransdell et al., 2013a). These CG neurons compensate for this change in excitability, presumably to homeostatically maintain a target level of excitability (Ransdell et al., 2012). However, none of the network level impacts of this perturbation and plasticity have been investigated. Indeed, it is difficult to study homeostatic plasticity in intact networks and to simultaneously take into account both properties of individual cells as well as their network interactions. In the present study, we discovered that LC variability makes the network vulnerable to desynchronization as a result of TEA exposure, but that compensation resynchronizes the network within 30-60 minutes via both intrinsic cellular and circuit-level physiological mechanisms. To examine the underlying mechanisms, we developed a biophysical computational model of the entire cardiac network. The network model enabled a

comprehensive search of the conductance space for potential compensatory mechanisms that preserved network synchrony, and we used these findings to guide further experimentation. Our study revealed cooperative homeostatic plasticity among intrinsic conductances and electrical coupling across multiple cells in the cardiac network. We interpret this as a novel homeostatic compensatory mechanism contributing to the overall robustness of CPG output.

MATERIALS AND METHODS:

Animals

Adult male Jonah crabs, *Cancer borealis*, were shipped overnight from The Fresh Lobster Company (Gloucester, MA). Crabs were maintained in artificial seawater at 12°C until used. Crabs were anesthetized by keeping them on ice for 30 minutes prior to dissection. The complete CG was dissected from the animal and pinned out in a Sylgard-lined petri dish in chilled physiological saline (440mM NaCl, 26mM $MgCl_2$, 13mM $CaCl_2$, 11mM KCl, and 10mM HEPES, pH 7.4-7.5, 12°C). Chemicals were obtained from Fisher Scientific unless otherwise noted.

BIOLOGICAL METHODS: Electrophysiology

The CG network is comprised of 9 cells: 4 Small Cell (SC) pacemaker interneurons which give simultaneous excitatory input to 5 Large Cell (LC) motor neurons. Superfusate of SCs can be separated from the anterior LC somata using petroleum jelly wells (Figure 1A). Intact network activity was monitored with intracellular recordings from anterior LCs along with extracellular recording of the network output. For most experiments, the posterior end of the ganglion was maintained in normal physiological saline and protected from TEA superfusate with a barrier of petroleum jelly. The anterior end of the preparation was superfused at a rate of approximately 2 ml/min. A schematic of this experimental setup is shown in Figure 1A. All experiments were performed at 12°C.

Extracellular recordings using a Model 1700 Differential AC Amplifier (A-M Systems, Carlsborg, WA) were taken with stainless steel pin electrodes from a petroleum jelly well on the ganglionic trunk containing axons of all 9 neurons in the CG. LC spikes on the extracellular

traces are easily distinguishable by their large amplitude. The LC somata were desheathed for sharp electrode recordings. Intracellular recordings were made using glass electrodes containing 3M KCl (8-25 M**Ω**) and AxoClamp 900A and AxoClamp 2B amplifiers (Molecular Devices, Sunnyvale, CA). Two-electrode voltage clamp (TEVC) and two-electrode current clamp (TECC) protocols were created and run using Clampex 10.3 software (Molecular Devices).

Somata were isolated for dynamic clamp experiments by tightening a thread ligature past the anterior branch point on the nerve containing the LC soma. Isolated cells were simultaneously driven with the same current stimulus, described previously (Ransdell et al., 2013a). Briefly, a stimulus protocol was generated by recording the voltage waveform from a LC somata during intact network activity. This consisted of a 20 second recording from a LC3 soma which included four burst potentials with both pacemaker cell EPSPs and LC back-propagating APs present. In addition to the stimulus current, dynamic clamp artificial coupling current was applied with NetClamp software (developed in the Fishberg Department of Neuroscience of the Mount Sinai School of Medicine and available at http://gothamsci.com/NetClamp/) at a sampling rate of 50 kHz according to the equation: $I_{gap} = g*(V_m1 - V_m2)$ where g is a non-rectifying coupling conductance under experimental control, and the voltage difference between the cells ($V_m1 - V_m2$) determines the driving force.

I_A was measured before and after compensation using voltage clamp protocols as described previously (Ransdell et al., 2012a). Briefly, outward currents were measured from a holding potential of -30 mV and stepped from -50mV to +5 mV in 5mV increments in order to measure the high threshold K^+ current I_{HTK} which is blocked by TEA. In LCs, I_{HTK} is predominantly a mix of BKKCa and delayed rectifier currents (Ransdell et al. 2012). A-Type K^+ current (I_A) was measured by performing an identical voltage clamp steps from a holding

potential of -80mV and subtracting I_{HTK}. P/N leak subtraction was used for all TEVC. Coupling in the intact network was measured using TECC in both cells during the sucrose block. Negative current steps ranging from 1-6 nA were injected into one cell at a time while measuring voltage changes in both cells. Coupling coefficients were calculated as the ratio: ($\Delta V_{coupled\ cell}$ / $\Delta V_{Injected\ Cell}$).

BIOLOGICAL METHODS: Measurements of Intrinsic Compensation

To determine whether intrinsic compensation may be contributing to restoration of synchrony in the biological network, we used a current stimulus protocol simulating realistic network inputs to LCs in order to deliver the same biologically relevant stimulus at 3 time points (Joseph L Ransdell et al., 2013a). Using this reversible sucrose block to suspend pacemaking activity, we were able to compare the similarity of responses of LC3 and LC5 to the same current injection at three time points. This allows us to test each cell in isolation with respect to its output waveform, but compensation occurs with full network activity after removal of the sucrose over the course of 1 hour. We measured individual LC responses to current injection in control saline, repeated after 5 minutes of TEA exposure (acute), and again after 1 hour of TEA exposure.

Our modeling results suggested that an increase in I_A may act in a manner to accomplish both the decrease in excitability and the restoration of synchrony seen in our biological data. In order to determine whether compensatory changes in I_A occur in the intact network, we performed two-electrode voltage clamp in the same LC before and after 1 hour of TEA exposure. In order to track changes in I_A in individual LCs we again used reversible sucrose block to perform voltage clamp immediately after acute TEA application and again after 1 hour of TEA perfusion. After voltage clamping anterior LCs, the sucrose was washed out and replaced with

physiological saline, allowing the network to resume normal activity. This process was repeated after 1 hour of compensation.

BIOLOGICAL METHODS: Data Analysis

Intracellular burst waveforms were considered to begin with the first EPSP from pacemaker activity and ended upon return of the waveform to resting membrane potential. Recordings were analyzed using Clampfit 10.3 (Molecular Devices) and Spike 2 version 7 (CED, Cambridge, UK) software. Statistical analyses were performed using SigmaPlot 11.0. Correlation coefficients (R-values) were obtained by a Pearson correlation, and squared to calculate the coefficient of determination (R^2). Most data are "before and after" effects within the same ganglion or cell, and therefore any two groups were compared with paired *t*-tests when the data were normally distributed, or Wilcoxon signed rank tests in the case of non-normality. The sample sizes for comparison of waveform synchrony were calculated with power analyses based on projected means and standard deviations from data reported in our previous study with very similar experimental manipulations of TEA exposure of LCs (Joseph L Ransdell et al., 2013a), which yielded target sample size of N=6-10 to yield a power of 0.8 to 0.97. Sample sizes for changes in network output and changes in I_A after TEA exposure were based on similar data in our previous work (Ransdell et al., 2012b), and yielded target sample sizes of N=5 to achieve a power of 0.909. Power analyses were conducted based on the use of paired *t*-tests to analyze the data. However, when data were not normally distributed we ended up using a Wilcoxon signed rank test, which was not utilized in our initial power analyses. All sample sizes used in our studies are reported in Figure Legends and/or in the Results section when significance values are reported.

To quantify synchrony of LC voltage waveforms, we performed a cross-correlation of the digitized voltage signal from LC pairs, as shown in Figure 2B. The first pacemaker spike was used to define the start of each LC burst, and bursts were considered to have terminated upon return to V_{Rest} in the LCs. The coefficient of determination from this cross-correlation (R^2) was used to examine how accurately one burst waveform could predict the waveform in another LC (see Ransdell et al. 2013a). This cross-correlation was performed for every burst across the full time-course of the experiment (Figure 2C, *left*). A decrease in R^2 therefore indicates a loss or reduction in waveform synchrony. R^2 values from 10 consecutive bursts were averaged for all data points presented as waveform synchrony data, save for the individual points found in Figures 2B and 2C.

Five different measures of excitability of LCs were calculated using both extracellular and intracellular recordings (Figure 2D). Extracellular recordings from the ganglionic trunk were used to calculate the number of spikes per burst and spike frequency. Because our hypothesis predicts both increased LC excitability and desynchronization with TEA exposure, it should be noted that there is a potential confound in distinguishing these effects based on extracellular analysis alone. Axons of all LCs run through the ganglionic trunk, thus the increased spike count observed could result from an increase in the total number of action potentials, desynchronization of action potentials across LCs, or both. We therefore included three additional measures of excitability that helped clarify the effect. We measured the latency between the onset of SC pacemaker bursting to the first LC spike in each burst (Figure 2D; SC-LC phase delay). Two other measures of excitability were calculated from intracellular voltage changes: burst amplitude and total burst depolarization. Burst amplitude was defined as the maximal voltage change from V_{Rest} to the highest peak of the burst, and total depolarization is

the area under the curve above V_{Rest}, measured in mV*sec. For all measures of excitability, values from 10 consecutive bursts were averaged at each time-point in each preparation (N=8).

MODEL METHODS: Single Cell Models

A detailed model was created with eight voltage-dependent conductances (G_A, G_{Kd}, G_{NaP}, G_{CaS}, G_{CaT}, G_{CAN}, $G_{SK(Ca)}$, $G_{BK(Ca)}$) and passive leak channels. These conductances are defined as: A-type potassium (G_A), delayed rectifier (G_{Kd}), persistent sodium (G_{NaP}), transient calcium (G_{CaT}), slow persistent calcium (G_{CaS}), calcium-dependent non-selective cation (G_{CAN}), two calcium-dependent potassium currents (G_{SKKCa} and G_{BKKCa}), and leak (G_{Leak}). A single compartment model with biological dimensions for soma (Joseph L Ransdell et al., 2013b; Ransdell et al., 2010) was created in NEURON and its capacitance (C_m) and leak conductance (G_{leak}) were tuned to match the observed biological membrane time constant (τ) and input resistance (R_{in}). This resulted in a soma with a length of 284.87 µm and a diameter of 125 µm, with a capacitance of 2.719 µF/cm^2. Channels were then added and their maximal conductances were tuned to match three biological properties observed, i.e., a) Total outward current b) Response to synaptic drive and c) Response to synaptic drive in the presence of TEA. These results were obtained from experiments performed on ligatured somata of *C. borealis* LCs (Joseph L Ransdell et al., 2013a, 2013b; Ransdell et al., 2012b). For the network studies another compartment termed Spike Initiation Zone (SIZ) was added to the model. This compartment was modeled as a cylinder with capacitance of 1 µF/cm^2, a length of 400 µm, and a diameter of 8 µm, and contained only sodium, potassium and passive leak channels. This compartment allowed us to obtain spiking activity in the model cells for spike synchrony analysis. The resulting model equations were as follows:

$$C\frac{dV}{dt} = -I_A - I_{Kd} - I_{NaP} - I_{CaS} - I_{CaT} - I_{CAN} - I_{SKKCa} - I_{BKKCa} - I_{Leak} \quad \text{(Soma)}$$

$$C\frac{dV}{dt} = -I_{Na} - I_{Kdr} - I_{Leak} \quad \text{(SIZ)}$$

The individual currents were modeled as $I_c = g_{max,c} m^p h^q (V - E_c)$, where $g_{max,c}$ is its maximal conductance, *m* its activation variable (with exponent *p*), *h* its inactivation variable (with exponent *q*), and E_c its reversal potential (a similar equation is used for the synaptic current but without *m* and *h*). The kinetic equation for each of the gating functions *x* (*m* or *h*) takes the form

$$\frac{dx}{dt} = \frac{x_\infty\left(V,[Ca^{2+}]_i\right) - x}{\tau_x(V,[Ca^{2+}]_i)}$$

where x_∞ is the steady state gating voltage- and/or Ca^{2+}- dependent gating variable and τ_x is the voltage- and/or Ca^{2+}- dependent time constant. The equations for the active channels in the soma compartment were fit using biological recordings for these currents from the cardiac ganglion of *Cancer borealis*. These currents were fit as follows: Voltage clamp data obtained with Clampfit were imported into MATLAB (Mathworks, Natick, MA) and fit using the MATLAB curve-fitting toolbox. Current data were converted to conductance data by dividing by ($V_m - E_{Rev}$), where E_{Rev} was as follows: E_{Na} = +55 mV, E_K = -80 mV, E_{Ca} = +45 mV, E_{Leak} = -50 mV, and E_{CAN} = -30 mV. The time axis was adjusted to start from 0 for the beginning of the clamp. The following parameterization was used:

$$g(t) = \sum_{i=1}^{n} A_i \left(1 - \exp\left(-t/\tau_{m,i}\right)\right)\left(h_i - (h_i - 1)\exp\left(-t/\tau_{h,i}\right)\right)$$

In this equation, $A_i = G_{i,max} \times m_i$ was the maximal conductance of the current *i* multiplied by its voltage-dependent steady-state activation (m_i), h_i was the steady-state inactivation value, and $\tau_{m,i}$ and $\tau_{h,i}$ were the time constants with which activation and inactivation reached steady-state, respectively. This fitting procedure assumed that ionic currents were completely deactivated (*m* = 0) and de-inactivated (*h* = 1) prior to the onset of the voltage clamp. This was fit to each trace in a voltage clamp experiment, giving values of each of the four parameters for each test clamp voltage (V_c). These values were then fit for each current as functions of V_c using the general forms as stated below. This procedure yielded equations for the currents recorded in voltage clamp that could be used in simulations according to the Hodgkin-Huxley mathematical formalism.

$$A(V_c) = G_{max} \times m(V_c) = G_{max} \times \left(1 + \exp\left(\left(V_c - V_{m,1/2}\right)/k_m\right)\right)^{-1}$$
$$h(V_c) = \left(1 + \exp\left(\left(V_c - V_{h,1/2}\right)/k_h\right)\right)^{-1}$$
$$\tau_m(V_c) = \tau_{base,m} + \tau_{amp,m}\left(\exp\left(\left(V_c - V_{\tau1,m}\right)/k_{\tau1,m}\right) + \exp\left(\left(V_c - V_{\tau2,m}\right)/k_{\tau2,m}\right)\right)^{-1}$$
$$\tau_h(V_c) = \tau_{base,h} + \tau_{amp,h}\left(\exp\left(\left(V_c - V_{\tau1,h}\right)/k_{\tau1,h}\right) + \exp\left(\left(V_c - V_{\tau2,h}\right)/k_{\tau2,h}\right)\right)^{-1}$$

All the maximal conductances ($G_{i,max}$) were in µS, time constants in ms and voltages in mV.

MODEL METHODS: Calcium Dynamics

Intracellular calcium modulates the conductance of the calcium-activated potassium currents (BKKCa and SKKCa), calcium-activated nonselective cation current (CAN), and influences the magnitude of the inward calcium current in the LC (Tazaki and Cooke, 1990). A calcium pool was modeled in the LC with its concentration governed by the first-order dynamics (Prinz et al., 2003; Soto-Treviño et al., 2005) below:

$$\tau_{Ca}\frac{d[Ca^{2+}]}{dt} = -F \times I_{Ca} - ([Ca^{2+}] - [Ca^{2+}]_{rest})$$

where F = 0.256 μM/nA is the constant specifying the amount of calcium influx that results per unit (nanoampere) inward calcium current; τ_{Ca} represents the calcium removal rate from the pool; and $[Ca^{2+}]_{rest}$ = 0.5 μM. Voltage-clamp experiments of the calcium current (Joseph L Ransdell et al., 2013b) showed the calcium buffering time constant to be around 690 ms (τ_{Ca}).

MODEL METHODS: Searching for LC Neurons within the Model Parameter Space

After creating a nominal LC model (Tables 1,2), we wanted to search the conductance space for other possible conductance combinations that might exhibit appropriate LC output. The properties that had to be maintained were; a) Input Resistance (R_{in}) and Resting Membrane Potential, b) Pre-TEA and Post TEA response to current injection c) Response to Synaptic drive obtained from biological cell.

The rules used to select the potential parameters were as follows (based on biological recordings): Synaptic Drive response should have an R^2 value of at least 0.8 or higher when compared to biological Synaptic Drive response. The duration of the pre-TEA response to a 6 nA, 50 ms current injection should be less than 120 ms. Also the peak should be less than -22 mV. The duration of the post-TEA (G_{BKKCa} and G_{Kd} reduced by 90%) response should be between 255-667 ms and its peak should be greater than -15 mV. A 9-D max conductance parameter space (5-fold variation over each conductance except G_{Leak}) was searched randomly for sets that satisfied the constraints above. We searched 20,000 different combinations of parameter sets with these criteria, and most of those which passed did not have a proper termination of activity following current injection (i.e., did not return to V_{rest}). We concluded this was due to an inappropriate relationship between I_{CAN} and I_{SKKCa}. Subsequent trials revealed that a given ratio range (~1:0.83 respectively) of these two currents was necessary for proper

termination of activity. Larger ratios cause V_{rest} to be higher due to the reversal potential (-30 mV) of CAN current. A higher fraction of I_{SKKCa} (reversal potential -80mV) caused a large AHP after termination and reduced the duration of the post-TEA response. Using the updated selection criteria with a ratio I_{CAN} to I_{SKKCa}, we found 180 parameter sets that passed. Of these 180 potential model sets, we selected only the ones that had Synaptic Drive response R^2 value > 0.9 compared to the biological Synaptic Drive response. This resulted in 49 potential parameter sets.

Biological data showed that I_A and I_{BKKCa} had a negative correlation in their magnitudes in LCs (Ransdell et al., 2012b). We added this to our criteria for screening potential parameter sets for the network studies. We converted biological I_A-I_{BKKCa} current data into factor data by dividing I_A and I_{BKKCa} by their respective factor average. G_A and G_{BKKCa} values of passed parameters were similarly divided by its average to get its factor data. The biological data was fit using a linear polynomial from 95% to 70% confidence intervals, in steps of 10%. For network studies we used a 70% confidence interval, which left us with 14 potential parameter sets that represented LC model neurons for use in modeling studies.

MODEL METHODS: Development and Validation of a Population of Conductance-Based Model Networks for Studying Mechanisms Restoring Network Synchrony

Our results demonstrate that intact cardiac ganglia are able to compensate for the loss of high-threshold K^+ currents and restore both excitability and synchrony within one hour of TEA blockade. We next set out to explore the mechanisms by which excitability and synchrony could be restored in this network. To maximize our ability to interrogate multiple parameters that may be responsible for compensation in this system, we constructed a population of conductance-based biophysical models of the CG network. This allowed us to simulate the TEA conductance

blockade and then manipulate individual conductances, both voltage-gated and synaptic, to examine their effects on network excitability and synchrony.

Our 14 parameter sets for LCs were used to create 50 random 5-cell networks of LCs, ensuring that the same model LC never appeared twice in the same network. The five cells within a network were then electrically coupled using conductance values tuned to reflect experimental observations of coupling coefficients. Small cell (SC) pacemaker drive was simulated as excitatory synapses via the NetStim function in NEURON. Parameters for the model of the synaptic drive onto LCs were tuned to get 6 to 9 spikes in the nominal LC model. It was observed biologically that frequency of SC firing increases within the slow wave oscillation cycle of LCs. Based on these recordings, the model SC burst initially fired at 18 Hz for first 440 ms and then increased to 25 Hz for 560 ms, with the burst terminating at 1000 ms.

Our experimental TEA block was simulated in these networks by reducing G_{BKKCa} and G_{Kd} conductances by 90% in the 3 anterior LCs based on biological data in LCs (Joseph L Ransdell et al., 2013a). We imposed a final set of selection criteria on the randomly generated model networks, rejecting networks that increased synchrony or decreased the total number of spikes after the simulated TEA block, as this was never observed in biological networks. This left 27 networks that reproduced the biological trends and these were used in subsequent analyses to explore potential conductance changes that could restore network synchrony.

Somatic burst potentials drive action potentials in LC axons, so divergent burst waveforms would be expected to cause desynchronized spiking. Our biological data qualitatively agreed with this, but a precise quantification of synchrony for all spikes within a burst is subject to many ambiguities. Our model networks easily provided precise spike times for each cell in the network, so we chose to examine actual spike synchrony in the model to complement the burst

waveform analysis in the biological preparation. Our analysis considered synchrony for paired anterior LCs with a nominal coupling conductance of 0.0182 S using a 25 ms bin width for spike-times (Wang and Buzsáki, 1996). Spikes occurring in both cells during the same bin were considered synchronized, while spikes that did not bin together were tallied as desynchronized. Using the definition of synchrony listed in the next section, these randomly generated model networks exhibited "control" synchrony scores ranging from 0.642 to 1.0 with a median value of 0.915 (matching data in biology), where 1.0 represents perfect spike synchrony.

MODEL METHODS: Data Analysis

In the models, spike synchrony between two cells was calculated based on spike times (Wang and Buzsáki, 1996). Spike times were recorded from each LC's Spike Initiation Zone (SIZ). The simulation time was divided into 25 ms bins. After initializing all bins to zero, each cell spike was added to the corresponding bin. Synchrony (SY) between two cells A and B was calculated using following equation:

$$SY_{AB} = \frac{\sum_{l=1}^{k} A(l)*B(l)}{\sqrt{\sum_{l=1}^{k} A(l)* \sum_{l=1}^{k} B(l)}}$$

where *l* is the current bin and *k* is the maximum number of bins. Spikes occurring in both cells during the same bin were considered synchronized, while spikes that did not bin together were tallied as desynchronized.

To compare the measures of spike and waveform synchrony in model networks, model waveform synchrony measures (Figure 3) were performed as described above on filtered voltage traces (Gaussian lowpass filter, 15 Hz cutoff frequency; Clampfit 10.3) that remove the influence of the axonal spikes on the voltage waveforms. Statistical analyses were performed in SigmaPlot v11.0. The effects of changing G_{max} on the number of spikes and synchrony among TEA-

"treated" model neurons were tested with paired *t*-tests. Analyses changes in spike number and spike synchrony with changing coupling and synaptic strengths (Figure 5) were analyzed with One-Way ANOVAs with post-hoc pairwise comparisons between a given percent change and the TEA case conducted via Holm-Sidak tests.

Table 1. Nominal model conductance values:

Conductance	Value (S/cm^2)
Leak	2e-4
A	6e-4
BKKCa	7.3e-3
g1_Kd	3e-4
g2_Kd	3.5e-5
CaS	1.7e-4
CAN	1.06e-4
SKKCa	8.79e-5
CaT	1.5e-4
NaP	3.06 e-4

Table 2. Model current parameters.

I_{ion}	x^p	x_∞	τ_x (msec)
I_A	m^3	$\frac{1}{1+\exp((V+21.46)/-17.96)}$	$3.002+\frac{4.073}{1+\exp((V+24.18)/2.592)}$
	h	$\frac{1}{1+\exp((V+21.14)/25.99)}$	$9.434+\frac{11.7}{1+\exp((V+1)/5.317)}$
I_{CaS}	m^2	$\frac{1}{1+\exp((V+24.75)/-5)}$	$20+\frac{50.2}{\exp((V+20.25)/1)}$
	h	$\frac{45}{40+[Ca^{2+}]}$	$\frac{1}{0.02}$
I_{CaT}	m	$\frac{1}{1+\exp((V+20)/-1.898)}$	$18.51-\frac{3.388}{\exp((V-6.53)/9.736)+\exp((V+12.39/-2.525)}$
	h	$\frac{1}{1+\exp((V+55.27)/6.11)}$	$20.23+\frac{40}{\exp((V+23.48)/-9.976)+\exp((V+5.196)/10.84)}$
I_{Kd}	m_1^4	$\frac{1}{1+\exp((V+24.19)/-10.77)}$	$25.049+\frac{25}{1+\exp((V+25.84)/6.252)}$
	h_1	$0.3+\frac{1-0.3}{1+\exp((V+15.87)/5.916)}$	$550+\frac{954.9}{\exp((V+10.8)/-15)}$
	m_2^4	$\frac{1}{1+\exp((V+23.32)/-10)}$	$100+\frac{550}{\exp((V+15)/12.46)}$
I_{NaP}	m^3	$\frac{1}{1+\exp((V+32.7)/-18.81)}$	$3.15+\frac{0.8464}{\exp((V+0.8703)/-6.106)}$

I_{CAN}	w	(0.0002 * [Ca^{2+}] ^2 / (0.0002 * [Ca^{2+}] ^2 + 0.05))	(40 / (0.0002 * [Ca^{2+}] ^2 + 0.05))
I_{SKKCa}	w	(0.0001 * [Ca^{2+}] ^2 / (0.0001 * [Ca^{2+}] ^2 + 0.1))	(4 / (0.0001 * [Ca^{2+}] ^2 + 0.1))
I_{BKKCa}	a	$\frac{[Ca^{2+}]}{(1+\exp((V-15+0.08*[Ca^{2+}])/-15)*(1+\exp((V+5+0.08*[Ca^{2+}])/-9)*(2+[}$	$\frac{1}{0.4}$
	b	$\frac{7}{5+[Ca^{2+}]}$	$\frac{1}{0.2}$

F = Faradays constant
R = Gas constant
V = Membrane voltage
[Ca^{2+}] = intracellular Calcium concentration

RESULTS

Exposure to TEA Desynchronizes LC Burst Waveforms and Increases Excitability

Ransdell et al. (2013a) were able to repeatably reduce the magnitude of high-threshold K^+ currents (I_{Kd} + I_{BKKCA}) by ~92% in isolated LCs with 25 mM TEA. We used this experimental manipulation on the 3 anterior LCs in intact CGs (Figure 1A) causing LCs in the same ganglion to change from identical (Figure 1B) to divergent, asynchronous output (Figure 2A, I, II) after exposure to TEA. After application of TEA, motor neurons became noticeably more depolarized during burst potentials and LC spiking seen on the extracellular recordings increased substantially (Figure 2A). Additionally, comparison of intracellular voltage waveforms revealed a loss of conserved output (Figure 2A). These results are consistent with the hypothesis that variable underlying conductances of the LCs makes them vulnerable to a uniform perturbation of a subset of conductances such as the TEA blockade that targets high-threshold K^+ conductances. Because our previous results demonstrated that the change in excitability that accompanies TEA exposure in LCs is accompanied by an increase in A-type K^+ current, we hypothesized that compensation may also occur at the network level to restores synchrony among LCs subsequent to the TEA block.

Compensation restores both excitability and synchrony following TEA Exposure

To determine whether compensatory responses can restore both excitability and synchrony of LC output following TEA block, anterior LCs were superfused with TEA for at least 1 hour while activity of the individual LCs and the network were continuously recorded. Our data demonstrate that both synchrony and excitability are restored towards baseline levels over a period of 30-60 minutes following TEA exposure. Figure 2A and 2B illustrate a typical

progression through the loss and subsequent restoration of synchrony among LCs during one hour of continuous exposure to TEA. Acutely after application of TEA, we saw a significant reduction in synchrony as measured by R^2 (see Methods; Ransdell et al. 2013a) across LC voltage waveforms (Figure 2B; 2C, time point II). Following this reduction, waveform synchrony values consistently recovered towards baseline levels, often by 30 minutes, and were no longer statistically different from baseline by 1 hour of treatment with TEA (Figure 2C, right). To monitor compensatory changes in excitability, five different measures of excitability were calculated using both extracellular and intracellular recordings (Figure 2D; see Experimental Methods). The spikes per burst, average spike frequency, total burst depolarization and burst amplitude all were significantly increased immediately after exposure to TEA ("acute"), while the small cell pacemaker (SC)-to-LC phase delay was significantly decreased (Figure 2D). All 5 measures also then showed a significant change back towards their baseline levels between the 30 minute and 60 minute time points. While all measures showed clear shifts towards restoration of baseline excitability, the number of spikes per burst, spike frequency within each burst, burst amplitude, and total burst depolarization were not completely restored to control levels; the exception was the SC-LC phase delay which was fully restored (Figure 2D). Preparations exposed to TEA for 2-3 hours showed no further change in excitability (data not shown). For this reason, time scales longer than 1 hour were not included in our analyses.

Model Predicts Multiple Mechanisms of Compensation based on Intrinsic Conductances

TEA exposure reduces LC synchrony and induces hyperexcitability. Our model development and selection criteria resulted in a population of 27 model CG networks with variable underlying conductances of the constituent neurons that successfully recapitulated the

biological data observed in TEA (see Methods, Supplemental Information). Our previous results identified an approximate 2.2 ± 0.8-fold change in I_A in LCs as a result of 60 minutes of TEA exposure (Ransdell et al. 2012). Therefore, we used the model networks to explore potential mechanisms of compensation by first increasing and decreasing each individual maximal membrane conductance by a similar factor of 2. We searched for changes that would increase LC spike synchrony while countering the hyperexcitability induced by TEA. To easily visualize the trends, each network was normalized to its initial value for spike synchrony. These data are shown for all conductances in Figure 3.

Our initial goal with the model was to determine whether changes in single conductances were sufficient to elicit compensatory changes in output that help restore both excitability and synchrony. While it is not difficult to conceive of a change in multiple aspects of the parameter set that could achieve restoration of output, it is perhaps not as intuitive – but presumably the most parsimonious solution – for a single conductance to have such an impact. True to this expectation, while various manipulations of G_{max} values improved either excitability or synchrony, very few conductance changes improved both. The optimal solution of significantly improving spike synchrony and also significantly decreasing the total number of action potentials was achieved in only one case: 2-fold increase in G_A resulted in a mean synchrony score that was significantly different from the TEA case ($P < 0.05$, paired *t*-test) but not significantly different from control ($P = 0.157$). No other change in a given conductance resulted in this combination of statistical outcomes. Not every model cell or networked improved uniformly with this conductance change. Therefore, while these results do not rule out a contribution for other conductances, they do suggest that an increase in G_A, as seen in previous experimental studies on isolated LCs (Ransdell et al., 2012a), may be the most likely candidate for a change in intrinsic

conductance promoting synchrony at the network level. These data suggest that while a single conductance change (increased G_A) can help restore both excitability and synchrony, variations in a single voltage-dependent conductance may not be sufficient to account for the full compensation response. In addition to perturbing only individual conductances, we also varied current kinetics and activation parameters (half-activation voltage $V_{1/2}$, ±10 mV, and slope factor *k*, by 0.5x and 2x (Ballo et al., 2012) and time constant by ±10 ms) for all the cell currents individually, and found that no changes in parameters for a single current could simultaneously restore excitability at the single cell level, and synchrony at the network level (data not shown). While the analysis has focused only on the parameters of a single current, simultaneous changes in parameters of multiple currents could also potentially provide similar compensation, and that remains to be explored. However, our analysis does reveal the substantial contribution of changing a single parameter – G_A – on multiple aspects of network compensation, to an extent that is beyond simple intuition. Importantly, the model also extends the biological data by demonstrating that waveform synchrony can translate into spike synchrony. Because of the electrotonic distance between the somata and axons of LCs, we cannot measure spike synchrony directly in this preparation. The model allows us to infer that waveform synchrony (and loss of synchrony) can indeed translate to the level of the most proximal cellular output – spiking.

Intrinsic Compensation Contributes to Restoration of Synchrony

Model runs predicted that increases in I_A help restore LC excitability and synchrony. To test this experimentally, we silenced pacemaker activity with isotonic sucrose solution (see Methods, Supplemental; Figure 1A), and tested the similarity of responses of each individual LC to a biologically realistic current stimulus (Ransdell et al. 2013a). We compared LC3 and LC5 to

the same current injection at three time points: control, 5 minutes post-TEA, and 1 hour post-TEA. Between current injections, pacemaker activity was restarted by removal of the sucrose block. This allows us to test each cell in isolation, but compensation occurs in the intact network. The initial voltage responses to our stimulation protocol in LC3 and LC5 in control conditions are highly similar to one another, and their level of waveform synchrony was not significantly different from the synchronous activity across these LCs during intact control network activity (Figure 4A,B). Immediately following TEA application, LC3 and LC5 show disparate output when driven with a common stimulus protocol (Figure 4A). Finally, our data show significant increases in R^2 of voltage activity within 1 hour across isolated LCs (Figure 4B), demonstrating that *intrinsic* compensation does improve *network* synchrony. However, after 1 hour the synchrony values were significantly lower than control values (Figure 4B,C), suggesting that intrinsic compensation alone is insufficient to restore synchrony. To determine whether compensatory changes in I_A occur in the intact network, we measured I_A with two-electrode voltage clamp in LCs before and after 1 hour of TEA exposure. Measurements were made while the network activity was temporarily halted with sucrose block, and compensation occurred with ongoing network activity. In all cases peak I_A current increased (Figure 4D), with a mean increase of 56% ($p<0.05$, N=6, Wilcoxon signed rank test). These data are consistent with the hypothesis that a compensatory increase in I_A can help promote synchrony in these networks.

Although the waveforms of LC3 and LC5 were not different from one another after 1 hour of compensation, anterior LC burst potentials did not reproduce their *original* waveform after compensation (see Figure 2; Panels I and IV). We also use the LCs from data shown in Figure 4A to compare the voltage responses of individual LCs to a fixed stimulus before and after compensation. Repeatable voltage responses under control conditions indicate that trial-to-

trial variability is negligible (mean $R^2 = 0.997$; Figure 4E, control). However, the voltage response after compensation was significantly different from the control voltage response ($p<0.01$, N=8, Wilcoxon signed rank test), indicating that intrinsic compensation does not restore the original cellular output (Figure 4E; control vs. 1 HR TEA).

Increased Model Electrical Coupling Conductance Helps Restore Synchrony

If intrinsic compensation does not fully restore synchrony, another mechanism must be present to explain the results observed during network compensation. LCs receive common excitatory inputs from the pacemakers and one hypothesis is that changing the strength of these chemical synapses might help to restore LC firing to appropriate levels. LCs in the network are also electrically coupled to one another via gap junctions which presumably promotes synchrony, although clearly the native coupling is not able to maintain LC synchrony in TEA (Cooke, 2002; Hagiwara et al., 1959; Tazaki and Cooke, 1983). A second hypothesis is that increased electrotonic coupling between LCs could buffer against disparate output and help to restore synchrony.

Using our set of model networks, we increased and decreased the strength of chemical synapses in 10% increments to test the effects on excitability and synchrony. We then did the same with model electrical coupling conductance. We found that increasing the strength of either chemical synapses or electrical coupling increased both synchrony and excitability (Figure 5 *left*). However, increasing the chemical synaptic conductance in conjunction with TEA blockade also increases spiking of the LCs ~25-30% in contrast with the biological decrease in excitability relative to the acute TEA exposure seen with compensation. Conversely, only a small change in LC spiking occurs with an increase in electrical coupling (~9%, Figure 5 *left*). Reducing the

strength of either chemical synapses or electrical coupling decreased overall spike synchrony (Figure 5 *right*), violating the assumptions of compensation based on the biological data. Reducing chemical synaptic strength eventually ceased LC firing altogether (data not shown).

Increased Electrical Coupling Helps Restore Synchrony across LCs in Experiments

Increased electrical coupling restored synchrony in model LCs with only a modest effect on excitability. To investigate this relationship in experiments, we isolated LCs and used dynamic clamp to add an artificial coupling conductance. Pairs of LCs from the same network were physically isolated by thread ligature, exposed to TEA, and simultaneously received the same stimulus protocol while dynamic clamp added a non-rectifying artificial coupling conductance (from 0 to 0.2 μS) between the cells. The driving force was equivalent to the voltage difference in membrane potential between the coupled cells. Increasing the artificial coupling conductance significantly increased the correlation coefficient of the waveform between the two cells (Figure 6A), with a synaptic conductance value of 0.2 μS able to rescue synchrony of LCs to levels observed in intact networks (Figure 6A). These results provided proof of principle that increasing electrical coupling could be responsible for resynchronization in the network.

We then measured coupling coefficients between LCs during compensation in the intact network. Coupling coefficients between cells increased significantly after 1 hour in TEA (mean increase 85%, $p<0.01$; Figure 6B,C). The coupling coefficient is a useful description of the functional relationship in coupling, but does not identify the electrophysiological mechanism. Plasticity of coupling properties can ultimately be influenced by two fundamentally different mechanisms: altered resistance of the non-junctional membrane of the coupled cells, or

modification of gap junctional conductance. Using two-electrode current clamp, we saw no significant differences in the apparent input resistance of LCs in control physiological saline, after acute TEA exposure, or after compensation (1 hour TEA exposure; Figure 6B,C). These results indicate that changes in passive membrane conductance (G_{Leak}) are not responsible for increased coupling coefficients.

To directly test whether coupling conductance between LCs increases as a result of TEA-induced compensation, we focused on LC4 and LC5 pairs within the same network. In the crab CG, anterior LCs exhibit strong local electrical and dye coupling (Tazaki and Cooke, 1983, 1979). The branch containing LC4 and LC5 somata can be separated and electrotonically "sealed" from the network by thread ligature to create ideal conditions for measuring coupling conductance. With two electrodes in each cell, we used hyperpolarizing current injections to measure resistance and calculate junctional conductance independent of membrane resistance (as in (Bennett, 1966); see Methods). Coupling conductance (G_C) between LC4 and LC5 significantly increased during 1 hour of TEA exposure (mean increase 49.5%, $p<0.01$, $N = 8$; Figure 6B,C).

Interaction of Intrinsic and Electrical Synaptic Compensation

Taken together, our experimental and modeling results suggest that although an increase in G_A is able to counter the increase in excitability of LCs in TEA in a compensatory fashion, as well as promote restoration of synchrony, such an intrinsic compensation was insufficient to restore synchrony fully. Additionally, our results suggest that an increase in coupling among LCs can greatly promote synchrony with only a modest effect on excitability. Therefore, we next used our model networks to investigate how G_A and G_C might interact to promote synchrony by

calculating synchrony scores as conductances of all 27 model networks were adjusted. First we increased G_A alone in 10% increments up to a 100% increase (Figure 7). Increasing G_A up to +40% promoted greater synchrony after TEA blockade, but was unable to fully restore synchrony even with increasing conductance levels, consistent with our biological data (Figure 4). Increasing G_A beyond +40% did not further improve synchrony (Figure 7), and ultimately caused LCs to cease firing altogether. We also increased model G_C incrementally (from +10% to +150%), and found that electrical coupling alone was capable of restoring synchrony fully, but this required a 140% increase in its value (Figure 7). Finally, we increased both G_A and G_C together in 10% increments, revealing a potentially synergistic relationship: a smaller increase of 70% in each conductance was able to produce spike synchrony that was indistinguishable from control (Figure 7).

DISCUSSION

Homeostatic or compensatory plasticity in the nervous system has been the subject of intense interrogation, with studies focusing on both homeostatic synaptic scaling (Lee et al., 2013; Turrigiano, 2012) and tuning of ionic conductance relationships to maintain a target level of excitability (Desai et al., 1999; Turrigiano et al., 1994). However, few studies have sought to integrate multiple mechanisms to directly address emergent network stability from compensatory processes acting at the level of single neurons. Moreover, only recently has there been an appreciation that variability in underlying cellular parameters such as conductance magnitudes (Pratt and Aizenman, 2007; Schulz et al., 2006; Wilhelm et al., 2009), activation properties of channels (Amendola et al., 2012; Olypher et al., 2006), and synaptic strengths (Grashow et al., 2010; Olypher and Calabrese, 2007; Wilhelm et al., 2009) may form part of the repertoire of

compensatory mechanisms that endow networks with remarkable robustness characteristics. Homeostatic plasticity has been reported in single isolated neurons (Ransdell et al., 2012a; Swensen and Bean, 2005), in artificial networks formed in culture (Desai et al., 1999; Ibata et al., 2008), or in thin sections of the CNS (Karmarkar and Buonomano, 2006; Lambo and Turrigiano, 2013).

Cortical slice preparations have demonstrated homeostatic plasticity of intrinsic conductances coordinated with chemical synaptic plasticity (Karmarkar and Buonomano, 2006; Lambo and Turrigiano, 2013), and Mauthner cells in fish have been shown to exhibit coordinated activity-dependent changes in both the chemical and electrical components of its mixed synapses (Pereda and Faber, 1996; Yang et al., 1990). While membrane conductances and properties of electrical coupling are known to interact in critically important ways to promote synchrony (Curti et al., 2012; Gutierrez and Marder, 2013), to our knowledge the present study is the first demonstration of coordinated homeostatic plasticity of intrinsic and electrical synaptic conductances in a comprehensive network-level example of homeostatic compensation.

We hypothesized that plasticity distributed throughout the network might provide robustness of network output. Using a combination of pharmacology, electrophysiology, and modeling approaches in intact neural networks, we first uncovered a striking vulnerability of neural networks to underlying cellular variability. We then demonstrated that an intact network has mechanisms that allow for robustness in output via synergistic compensatory changes across individual cell (ionic conductance) as well as trans-cellular (electrical coupling) properties. The interplay of intrinsic and synaptic parameters, and distributed plasticity in determining network output, is difficult, if not impossible, to unravel experimentally. This makes investigations via biophysical models an attractive alternative to narrow possibilities, and complement

experiments, as we have demonstrated.

Multi-component Compensation Can Synergistically Restore Network Output

Previous modeling studies found that K^+ currents can increase or help restore synchrony between electrically coupled neurons (Pfeuty et al., 2003), so we first hypothesized that a compensatory increase in A-Type K^+ membrane conductance could be a mechanism underlying both restored excitability and resynchronization. Over the course of 30-60 minutes, increased I_A was associated with decreasing cellular excitability [see also (Golowasch et al., 1999)] and improvement of coordinated motor neuron firing. However, intrinsic compensation alone was insufficient to fully restore synchrony across LCs. A concomitant increase in electrotonic coupling ensured virtually complete resynchronization. Our modeling results suggest that although a sufficient increase in electrical coupling alone could restore full synchrony (140% increase), it could not simultaneously restore the original level of excitability. Only a 70% increase was necessary when accompanied by a concomitant increase in G_A. Therefore, we conclude that multi-component mechanisms are not only necessary for full compensation, but also that their synergistic action is potentially more efficient than either mechanism operating in isolation.

Comparison of Our Results in the Context of Behavioral/Motor Plasticity

While our results occurred in a compensatory context, the underlying mechanisms bear striking similarity to motor output plasticity induced by operant conditioning in *Aplysia*. In a series of elegant experiments, it has been shown that chaotic exploratory and consummatory radula biting movements of *Aplysia* during food searching behavior can be stably modified by

operant conditioning, leading to prolonged bouts of radula movements with increased frequency and more stereotyped rhythmic organization (Nargeot and Simmers, 2011; Nargeot et al., 2007). Chaotic biting patterns result from inherently variable and unsynchronized bursting of CPG neurons that are each randomly capable of triggering bites (Nargeot et al., 2009). Following operant conditioning, induction of regular and synchronized bursting of pattern-initiating cells can be attributed to changes in both intrinsic excitability and electrical coupling strength. Specifically, changes in intrinsic excitability attributed to changes in leak conductance underlie the increase in frequency of motor output, while increases in coupling strength allow for the synchronization and regularization of bursting (Nargeot et al., 2009; Sieling et al., 2014). The full shift in behavioral and circuit output is therefore the additive influence of both intrinsic and electrical synaptic conductances. The striking similarity in these underlying mechanisms suggests that these kinds of circuit-level mechanisms may be a conserved strategy for stabilization of synchrony within network output, be it compensatory or in the context of behavioral plasticity.

Physiological Regulation of Coupling Conductance

The speed (within 30 minutes) and magnitude (up to a doubling of effective coupling) of physiological changes seen in electrical coupling was remarkable. Although electrical coupling has long been known to promote synchrony in many systems, including the CG (Bennett and Zukin, 2004; Tazaki, 1972), the physiological interaction of electrical coupling with intrinsic conductances to affect a compensatory output has not been examined. Previous work in the crustacean STG has demonstrated how synchronized activity of pacemaker cells is dependent on an interaction of intrinsic conductances and electrical coupling (Soto-Treviño et al., 2005; Szücs

et al., 2001, 2000), and that distinct circuits can be brought into synchrony via manipulations of electrical and chemical synapses (Elson et al., 1998; Szücs et al., 2009, 2000). But none of these studies have addressed the interaction of membrane conductance and electrical coupling in a compensatory context. Similarly, plasticity of electrical synapses has drawn considerable attention after being discovered in the mammalian central nervous system, including the thalamic reticular nucleus (Haas et al., 2011; Landisman and Connors, 2005), inferior olive (Lefler et al., 2014; Mathy et al., 2014), and retina (Kothmann et al., 2009; Völgyi et al., 2013). Studies in the thalamic reticular nucleus have suggested that potentially compensatory changes in coupling are important to maintain network stability as large changes in intrinsic excitability occur across development (Parker et al., 2009). These discoveries increased awareness of the complex functional roles and plasticity of coupling (Haas, 2015; O'Brien, 2014; Pereda et al., 2013), and also spurred research to identify molecular mechanisms that underlie plasticity and maintenance of these structures (Flores et al., 2012; Li et al., 2012; Turecek et al., 2014). Our study adds to this growing appreciation for plasticity of electrical synaptic connections in the context of homeostatic plasticity.

Variability, Plasticity, and Network Output – The Bigger Picture

Stable levels of intrinsic neuronal excitability and temporal coordination within networks are critical features across all nervous systems. Underlying both neuronal and network outputs are complex, and often highly variable intrinsic and synaptic properties of constituent neurons (Marder, 2011a; Norris et al., 2011). Our data demonstrate that intrinsic variability among cells of the same type can make networks vulnerable to loss of temporal coordination, in this case desynchronization of motor neuron output. Although LC activity was fully resynchronized

within 1 hour, recovered LCs never recapitulated their original voltage waveforms. While the intrinsic conductances involved in our manipulation and compensation (G_{Kd}, G_{BKKCa}, G_A) have overlapping functions and characteristics (Ransdell et al., 2012a), our findings demonstrate that individual conductances are not truly redundant. Degeneracy of ion channel properties leading to this type of relationship has been put forth as a mechanism underlying robustness and adaptability in neural networks (Marder and Goaillard, 2006; Tononi et al., 1999), but our study suggests physiological limits to neural network compensation and robustness. These limits may themselves be a contributing factor to the nature and progression of pathology in neurodegenerative diseases (Beck and Yaari, 2008; Small, 2008; Trasande and Ramirez, 2007).

We induce desynchronization and compensation in our studies through pharmacological block of a subset of K^+ conductances with TEA. However, the precise role these mechanisms play in fully intact biological networks is unclear. Intrinsic conductances can be differentially affected by ubiquitous natural mechanisms such as neuromodulation (Marder, 2012, 2011b) or temperature changes (Marder et al., 2015; Tang et al., 2012). Further, the effectiveness of electrical coupling can be affected by modulation of intrinsic cellular conductances (Szabo et al., 2010). Maintaining reliable synchronization of output under changing conditions is not trivial, and understanding the robustness and constraints of homeostatic systems that cope with such perturbations remains an important area for future investigation (Marder et al., 2014).

AUTHOR CONTRIBUTIONS

Conception and design: BJL, PS, JLR, SSN, DJS

Acquisition of data: BJL, PS, JLR

Analysis and interpretation of data: BJL, PS, JLR, SSN, DJS

Drafting or revising the article: BJL, PS, SSN, DJS

ACKNOWLEDGMENTS

This work was supported by NIH grant MH46742 (DJS and E. Marder), NIH grant MH087755 (SSN), NIH grant NIGMS 5T32GM008396, and a grant from the University of Missouri Research Board (DJS and SSN).

This chapter is modified from its original publication in the journal eLife (2016), under Creative Commons Attribution license.

COMPETING INTERESTS

The authors declare they have no competing financial interests.

REFERENCES

Amendola, J., Woodhouse, A., Martin-Eauclaire, M.-F., Goaillard, J.-M., 2012. Ca^{2+}/cAMP-sensitive covariation of I(A) and I(H) voltage dependences tunes rebound firing in dopaminergic neurons. J. Neurosci. 32, 2166–81.

Beck, H., Yaari, Y., 2008. Plasticity of intrinsic neuronal properties in CNS disorders. Nat. Rev. Neurosci. 9, 357–369.

Bennett, M., Zukin, R., 2004. Electrical Coupling and Neuronal Synchronization in the Mammalian Brain. Neuron 41, 495–511.

Bennett, M. V, 1966. Physiology of electrotonic junctions. Ann. N. Y. Acad. Sci. 137, 509–39.

Ciarleglio, C.M., Khakhalin, A.S., Wang, A.F., Constantino, A.C., Yip, S.P., Aizenman, C.D., 2015. Multivariate analysis of electrophysiological diversity of Xenopus visual neurons during development and plasticity. Elife 4.

Cooke, I.M., 2002. Reliable, responsive pacemaking and pattern generation with minimal cell numbers: the crustacean cardiac ganglion. Biol. Bull. 202, 108–36.

Curti, S., Hoge, G., Nagy, J.I., Pereda, A.E., 2012. Synergy between electrical coupling and membrane properties promotes strong synchronization of neurons of the mesencephalic trigeminal nucleus. J. Neurosci. 32, 4341–59.

Desai, N.S., 2004. Homeostatic plasticity in the CNS: synaptic and intrinsic forms. J. Physiol. Paris 97, 391–402.

Desai, N.S., Rutherford, L.C., Turrigiano, G.G., 1999. Plasticity in the intrinsic excitability of cortical pyramidal neurons. Nat. Neurosci. 2, 515–20.

Elson, R., Selverston, A., Huerta, R., Rulkov, N., Rabinovich, M., Abarbanel, H., 1998. Synchronous Behavior of Two Coupled Biological Neurons. Phys. Rev. Lett. 81, 5692–5695.

Flores, C.E., Nannapaneni, S., Davidson, K.G. V, Yasumura, T., Bennett, M.V.L., Rash, J.E., Pereda, A.E., 2012. Trafficking of gap junction channels at a vertebrate electrical synapse in vivo. Proc. Natl. Acad. Sci. U. S. A. 109, E573–82.

Golowasch, J., Abbott, L.F., Marder, E., 1999. Activity-dependent regulation of potassium currents in an identified neuron of the stomatogastric ganglion of the crab Cancer borealis. J. Neurosci. 19, RC33.

Grashow, R., Brookings, T., Marder, E., 2010. Compensation for variable intrinsic neuronal excitability by circuit-synaptic interactions. J. Neurosci. 30, 9145–56.

Grashow, R., Brookings, T., Marder, E., 2009. Reliable neuromodulation from circuits with variable underlying structure. Proc. Natl. Acad. Sci. U. S. A. 106, 11742–6.

Günay, C., Edgerton, J.R., Jaeger, D., 2008. Channel density distributions explain spiking variability in the globus pallidus: a combined physiology and computer simulation database approach. J. Neurosci. 28, 7476–91.

Gutierrez, G.J., Marder, E., 2013. Rectifying electrical synapses can affect the influence of synaptic modulation on output pattern robustness. J. Neurosci. 33, 13238–48.

Haas, J.S., 2015. A new measure for the strength of electrical synapses. Front. Cell. Neurosci. 9, 1–5.

Haas, J.S., Zavala, B., Landisman, C.E., 2011. Activity-dependent long-term depression of electrical synapses. Science 334, 389–93.

Hagiwara, S., Watanabe, A., Saito, N., 1959. Potential changes in syncytial neurons of lobster cardiac ganglion. J. Neurophysiol. 22, 554–72.

Ibata, K., Sun, Q., Turrigiano, G.G., 2008. Rapid synaptic scaling induced by changes in

postsynaptic firing. Neuron 57, 819–26.
Karmarkar, U.R., Buonomano, D. V., 2006. Different forms of homeostatic plasticity are engaged with distinct temporal profiles. Eur. J. Neurosci. 23, 1575–1584.
Kothmann, W.W., Massey, S.C., O'Brien, J., 2009. Dopamine-stimulated dephosphorylation of connexin 36 mediates AII amacrine cell uncoupling. J. Neurosci. 29, 14903–11.
Krubitzer, L., Kahn, D.M., 2003. Nature versus nurture revisited: an old idea with a new twist. Prog. Neurobiol. 70, 33–52.
Lambo, M.E., Turrigiano, G.G., 2013. Synaptic and intrinsic homeostatic mechanisms cooperate to increase L2/3 pyramidal neuron excitability during a late phase of critical period plasticity. J. Neurosci. 33, 8810–9.
Landisman, C.E., Connors, B.W., 2005. Long-term modulation of electrical synapses in the mammalian thalamus. Science 310, 1809–13.
Lee, K.F.H., Soares, C., Béïque, J.-C., 2013. Tuning into diversity of homeostatic synaptic plasticity. Neuropharmacology 1–7.
Lefler, Y., Yarom, Y., Uusisaari, M.Y., 2014. Cerebellar Inhibitory Input to the Inferior Olive Decreases Electrical Coupling and Blocks Subthreshold Oscillations. Neuron 81, 1389–1400.
Li, X., Lynn, B.D., Nagy, J.I., 2012. The effector and scaffolding proteins AF6 and MUPP1 interact with connexin36 and localize at gap junctions that form electrical synapses in rodent brain. Eur. J. Neurosci. 35, 166–81.
Maffei, A., Bucher, D., Fontanini, A., 2012. Homeostatic plasticity in the nervous system. Neural Plast. 2012, 913472.
Marder, E., 2012. Neuromodulation of neuronal circuits: back to the future. Neuron 76, 1–11.
Marder, E., 2011a. Variability, compensation, and modulation in neurons and circuits. Proc. Natl. Acad. Sci. U. S. A. 108 Suppl , 15542–8.
Marder, E., 2011b. Variability, compensation, and modulation in neurons and circuits. Proc. Natl. Acad. Sci. U. S. A. 108 Suppl , 15542–8.
Marder, E., Goaillard, J.-M., 2006. Variability, compensation and homeostasis in neuron and network function. Nat. Rev. Neurosci. 7, 563–74.
Marder, E., Haddad, S. a., Goeritz, M.L., Rosenbaum, P., Kispersky, T., 2015. How can motor systems retain performance over a wide temperature range? Lessons from the crustacean stomatogastric nervous system. J. Comp. Physiol. A 201, 851–856.
Marder, E., O'Leary, T., Shruti, S., 2014. Neuromodulation of circuits with variable parameters: single neurons and small circuits reveal principles of state-dependent and robust neuromodulation. Annu. Rev. Neurosci. 37, 329–46.
Mathy, A., Clark, B. a., Häusser, M., 2014. Synaptically induced long-term modulation of electrical coupling in the inferior olive. Neuron 81, 1290–6.
Nargeot, R., Le Bon-Jego, M., Simmers, J., 2009. Cellular and Network Mechanisms of Operant Learning-Induced Compulsive Behavior in Aplysia. Curr. Biol. 19, 975–984.
Nargeot, R., Petrissans, C., Simmers, J., 2007. Behavioral and In Vitro Correlates of Compulsive-Like Food Seeking Induced by Operant Conditioning in Aplysia. J. Neurosci. 27, 8059–8070.
Nargeot, R., Simmers, J., 2011. Neural mechanisms of operant conditioning and learning-induced behavioral plasticity in Aplysia. Cell. Mol. Life Sci. 68, 803–16.
Nelson, S.B., Turrigiano, G.G., 2008. Strength through diversity. Neuron 60, 477–82.
Norris, B.J., Wenning, A., Wright, T.M., Calabrese, R.L., 2011. Constancy and variability in the

output of a central pattern generator. J. Neurosci. 31, 4663–74.
O'Brien, J., 2014. The ever-changing electrical synapse. Curr. Opin. Neurobiol. 29, 64–72.
Olypher, A., Cymbalyuk, G., Calabrese, R.L., 2006. Hybrid systems analysis of the control of burst duration by low-voltage-activated calcium current in leech heart interneurons. J. Neurophysiol. 96, 2857–67.
Olypher, A. V, Calabrese, R.L., 2007. Using Constraints on Neuronal Activity to Reveal Compensatory Changes in Neuronal Parameters. J. Neurophysiol. 98, 3749–3758.
Parker, P.R.L., Cruikshank, S.J., Connors, B.W., 2009. Stability of electrical coupling despite massive developmental changes of intrinsic neuronal physiology. J. Neurosci. 29, 9761–70.
Pereda, A.E., Curti, S., Hoge, G., Cachope, R., Flores, C.E., Rash, J.E., 2013. Gap junction-mediated electrical transmission: regulatory mechanisms and plasticity. Biochim. Biophys. Acta 1828, 134–46.
Pereda, A.E., Faber, D.S., 1996. Activity-dependent short-term enhancement of intercellular coupling. J. Neurosci. 16, 983–92.
Pfeuty, B., Mato, G., Golomb, D., Hansel, D., 2003. Electrical synapses and synchrony: the role of intrinsic currents. J. Neurosci. 23, 6280–94.
Pratt, K.G., Aizenman, C.D., 2007. Homeostatic regulation of intrinsic excitability and synaptic transmission in a developing visual circuit. J. Neurosci. 27, 8268–77.
Prinz, A.A., Billimoria, C.P., Marder, E., 2003. Alternative to hand-tuning conductance-based models: construction and analysis of databases of model neurons. J. Neurophysiol. 90, 3998–4015.
Ransdell, J.L., Faust, T.B., Schulz, D.J., 2010. Correlated Levels of mRNA and Soma Size in Single Identified Neurons: Evidence for Compartment-specific Regulation of Gene Expression. Front. Mol. Neurosci. 3, 116.
Ransdell, J.L., Nair, S.S., Schulz, D.J., 2013. Neurons within the Same Network Independently Achieve Conserved Output by Differentially Balancing Variable Conductance Magnitudes. J. Neurosci. 33, 9950–9956.
Ransdell, J.L., Nair, S.S., Schulz, D.J., 2013a. Neurons within the Same Network Independently Achieve Conserved Output by Differentially Balancing Variable Conductance Magnitudes. J. Neurosci. 33, 9950–9956.
Ransdell, J.L., Nair, S.S., Schulz, D.J., 2012a. Rapid homeostatic plasticity of intrinsic excitability in a central pattern generator network stabilizes functional neural network output. J. Neurosci. 32, 9649–58.
Ransdell, J.L., Nair, S.S., Schulz, D.J., 2012b. Rapid homeostatic plasticity of intrinsic excitability in a central pattern generator network stabilizes functional neural network output. J. Neurosci. 32, 9649–58.
Ransdell, J.L., Temporal, S., West, N.L., Leyrer, M.L., Schulz, D.J., 2013b. Characterization of inward currents and channels underlying burst activity in motoneurons of crab cardiac ganglion. J. Neurophysiol. 110, 42–54.
Roffman, R.C., Norris, B.J., Calabrese, R.L., 2012. Animal-to-animal variability of connection strength in the leech heartbeat central pattern generator. J. Neurophysiol. 107, 1681–93.
Schulz, D.J., Goaillard, J.-M., Marder, E., 2006. Variable channel expression in identified single and electrically coupled neurons in different animals. Nat. Neurosci. 9, 356–62.
Sieling, F., Bédécarrats, A., Simmers, J., Prinz, A.A., Nargeot, R., 2014. Differential Roles of Nonsynaptic and Synaptic Plasticity in Operant Reward Learning-Induced Compulsive Behavior. Curr. Biol. 24, 941–950.

Small, D.H., 2008. Network dysfunction in Alzheimer's disease: does synaptic scaling drive disease progression? Trends Mol. Med. 14, 103–8.
Soto-Treviño, C., Rabbah, P., Marder, E., Nadim, F., 2005. Computational model of electrically coupled, intrinsically distinct pacemaker neurons. J. Neurophysiol. 94, 590–604.
Swensen, A.M., Bean, B.P., 2005. Robustness of burst firing in dissociated purkinje neurons with acute or long-term reductions in sodium conductance. J. Neurosci. 25, 3509–20.
Szabo, T.M., Caplan, J.S., Zoran, M.J., 2010. Serotonin regulates electrical coupling via modulation of extrajunctional conductance: H-current. Brain Res. 1349, 21–31.
Szücs, A., Elson, R.C., Rabinovich, M.I., Abarbanel, H.D., Selverston, A.I., 2001. Nonlinear behavior of sinusoidally forced pyloric pacemaker neurons. J. Neurophysiol. 85, 1623–1638.
Szücs, A., Huerta, R., Rabinovich, M.I., Selverston, A.I., 2009. Robust Microcircuit Synchronization by Inhibitory Connections. Neuron 61, 439–453.
Szücs, A., Varona, P., Volkovskii, A.R., Abarbanel, H.D., Rabinovich, M.I., Selverston, A.I., 2000. Interacting biological and electronic neurons generate realistic oscillatory rhythms. Neuroreport 11, 563–569.
Tang, L.S., Taylor, A.L., Rinberg, A., Marder, E., 2012. Robustness of a rhythmic circuit to short- and long-term temperature changes. J. Neurosci. 32, 10075–85.
Tazaki, K., 1972. The burst activity of different cell regions and intercellular co-ordination in the cardiac ganglion of the crab, Eriocheir japonicus. J. Exp. Biol. 57, 713–26.
Tazaki, K., Cooke, I., 1983. Topographical localization of function in the cardiac ganglion of the crab, Portunus sanguinolentus. J. Comp. Physiol.
Tazaki, K., Cooke, I., 1979. Spontaneous electrical activity and interaction of large and small cells in cardiac ganglion of the crab, Portunus sanguinolentus. J. Neurophysiol. 42, 975–999.
Tazaki, K., Cooke, I.M., 1990. Characterization of Ca current underlying burst formation in lobster cardiac ganglion motorneurons. J. Neurophysiol. 63, 370–384.
Tononi, G., Sporns, O., Edelman, G.M., 1999. Measures of degeneracy and redundancy in biological networks. Proc. Natl. Acad. Sci. U. S. A. 96, 3257–62.
Trasande, C.A., Ramirez, J.-M., 2007. Activity deprivation leads to seizures in hippocampal slice cultures: is epilepsy the consequence of homeostatic plasticity? J. Clin. Neurophysiol. 24, 154–64.
Turecek, J., Yuen, G.S., Han, V.Z., Zeng, X.-H., Bayer, K.U., Welsh, J.P., 2014. NMDA receptor activation strengthens weak electrical coupling in mammalian brain. Neuron 81, 1375–88.
Turrigiano, G., 2012. Homeostatic synaptic plasticity: local and global mechanisms for stabilizing neuronal function. Cold Spring Harb. Perspect. Biol. 4, a005736.
Turrigiano, G., Abbott, L.F., Marder, E., 1994. Activity-dependent changes in the intrinsic properties of cultured neurons. Science 264, 974–7.
Turrigiano, G.G., 2008. The self-tuning neuron: synaptic scaling of excitatory synapses. Cell 135, 422–35.
Turrigiano, G.G., Nelson, S.B., 2004. Homeostatic plasticity in the developing nervous system. Nat. Rev. Neurosci. 5, 97–107.
Völgyi, B., Kovács-Oller, T., Atlasz, T., Wilhelm, M., Gábriel, R., 2013. Gap junctional coupling in the vertebrate retina: variations on one theme? Prog. Retin. Eye Res. 34, 1–18.
Wang, X.J., Buzsáki, G., 1996. Gamma oscillation by synaptic inhibition in a hippocampal

interneuronal network model. J. Neurosci. 16, 6402–13.
Wilhelm, J.C., Rich, M.M., Wenner, P., 2009. Compensatory changes in cellular excitability, not synaptic scaling, contribute to homeostatic recovery of embryonic network activity. Proc. Natl. Acad. Sci. U. S. A. 106, 6760–5.
Yang, X.D., Korn, H., Faber, D.S., 1990. Long-term potentiation of electrotonic coupling at mixed synapses. Nature 348, 542–5.

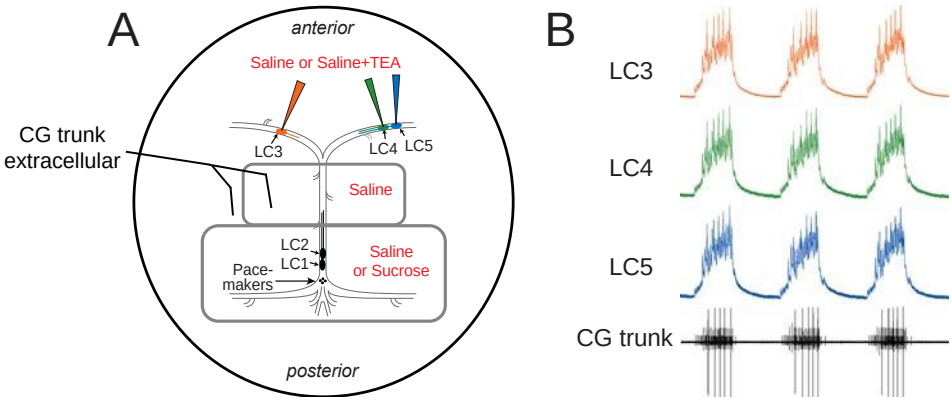

FIGURE 1.1: *Simultaneous recordings from multiple LCs in the same network reveal loss of synchronous activity after TEA exposure*. **A.** Experimental setup for the recording and superfusion of CG neurons. Petroleum jelly wells (gray) allow the posterior LC1 and LC2 as well as the pacemaker small cells (SCs) to be pharmacologically isolated from the anterior large cells (LC3, LC4, LC5). Pacemaker cells can be maintained in physiological saline, or the network can be temporarily shut down by replacing saline with 750 mM sucrose. Extracellular recordings are performed with stainless steel pin electrodes from the "trunk" nerve that contains the axons of all 5 LCs and the pacemaker cells. Intracellular recordings are taken from the anterior LCs. The area outside the petroleum jelly wells is superfused with pharmacological agents to target only the anterior large cells. **B.** Simultaneous intracellular recordings from the three anterior LCs and extracellular recording of the network output via the trunk nerve, demonstrating synchrony among LCs in the control outgoing rhythm. Scale bars = 10 mV, recording duration = 9 s.

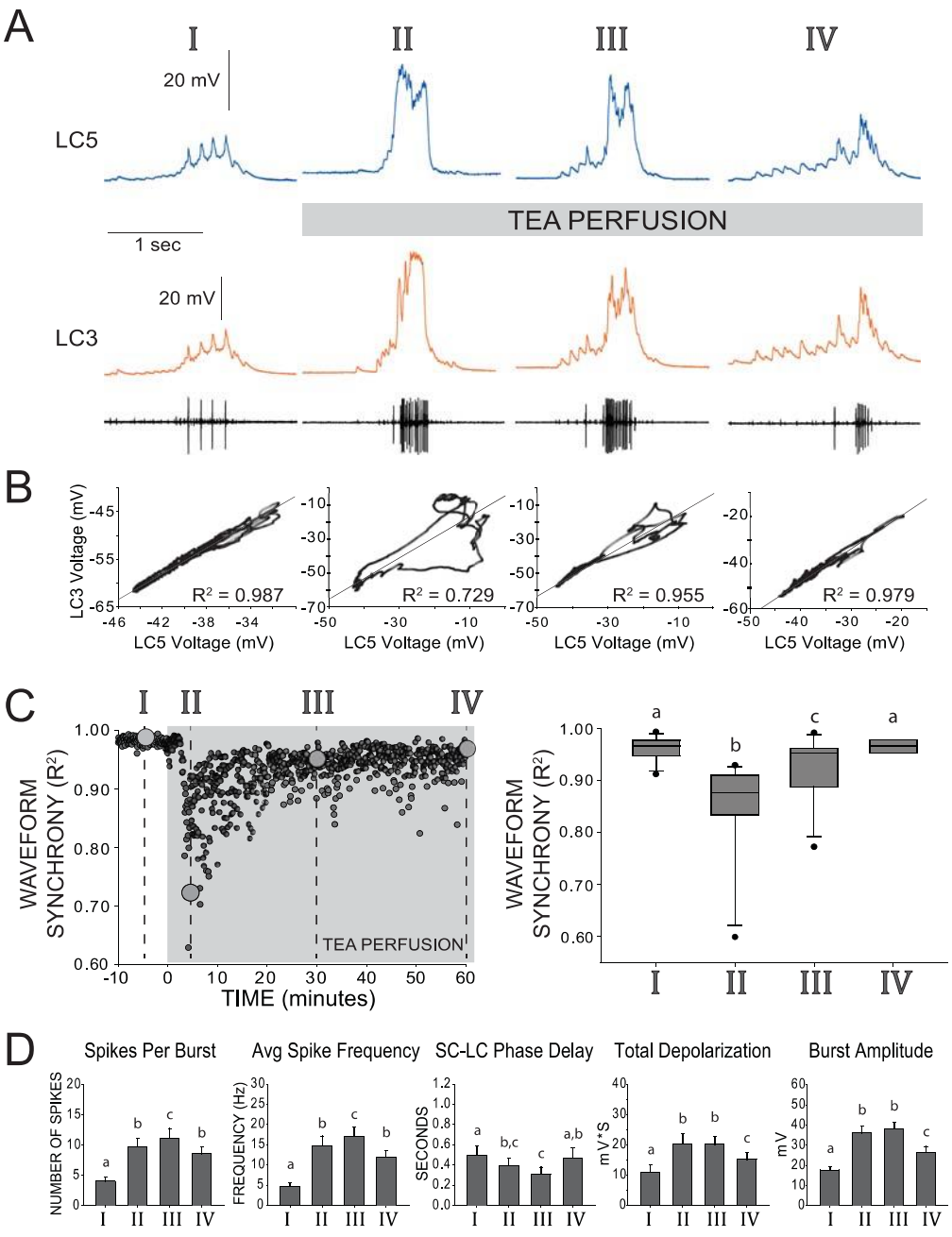

FIGURE 1.2: *Restored excitability and waveform synchrony among LCs after 1 hour of TEA exposure.* **A.** Representative recordings of LC3 and LC5 and of network activity over one hour of TEA exposure. Roman numerals (I, II, III, IV) designate time points of reference throughout the remainder of the figure, as follows: I – control saline, II – acute TEA exposure identified as the maximum effect on loss of synchrony across LCs (i.e.

lowest R^2 value), III – 30 minutes of TEA exposure, IV – 60 minutes of TEA exposure. **B.** Scatterplots show pairwise correlation of time-matched voltages (sampled at 10 kHz) of the waveforms shown in the representative traces. R^2 values are calculated from Pearson's correlation tests for these two cells. Loss and restoration of conserved output is demonstrated by changes in coherence in the scatterplot as well as in R^2 value. **C.** Synchrony of waveforms of the two cells seen in panels A and B plotted as R^2 values over the entire time course of the experiment. Roman numerals and large gray circles represent the values that were obtained from the scatterplots as each time point shown in panel B. TEA perfusion persists from time zero through 60 minutes. Box plots show distributions of R^2 values from cross-correlation analyses of LC voltage waveforms for pairs of LCs from N = 11 preparations. Lines within boxes mark the median, box boundaries represent 25^{th} and 75^{th} percentiles, whiskers represent 5^{th} and 95^{th} percentiles, and points represent outlying observations. Groups with significant differences in median synchrony ($P < 0.05$; Wilcoxon signed rank tests) are denoted with different letters. **D.** Excitability of LCs was quantified by five measurements (mean ±SD). Analysis of each preparation used the average of 10 consecutive bursts at each time point (N = 8 preparations). Number of spikes per burst, spike frequency within each burst, and the latency between pacemaker firing and first motor neuron spike (SC-LC Phase Delay) were calculated from extracellular traces. Total depolarization and amplitude of each burst are based on intracellular recordings. Significant differences across groups ($P < 0.05$; paired *t*-tests) are denoted with different letters, such that any two bars with a letter in common are not significantly different.

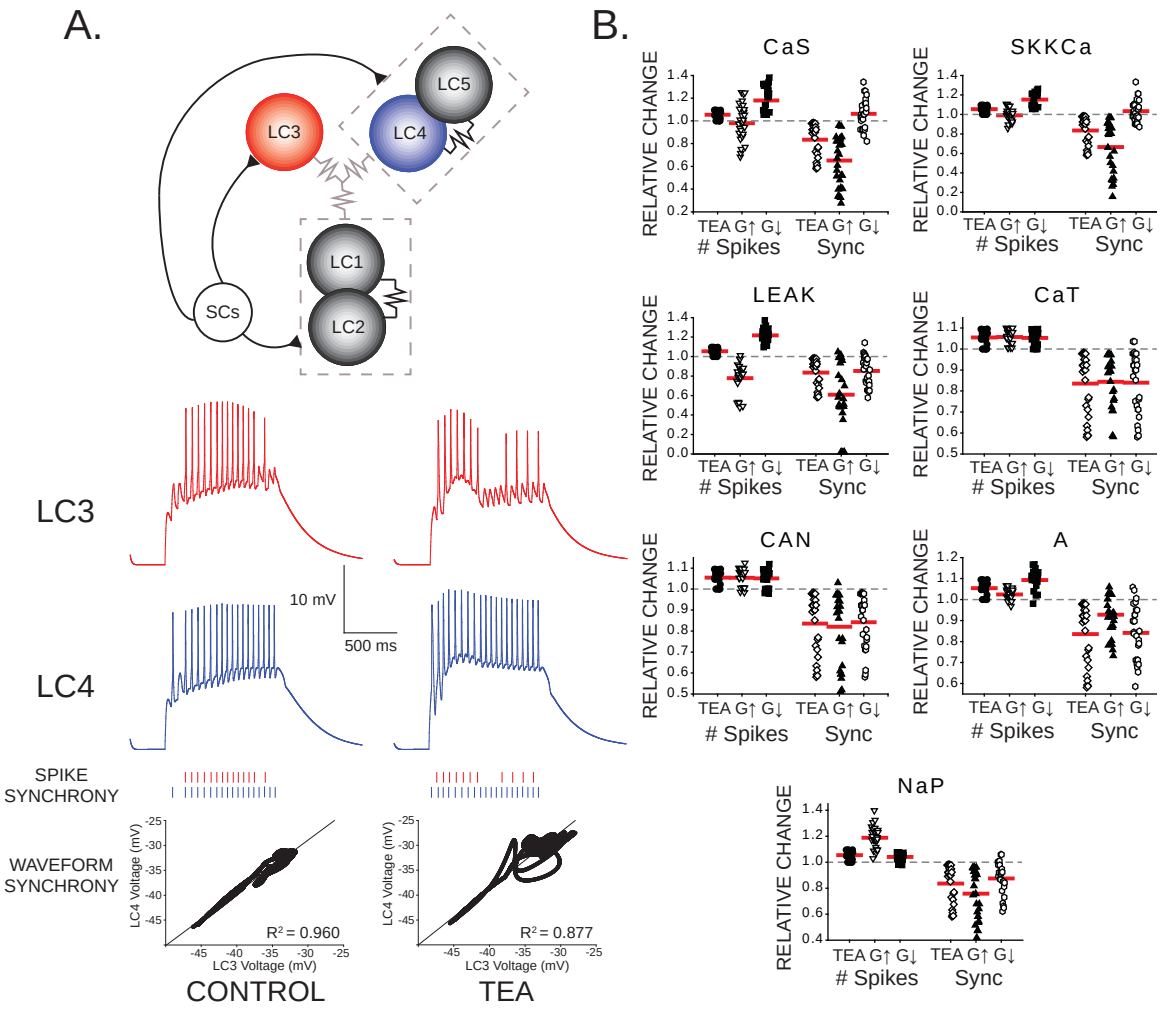

FIGURE 1.3: *Effects of increasing and decreasing individual ionic conductances on excitability and synchrony in model CG networks*. **A.** Schematic representation of model network organization and connectivity. Five large cell (LC) motor neurons are innervated via excitatory synapses from a common small cell pacemaker input (SCs). LC model neurons consist of two compartments - soma and axon - of which only the somata are pictured. Somata contain 9 conductances: G_{CaS}, G_{CaT}, G_{LEAK}, G_{CAN}, G_A, G_{BKKCa}, G_{SKKCa}, G_{Kd}, and G_{NaP}. Paired LCs (1+2, 5+6) have stronger local coupling (black resistor symbols), and all 5 LCs are reciprocally electrically coupled via weaker gap junctions

(gray resistor symbols). An example of LC3 and LC4 model output within a network burst activity is shown in the red and blue traces under both control and TEA (90% reduction in both G_{Kd} and G_{BKKCa}) conditions. Graphical representations of spike synchrony (raster plots) and waveform synchrony (scatterplots; as in Figure 2) are shown for the model neurons, demonstrating that both measures reflect the loss of LC synchrony as a result of TEA. **B**. Measurements of both output variables (# of spikes and spike synchrony) were made under three model conditions: control, TEA, and TEA + either a 2x increase (G↑) or 2x decrease (G↓) in a given conductance. N = 27 distinct model networks. All output measurements are normalized to their initial (control) conditions. Red lines represent the mean for a given group. Dashed line represents the 1.0 value (baseline) for a given measure. Compensatory responses that restore excitability and synchrony will tend to move the mean towards baseline.

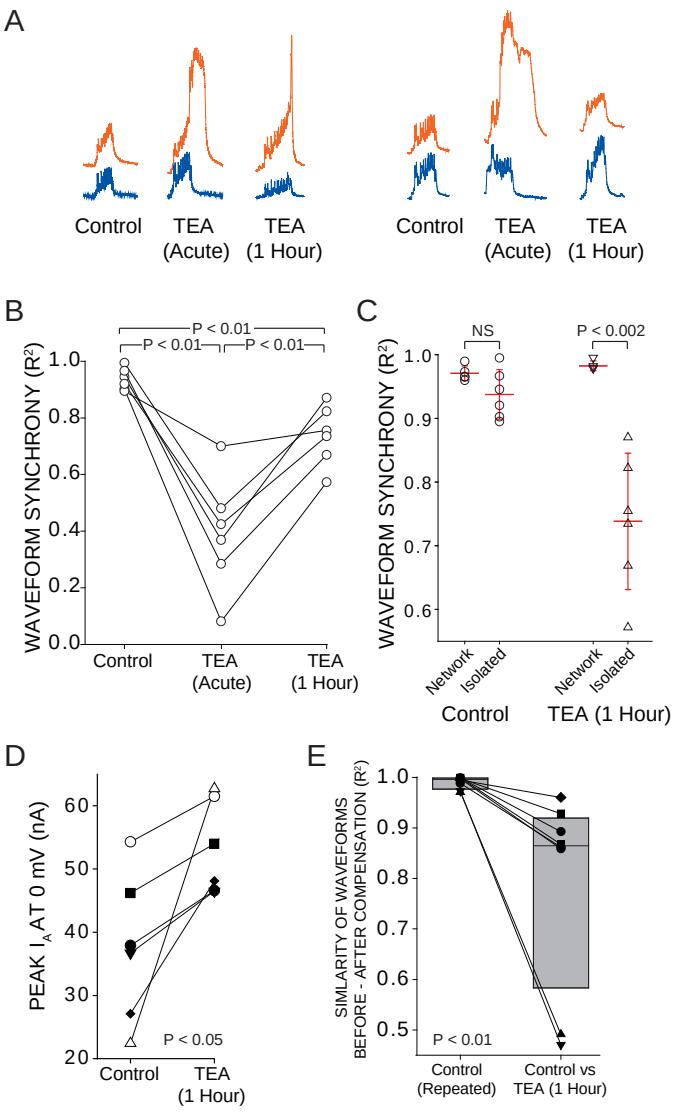

FIGURE 1.4: *Intrinsic compensation involving GA partially restores synchrony after TEA block.* A reversible sucrose block was used to temporarily stop network activity and a current stimulus protocol was delivered to individual LCs at three time points: control, after 5 minutes of TEA perfusion (acute), and after 1 hour of TEA perfusion (after compensation). **A.** Representative traces from 2 different preparations compare the responses of LC3 (orange) and LC5 (blue) to the same current injection (Stimulus Protocol) at each of the three time points. **B.** R^2 values for N = 6 preparations at each time point are plotted with the same preparation connected across time points. All 3 conditions

were significantly different from one another ($p<0.01$; paired *t*-tests). **C.** When isolated cell output was compared with output in the network, there was no difference in R^2 at the control state, but following 1 hour of compensation in the network, there was a significant ($P < 0.002$ – *t*-test) difference in synchrony scores (mean ± SD) between cells when isolated vs. when they are in the intact network. **D.** I_A was measured by two-electrode voltage clamp before and after compensation in N = 6 LCs in the intact CG. Voltage clamp data were obtained by temporarily silencing network activity with 750 mM sucrose. There was a significant increase in I_A after 1 hour in TEA (mean 56 +/- 65% increase, $p< 0.05$ –Wilcoxon signed rank test). **E**. Similarity of waveform in the same neurons before and after 1 hour TEA exposure. R^2 values were calculated for the output of the same cells before and after TEA exposure, and are shown as before-and-after values in the same cell connected by a line. Box plots show distributions of R^2 values from cross-correlation analysis of LC voltage waveforms N = 8 cells. Lines within boxes mark the median, box boundaries represent 25th and 75th percentiles. "Control" is the comparison of voltage waveforms to 2 separate rounds of current injection in the absence of TEA. Although there was improvement in similarity of waveforms after 1 hour in TEA (panel A), the newly compensated output after 1 hour of TEA exposure does not recapitulate the original response to the stimulus protocol (significantly different from control; $P < 0.01$ – Wilcoxon signed rank test).

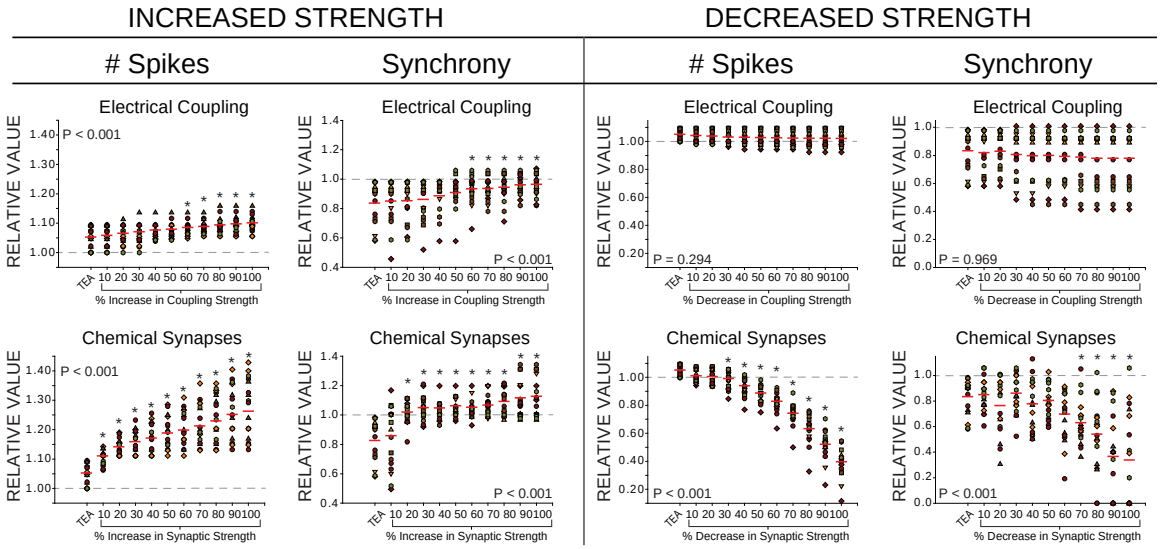

FIGURE 1.5: *Effects of increased or decreased strength of chemical synapses and electrical coupling on excitability and synchrony in model CG networks*. Measurements of two output variables (# of spikes and synchrony) were made under three model conditions: control, TEA (90% reduction in both G_{Kd} and G_{BKKCa}), and TEA + an incremental increase or decrease (up to 100% by 10% increments) for both chemical (pacemaker to LC) or electrical (LC to LC) connections. N = 27 distinct model networks. All output measurements are normalized to their initial (control) conditions to visualize trends. Red lines represent the mean for each group. Each different color and shape for points corresponds to one model network, and the same networks are shown across conductance levels. P-values in each plot refer to the results of a one-way ANOVA across all groups. Asterisks (*) denote groups in each plot that were significantly different from the TEA group via Holm-Sidak post-hoc tests.

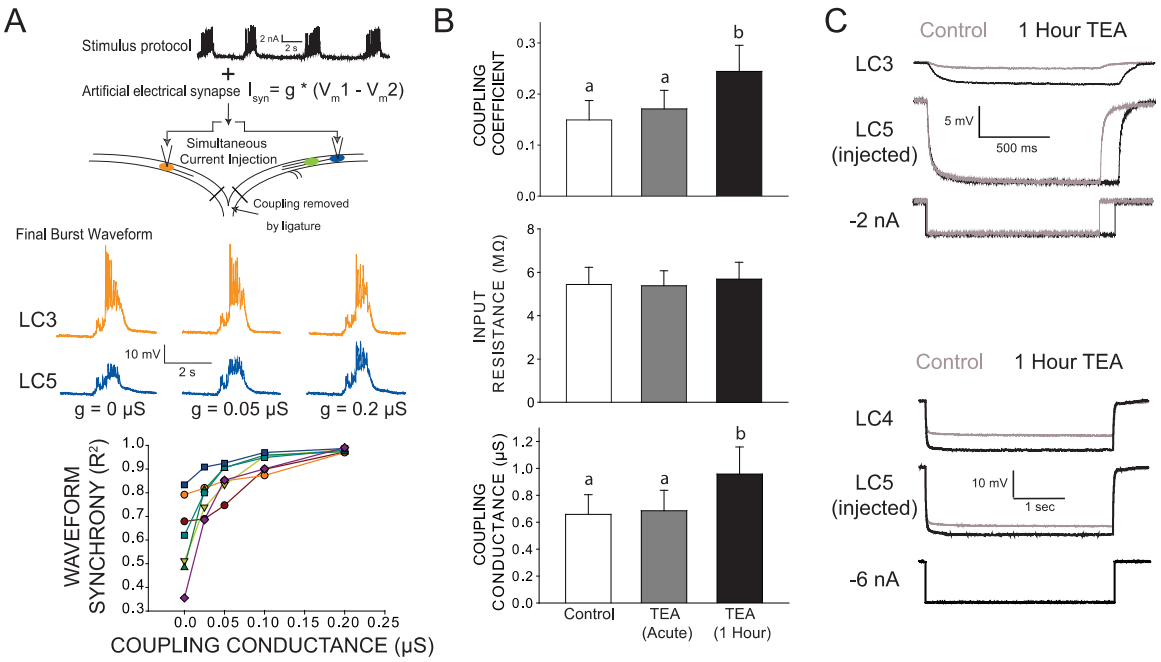

FIGURE 1.6: *Changes in electrical coupling associated with compensation in biological CG networks*. **A**. Artificial electrical coupling restores synchrony in isolated LCs. With acute exposure to TEA, isolated LCs produce disparate output in response to an identical stimulus. The stimulus protocol consists of current injections that mimic biological synaptic currents and back propagating action potentials (see Ransdell et al., 2013a) from four consecutive bursts of network activity. Current was injected simultaneously into isolated cells, while dynamic clamp was used to provide an artificial coupling conductance. Representative traces of the same two cells shown in TEA with different levels of synaptic current applied. Only the final burst of the four-burst input stimulus is shown for clarity. N = 7 different preparations (bottom panel) show an increase in synchrony with increasing coupling conductance. **B**. Biological coupling increases during network compensation. Hyperpolarizing current injections were used to measure coupling coefficients between LC3 and LC5 during control conditions, with acute TEA exposure (5 minutes) and after 1 hour compensation in TEA. Input resistance of LCs was measured

and showed no significant change at any time point. No significant differences were observed for coupling coefficient or coupling conductance between control and acute TEA conditions. Coupling coefficient significantly increased after 1 hour in TEA (Mean increase 85 ± 82% from control, N=11, $P < 0.01$, Wilcoxon signed rank test). Measurements from LC4 and LC5 show that coupling conductance increased significantly as a result of 1 hour TEA exposure (mean increase 49.5 ± 36% from control, N=13, $P < 0.001$, Wilcoxon signed rank test). Significant differences across groups are denoted with different letters. Plots show mean ± SD. **C.** Representative traces from two different preparations of changes in coupling observed before (Control) and after 1 hour of TEA exposure. Top traces are between LC3-LC5 and the bottom traces are between LC4-LC5. Measurements were made in two-electrode current clamp, and current was injected into LC5. Because current injections were manually timed to occur between bursts of network activity, slightly different durations of current pulses occurred in the two recordings in the top recordings. Recordings from LC4-LC5 were used for coupling conductance measurements seen in panel B, as their close proximity allows for much less influence of electrotonic distance on calculations of conductance.

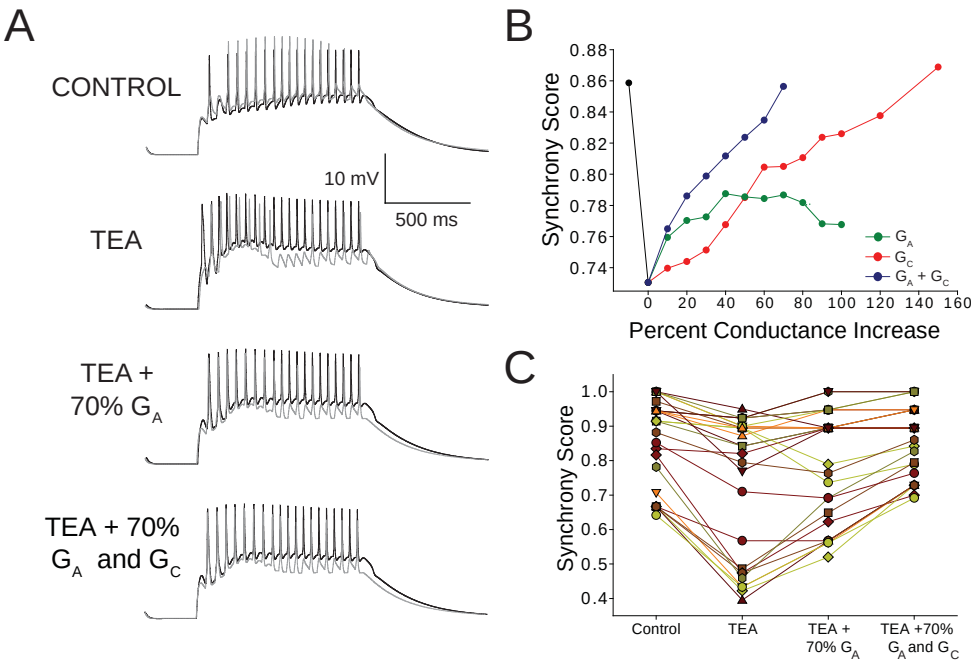

FIGURE 1.7: *Increased G_A and coupling conductance (G_C) among LCs act in concert to help restore synchrony across LCs in model networks*. **A.** Voltage response of a typical network LC3 (gray) and LC4 (black) cells under three model conditions: control, TEA (90% reduction in both G_{Kd} and G_{BKKCa}), TEA + 70% increase in G_A, and TEA + 70% increase in G_A and G_C. **B.** Effects of increasing G_A alone, G_C alone, or both G_A and G_C on synchrony in model networks. Dashed lines represent simple linear regression fits to the points for each condition. Black line represents the change in synchrony from control to TEA. Points shown are the average values for N = 27 networks. **C.** Summary of Synchrony Score shown for all 27 model networks. Stepwise changes are shown from Control, TEA, TEA + increasing G_A by 70%, and TEA + increasing both G_A and G_C by 70% (the point at which maximal synchrony is restored as per the analysis in panel B). Individual points correspond to those used to generate averages in panel A at the 70% level to give an idea of variability in the data set. Individual preparations are connected with lines to show trends across networks.

CHAPTER 2

Dopamine has a neuroprotective effect on network synchrony via direct modulation of gap junctions in the crustacean cardiac ganglion

Brian J. Lane, David K. Wilson, David J. Schulz

ABSTRACT

Motor neurons of the crustacean cardiac ganglion have variable intrinsic conductance magnitudes, yet produce virtually identical synchronized voltage activity. However, it is not known whether this variability makes cells vulnerable to desynchronization during neuromodulation. Previous work has investigated whether neuromodulation of variable networks can produce reliable responses in particular features of network output, but these studies have not examined this question as it relates to synchrony. To investigate this, we exposed the cardiac ganglion to the amine modulators serotonin and dopamine while recording from multiple motor neurons. Each amine had distinct excitatory effects, and serotonin caused desynchronized activity whereas dopamine did not. Dopamine was found to directly modify gap junctional conductance, and co-application of both modulators induced a serotonin-like response in network activity, but burst waveforms remained synchronized. Dopamine was also able to prevent desynchronization induced by the K^+ channel blocker tetraethylammonium (TEA), suggesting that dopaminergic modulation of electrical coupling potentially plays

a broadly protective role in maintaining network synchrony during perturbation.

INTRODUCTION

Neural networks must be capable of producing output that is robust and reliable, yet also flexible enough to meet changing environmental demands. One mechanism providing flexibility of network activity is neuromodulation, which reconfigures network output by altering a subset of cellular and synaptic conductances (Bargmann, 2012; Daur et al., 2016; Harris-Warrick, 2011).

However, even relatively simple networks achieve stable output by a variety of solutions; intrinsic cellular conductances and synaptic strengths can be highly variable yet still produce nearly identical physiological activity (Ball et al., 2010; Calabrese et al., 2011; Marder, 2011; Joseph L Ransdell et al., 2013a). This variability raises a fundamental question about neuromodulation that remains open, as highlighted in a recent review by Marder et al. (2014). The authors ask whether modulation of networks with variable underlying parameters can produce predictable and reliable results. In this review they demonstrate computationally that modulation of neurons with similar outputs arising from variable underlying conductances can cause anywhere from relatively small to fairly substantial differences in output (Marder et al., 2014). Therefore, the response of any neural network to modulation is likely state-dependent (Goldman et al., 2001; Gutierrez et al., 2013; Marder et al., 2014; Nadim et al., 2008; Williams et al., 2013), and potentially unpredictable as a result of these varying underlying conductances (Marder et al., 2014).

Neuromodulation faces the unique challenge of preserving critical features of network output while simultaneously modifying others. Neuromodulation generally alters a subset of conductances in cells and networks to reconfigure the output of a network, but it is not clear whether this reconfiguration should produce predictable and reliable changes in neurons and networks with variable underlying physiological properties. Other studies have addressed this broad question by examining half-center oscillator networks and choosing to focus on particular characteristics of network output such as production of sustained network oscillations, cycle period, or spike frequency in order to ask how sensitive or robust the feature of interest is to parameter changes (Dethier et al., 2015; Doloc-Mihu and Calabrese, 2016; Grashow et al., 2009). In some cases it seems that neuromodulation can expand the parameter space in which a given activity feature is maintained (Grashow et al., 2009), and this could potentially lead to neuroprotective effects of modulation that ensures robust network output (Städele et al., 2015). This study is the first to focus on the whether synchronized activity is maintained across variable neurons during neuromodulation.

The crustacean cardiac ganglion (CG) is a small central pattern generator network that produces reliable rhythmic bursts with precisely synchronized activity across the Large Cell motor neurons (LCs)(Lane et al., 2016). The CG is modulated by multiple substances, including neuropeptides and biogenic amines (Cooke, 2002; Cruz-Bermúdez and Marder, 2007). Despite virtually identical output within a given network, LCs display a great deal of variability in their intrinsic ionic conductances (J. L. Ransdell et al., 2013), which makes LCs vulnerable to desynchronization in response to a uniform perturbation with ion channel blockers (Lane et al., 2016; J. L. Ransdell et al., 2013).

Because altering a subset of cellular conductances can desynchronize network activity, the present study extends this principle to ask whether LCs are able to maintain stable synchrony during neuromodulation.

We hypothesize that due to the variability of conductances across LCs, modifying their activity with neuromodulation will desynchronize LC activity. We test this hypothesis by exposing the CG to two different amine modulators, serotonin (5HT) and dopamine (DA). We measured the effects of the modulators on excitability and synchrony individually and then in combination. We found that serotonergic modulation desynchronized LC voltage waveforms, and in most cases elicited prolonged pacemaker bursts driving two distinct bursts in LCs before the cycle was reset. In contrast, DA did not desynchronize LC activity, and did not elicit the burst doublets seen in 5HT. When co-applied, DA was able to prevent the 5HT-induced desynchronization without occluding the distinctive burst doublets caused by 5HT. Likewise, DA prevented desynchronization even during TEA application. Our results suggest that DA exerts a broadly protective effect on network synchrony by targeting electrical synaptic conductance. This may serve to maintain robust synchrony in the cardiac network while still being permissive to plasticity of output caused by other modulators.

EXPERIMENTAL PROCEDURES:

Animals:

Adult male Jonah crabs, *Cancer borealis*, were purchased and shipped overnight

from The Fresh Lobster Company (Gloucester, MA). Crabs were maintained in artificial seawater at 12°C until used. Crabs were anesthetized by keeping them on ice for 30 minutes prior to dissection. The complete cardiac ganglion was dissected from the animal and pinned out in a Sylgard-lined petri dish in chilled physiological saline (440mM NaCl, 26mM $MgCl_2$, 13mM $CaCl_2$, 11mM KCl, and 10mM HEPES, pH 7.4-7.5, 12°C). Chemicals were obtained from Fisher Scientific unless otherwise noted.

Electrophysiology:

The CG network is comprised of 9 cells: 4 Small Cell (SC) pacemaker interneurons which give simultaneous excitatory input to 5 Large Cell (LC) motor neurons. Stainless steel pin electrodes were connected to differential AC Amplifier (A-M Systems model 1700) for extracellular recording. One pin was placed inside a petroleum jelly well built around the ganglionic trunk and the other placed in the bath outside the well. The ganglionic trunk contains axons from all 9 cells, and thus serves to monitor the spiking output of the entire network. During normal activity, LCs produce consistent levels of rhythmic output and pairs of LCs show nearly identical voltage waveforms. LC spikes and pacemaker spikes are easily distinguishable by their relative amplitudes on extracellular recordings, and also by membrane potential changes observed by recording from LC somata using intracellular sharp electrodes.

LC somata are easily visible within the nerve and can be individually desheathed to allow for intracellular recordings. Intracellular sharp electrodes containing 3M KCl (8-25 M**Ω**) were used to simultaneously monitor the voltage activity in the somata of two anterior LCs. All paired intracellular recordings were from LC3 and either LC4 or LC5.

Amplifiers from Axon Instruments were used (AxoClamp 900A, MultiClamp 700B, AxoClamp 2B). Current clamp protocols were created and run using Clampex 10.3 software (Molecular Devices). Electrical coupling in the intact network was measured by hyperpolarizing current injection (1-6 nA) when LCs reached resting membrane potential between bursts. Cells were injected one at a time while measuring voltage changes in both cells. Coupling coefficients were calculated as the ratio: ($\Delta V_{\text{coupled cell}} / \Delta V_{\text{Injected Cell}}$). For both amines, the coupling coefficient at control was compared to the measured value after 15 minutes of modulation. Changes in coupling coefficient could ultimately be influenced by two fundamentally different mechanisms: altered conductance of the non-junctional membrane, or modification of gap junctional conductance. LC3 and LC5 are coupled to one another and to the rest of the network distal to the site of our recordings, making calculation of coupling conductance between these two cells problematic. A thread ligature tied around the anterior branch containing LC4 and LC5 can be used to create an electrotonically compact two-cell preparation in which coupling conductance can be calculated (Bennett, 1966)(Lane et al., 2016).

Perfusion:

Serotonin (5HT), dopamine (DA), and tetraethylammonium (TEA) were obtained from Tocris Bioscience (Bristol, UK). Whenever present, concentrations were as follows: 10^{-6} M 5HT, 10^{-5} M DA, 25mM TEA. All perfusions occurred at a rate of approximately 2 ml/min. Solutions were pre-chilled to maintain the preparation at a constant temperature of 12°C.

LC variability can be exploited by applying the K^+ channel blocker TEA exclusively to anterior LCs to desynchronize their activity (Lane et al., 2016). To test whether neuromodulation could desynchronize LC activity, we considered perfusion of neuromodulators over the entire network to provide a more biologically relevant challenge to test synchrony. There is no reason to suspect any biological conditions in which only the anterior LCs would be exposed to modulators. *In vivo*, the entire CG is exposed to both serotonin (5HT) and dopamine (DA) as hormonal modulators released from the pericardial organ or other neurohormonal sites (Cooke, 1966; Fort et al., 2004; Marder et al., 2005; Maynard and Welsh, 1959). In addition, a pair of extrinsic dopaminergic fibers innervates the CG from the thoracic ganglion and forms abundant synaptic contacts in both the anterior and posterior regions of the ganglion which provides a rapid and direct route for dopaminergic modulation (Cooke, 2002; Fort et al., 2004). Baseline activity was measured during a sham perfusion of physiological saline before the source of the perfusion was switched to saline containing neuromodulators and/or channel blockers. Simultaneous intracellular recordings monitored somatic burst potentials from multiple anterior LCs, and an extracellular well on the ganglionic trunk monitored activity of the entire network.

In some experiments, a petroleum jelly well was used to protect the posterior end of the ganglion from the perfusate in order to selectively expose only the anterior LCs to 5HT, DA, or DA+TEA. For experiments in which TEA was applied only to the anterior portion of the network, whole-network modulation was achieved by adding DA to the posterior end of the ganglion coincident with the onset of DA perfusion of the anterior

LCs.

Data Analysis:

Intracellular burst waveforms were considered to begin with the first EPSP from pacemaker activity and ended upon return to resting membrane potential. Recordings were analyzed using Clampfit 10.3 (Molecular Devices) and Spike 2.7 (CED, Cambridge, UK) software, including a custom script written by Dirk Bucher to define the initiation and termination of each burst for cross-correlation of intracellular voltage waveforms. Statistical analyses were performed using Sigmaplot 11.0. All data are expressed as median ± SD unless otherwise stated. *R*-values (and R^2) are obtained by a Pearson correlation. Changes in burst characteristics, coupling coefficients, coupling conductance, and synchrony were analyzed with paired *t*-tests when data was normally distributed, or signed rank tests in the case of non-normality.

All comparisons for measures of network output between control and modulation are after 15 minutes of modulation. Each burst characteristic quantified was averaged for 10 consecutive cycles at control and at 15 minutes. The values obtained were then averaged across all preparations for the data presented in Table 1.

RESULTS

Cardiac ganglion LC motor neurons are sensitive to both 5HT and DA

We hypothesized that variable cellular and/or synaptic properties in the CG could lead to desynchronized activity of LCs during neuromodulation. We therefore first sought to identify neuromodulators that directly affect LC activity. Both 5HT (10^{-6}M) and DA

(10^{-5}M) are excitatory when applied to the entire CG of *C. borealis* (Cruz-Bermúdez and Marder, 2007). When applied focally to the anterior LCs at these same concentrations, our results demonstrate that both amines have direct excitatory effects on LCs (Table 1). 5HT applied to the LCs increased the number of spikes per burst (5.850 ±2.72 in control; 10.85 ± 2.96 in 5HT; $p<0.01$), the spike frequency within each burst (6.24 ±3.18 Hz in control; 11.53 ± 3.39 Hz in 5HT; $p<0.01$), burst duration (0.642 ± 0.367 sec in control; 0.739 ± 0.411 sec in 5HT; $p<0.05$), LC duty cycle (0.183 ±0.059 in control; 0.232 ±0.063 in 5HT; $p<0.01$) and decreased the interburst interval (3.15±0.68 in control; 2.761 ±0.658 in 5HT; $p<0.01$). DA also affected LC output, significantly increasing the number of spikes per burst (4.45 ±3.42 in control and 10.20 ±6.41 in DA; $p<0.05$) and spike frequency within each burst (5.85 ±4.95 in control and 10.38 ±10.16 in DA; $p<0.05$).

5HT and DA have distinct excitatory effects when applied to the entire network

Our primary goal was to determine the network-level consequences of variability, and whether naturalistic perturbations such as neuromodulation should be expected to cause desynchronized activity. We therefore considered modulation of the entire network to be the most relevant test of the network's ability to maintain stable synchrony during neuromodulation. Subsequent experiments therefore exposed the entire network to 5HT and DA.

5HT increased overall network excitability (Figure 2A, Table 1). 5HT significantly increased pacemaker burst duration, and in 6 out of 8 experiments switched the network to a distinct output consisting of a single prolonged pacemaker burst driving two distinct

LC bursts (Figure 2A). Changes in network output in 5HT were quantified by statistical analysis of LC spiking from extracellular recordings (Table 1). 5HT significantly decreased interburst interval (4.15±3.07 in control; 2.04±0.46 in 5HT; $p<0.05$) and cycle period (5.149±3.086 in control; 2.607±0.563 in 5HT; $p<0.05$). 5HT increased the number of spikes per burst (6.250±1.883 in control and 9.625±2.789 in 5HT; $p<0.01$), the spike frequency within each burst (5.640±3.995 in control and 16.133±3.417 in 5HT; $p<0.01$), and LC duty cycle (0.161±0.0799 in control and 0.241±0.0530 in 5HT; $p<0.05$).

DA also increased network excitability, but in distinct ways from 5HT (Figure 2D). DA did not induce doublet bursting, but significantly increased the number of spikes per burst (8.850±3.978 in control; 11.225±5.337 in DA; $p<0.05$), spike frequency (8.854±4.878 in control; 11.268±7.434 in DA; $p<0.05$), burst duration (0.715±0.280 in control; 0.806±0.281 in DA; $p<0.05$), and LC duty cycle (0.164±0.0744 in control; 0.211±0.0411 in DA; $p<0.05$) (Table 1, N=8).

5HT Desynchronizes Burst Waveforms But DA Does Not

The degree of synchrony in burst waveforms was quantified as described previously (Lane et al., 2016, see Methods). Briefly, for each burst the digitized voltage waveform from two intracellular recordings were used to perform a cross-correlation. The coefficient of determination (R^2) was then used to quantify how accurately the voltage of one cell predicts the voltage of the other. This provides a baseline measure of synchrony for each burst and allowed us to track relative changes.

At the onset of serotonergic modulation (10^{-6}M), there was an acute reduction in synchrony as measured by R^2. Figure 2A illustrates typical acute effects of 5HT application. Differences in voltage waveforms appear between LC3 and LC5 after 5HT perfusion. R^2 values for every burst during a typical experiment are plotted in Figure 2B to visualize the changes in synchrony during these experiments. Synchrony reliably reached a minimum within several minutes (mean = 9.1 minutes) before stabilizing and showing a slow but modest recovery of synchrony. For statistical analysis in Figure 2C, R^2 values from 10 consecutive bursts were averaged at 3 time points: Control (5 minutes prior to modulation), acute 5HT modulation (sampled at the point of maximum desynchronization), and again after 30 minutes of exposure to 5HT (N=8 preparations). Synchrony significantly decreased in 5HT (R^2 = 0.967±0.012 control, 0.893±0.081 5HT; $p<0.01$, Signed rank test). There was a significant increase in synchrony between acute co-modulation and 30 minutes of continuous 5HT perfusion (0.927±0.066) ($p<0.01$, Signed rank test), but the cause of this increase is not clear. However, synchrony was still significantly below baseline after 30 minutes ($p<0.05$, Signed rank test).

During 5HT-induced doublets, the first and second of the two bursts typically displayed distinct waveform synchrony values. This can be seen from about 10-30 minutes for the experiment shown in Figure 2B, in which R^2 values alternated between the upper and lower bands. The R^2 values for both the 1st and 2nd burst were below control ($p<0.01$, signed rank test), but which of the two bursts had lower R^2 values varied across preparations.

In DA, burst waveforms remain completely synchronized (Figure 2D). The scatterplot in Figure 2E shows R^2 for each burst during a full 30 minutes of DA

perfusion. There were no noticeable changes in synchrony during any DA perfusion experiment (Figure 2E; 2F): there were no significant changes in R^2 from control (0.964±0.026), acute DA modulation (0.966±0.025), and 30 minutes of DA modulation (0.966±0.024). The acute data point was sampled at 9.1 minutes to match the mean time point used for sampling in 5HT.

DA, but not 5HT, modulates coupling conductance

We hypothesized that modulation of electrical coupling may be responsible for the different effects of 5HT and DA on LC synchrony. One possibility is that modulation with 5HT decreases the strength of electrical coupling, resulting in desynchronization. Alternatively, DA may increase coupling strength to ensure synchrony.

As an indicator of the strength of electrical coupling, we measured the coupling coefficient (see Methods) between LC3 and LC5 at control and after 15 minutes of modulation. Coupling coefficients were not significantly different between control (0.043± 0.035) and 15 minutes modulation in 5HT (0.037 ± 0.042) (Figure 3A; N=8). In contrast, DA increased coupling coefficient by 41% (0.035±0.030 in control; 0.049±0.043 in DA) ($p<0.01$, N=6; Figure 3A). Input resistance was not significantly changed in either 5HT (3.62±4.40 MΩ in control; 3.78± 4.11 MΩ in 5HT) or DA (3.85±2.34 MΩ in control; 3.33±1.77 MΩ in DA) (Figure 3A).

The coupling coefficient is a useful description of the functional relationship in coupling, but does not identify the electrophysiological mechanism. The somata of LC4 and LC5 exhibit strong local electrical coupling, and the branch containing only these two somata can be separated from the network by thread ligature to create ideal

conditions for calculating coupling conductance (Figure 3B). With two electrodes in each cell, we used hyperpolarizing current injections to calculate the junctional resistance independently of membrane resistance (see Methods). 5HT had no direct effect on coupling conductance, while DA significantly increased coupling conductance in both directions (Figure 3C; 3D).

Co-application of DA and 5HT Prevents Desynchronization and Induces Doublet Bursting

Our previous study demonstrated that increased electrical coupling among LCs was able to rescue loss of synchrony after treatment with the channel blocker TEA. The relatively rapid and large increase in electrical coupling upon exposure to DA led us to hypothesize that co-modulation with DA may be capable of *preventing* desynchronization caused by other modulators. Our next experiments tested the ability of DA to maintain network synchrony during co-modulation with 5HT. We followed the same perfusion and recording protocol, this time including both DA (10^{-5} M) and 5HT (10^{-6} M) into the test saline.

Individual preparations treated with DA+5HT sometimes showed a small increase or transient decrease in synchrony, which occurred over the same time scale as preparations exposed to 5HT alone. However, across the full set of N=8 preparations there was no significant change in synchrony when DA and 5HT were co-applied. Interestingly, 5 out of 8 preparations transitioned to the doublet bursting mode seen in 5HT alone. However, this time the double-bursting pattern displayed highly synchronized waveforms. Representative traces in Figure 4A show an example of a 5HT-

like double-burst without loss of waveform synchrony in DA+5HT. The scatterplot in Figure 4B shows R^2 for all bursts across a full experiment, in this case revealing a slight increase in synchrony from baseline after the onset of co-modulation and no clear segregation of the R^2 values for the 1st and 2nd burst in each doublet (in contrast with Figure 2B). Overall, there was no significant difference between in synchrony of control ($R^2 = 0.971 \pm 0.01$) and acute co-modulated preparations ($R^2 = 0.969 \pm 0.01$; Figure 4C). However there was a significant increase between acute and 30 minutes ($R^2 = 0.983 \pm 0.006$; $p<0.01$), suggesting a longer-term enhancement of coupling throughout the experiment.

Overall, DA+5HT co-modulation was strongly excitatory. Table 1 shows how various characteristics of LC output were affected by co-modulation, including significant changes in the number of spikes per burst (2.600±4.034 in control and 11.53 ±3.58 in DA+5HT; $p<0.01$), spike frequency (4.840±3.818 in control and 10.345±3.144 in DA+5HT; $p=0.05$), burst duration (0.403±0.361 in control and 1.074±0.447 in DA+5HT; $p<0.05$), interburst interval (3.829±3.321 in control and 2.779±1.816 in DA+5HT; $p<0.05$), and LC duty cycle (0.0953±0.0425 in control and 0.275±0.0831 in DA+5HT; $p<0.01$).

DA Prevents Desynchronizing Effect of TEA

We hypothesize that DA may play a protective role in preventing desynchronization against a variety of perturbations by modulating electrical coupling strength. Our previous studies showed that exposing the anterior LCs to the K^+ channel blocker TEA produces a powerful deleterious effect on LC synchrony and a large

increase in the number of spikes per burst and spike frequency (Lane et al., 2016). For reference, Figure 6A includes representative traces of TEA-induced desynchronization.

If DA can act in a protective fashion to maintain synchrony, then DA should prevent desynchronization in TEA. To test this, a barrier of petroleum jelly was built to protect the posterior (pacemaking) end of the ganglion from the perfusate while leaving anterior LCs exposed. The entire network was pre-incubated with DA for 5 minutes, and then the perfusion switched to saline containing both DA and TEA. The preparations pre-incubated in DA for 5 minutes did not show any loss of synchrony as a result of TEA. Sample traces (Figure 6A) include 4 time points to show R^2 at control (0.950±0.0149), 5 min DA (0.958±0.010), acute exposure to DA+TEA (0.953±0.011), and 30 minutes exposure to DA+TEA (0.968±0.008). Excitability increased after 5 minutes with the addition of DA, similar to those found after 15 minutes of DA in previous experiments (Table 1). After the addition of TEA at 5 minutes, there was a further increase in the number of spikes per burst (7.89±5.34 in DA and 16.39±7.65 in DA+TEA; $p<0.01$), spike frequency (8.25±7.95 in DA and 15.19±8.06 in DA+TEA;$p<0.01$), and cycle period (3.34±0.77 in DA and 3.97±1.06 in DA+TEA;$p<0.01$).

DISCUSSION

Modulation and LC synchrony

While these experiments do not fully address the broad fundamental question raised by Marder et al (2014), they do help to address whether variable cells within a

network are able to maintain synchrony during modulation. We found that serotonergic neuromodulation can lead to differential output across LCs, suggesting that the network needs mechanisms to safeguard against desynchronization caused by neuromodulation. Additionally, they also indicate that dopaminergic modulation is capable of playing that role by modulating gap junctional conductance without occluding the effects of other modulators.

Our experiments examined the effects of network-level modulation on LC synchrony in order to produce biologically relevant modulatory conditions. Our initial prediction of desynchronization was based on the variability of intrinsic conductances in LCs, and the results of our focal application of modulators to anterior LCs suggests that intrinsic conductances are modulated by 5HT and DA. Blocking I_{HTK} or I_A can lead to differential output across isolated LCs (J. L. Ransdell et al., 2013), and if these currents are targeted by 5HT it may help to explain its effects on synchrony. Additionally, DA increases LC excitability and is likely to have additional unidentified targets aside from coupling conductance. However, it remains possible that modulation of pacemaker inputs influences LC synchrony. The variability of intrinsic conductances across LCs has been firmly established in previous work (Joseph L Ransdell et al., 2013a, 2013b; Ransdell et al., 2012), but less is known about variability in chemical synaptic strength between pacemaker cells and LCs. It is known from other systems that synaptic strength between identified neurons varies two- to five-fold across animals for networks underlying the same motor pattern (Goaillard et al., 2009; Roffman et al., 2012). A more nuanced understanding of pacemaker activity and synaptic input to LCs could provide

more insights into the robust maintenance of network synchrony during neuromodulation and other perturbations of network activity. The precise intrinsic or synaptic conductance(s) affected by 5HT remain to be identified, along with a mechanistic description of how that change leads to desynchronized voltage waveforms. Further exploration of the cellular and network-level parameters modified by 5HT and DA in the CG could therefore help to reveal principles important for the robust maintenance of network synchrony during neuromodulation.

Protective Effects of Modulation

Regardless of how 5HT modulation leads to desynchronization, it is notable that coapplication of DA is able to not only prevent this loss of synchrony, but do so without occluding the doublet-bursting caused by 5HT. This mode of activity can be seen in extracellular recordings of the *C. borealis* CG exposed to 5HT in previous work (Cruz-Bermúdez and Marder, 2007), and also resembles the effects of proctolin described in the *Homarus* CG (Miller and Sullivan, 1981; Sullivan and Miller, 1984). We interpret that DA is capable of playing a protective role in maintaining LC synchrony while still being permissive to flexibility of network output provided by other modulators. TEA can also desynchronize LCs when applied to the anterior end of the network, but here we found that a 5 minute pre-incubation with DA was sufficient to prevent desynchronization under these conditions. This further supports a broadly protective role for DA in maintaining network synchrony against a variety of potential perturbations. Recent studies in the stomatogastric ganglion have demonstrated a role for extrinsic neuromodulation in counterbalancing the destabilizing effects of temperature change (Städele et al., 2015).

Our findings suggest that DA may play a similar role in stabilizing CG output in response to perturbation. Only three pairs of axons provide extrinsic innervation of the CG. One of these pairs is dopaminergic, while the others are cholinergic and GABAergic. The dopaminergic fibers make abundant synaptic contacts on anterior LCs and their neuropil in the vicinity of the sites of electrical coupling as well as the posterior end near the pacemaker cells (Fort et al., 2004). In addition to hormonal exposure to DA, this provides a potential means for direct delivery of these modulators to the CG through fibers that are rapidly responsive to physiologically relevant stimuli (Fort et al., 2004; Guirguis and Wilkens, 1995; Jury and Watson, 2000; Maynard, 1953).

Modulation of Electrical Coupling

DA has also been found to directly modulate gap junctional conductance and network activity in horizontal cells (He et al., 2000; Piccolino, 1984) AII amacrine cells (Kothmann et al., 2009), and rod cells (Jin et al., 2015) of the retina. DA modulation of coupling conductance is involved in sensorimotor function during copulation in *C. elegans* (Correa et al., 2015), and is one of several substances capable of modulating the electrical component of the mixed electrical-chemical synapses of auditory afferents onto the fish Mauthner cell (Cachope and Pereda, 2015; Cachope et al., 2007; Pereda et al., 1992). While electrical coupling is known to support synchronized activity in many systems, to our knowledge this is the first study that directly implicates the modulation of gap junctional conductance in countering desynchronizing perturbations.

Studies in the stomatogastric ganglion have shown that while neuromodulation can alter network output, it can also exert effects that help to stabilize and maintain critical aspects

of network output (Harris-Warrick and Johnson, 2010; Marder, 2012; Städele et al., 2015). It has also been used for detailed studies of amine modulation of electrical coupling (R. Flamm and Harris-Warrick, 1986a; R. E. Flamm and Harris-Warrick, 1986; Johnson and Harris-Warrick, 1990; Johnson et al., 1994, 2005; B. R. Johnson et al., 1993).

These modulators have both been extensively studied in the crustacean stomatogastric ganglion. 5HT and dopamine each have unique constellations of effects on cell types and synapses that are ultimately able to functionally reorganize the pyloric rhythm in distinct ways (R. Flamm and Harris-Warrick, 1986a, 1986b; Johnson et al., 1995; Spitzer et al., 2008). Modulation of the stomatogastric ganglion with either 5HT or DA can alter input resistance and coupling coefficients and have distinct effects on coupling coefficients between particular pairs of stomatogastric neurons, and some of these changes may be due to direct modulation of gap junctions, although precise calculations of coupling conductance are more problematic in the stomatogastric ganglion than in our reduced 2-cell preparation (B. Johnson et al., 1993). However, it is generally recognized that direct modulation of gap junctions could help to provide flexibility and robustness in the pyloric motor pattern (Gutierrez and Marder, 2013; Kepler et al., 1990; Marder et al., 2016). Similarly, our results implicate that dopaminergic modulation potentially provides flexibility and robustness to the CG by directly modulating gap junctional conductance to buffer against desynchronization of voltage activity in LCs.

REFERENCES

Ball, J.M., Franklin, C.C., Tobin, A.-E., Schulz, D.J., Nair, S.S., 2010. Coregulation of ion channel conductances preserves output in a computational model of a crustacean cardiac motor neuron. J. Neurosci. 30, 8637–49. doi:10.1523/JNEUROSCI.6435-09.2010

Bargmann, C.I., 2012. Beyond the connectome: How neuromodulators shape neural circuits. BioEssays 34, 458–465. doi:10.1002/bies.201100185

Bennett, M. V, 1966. Physiology of electrotonic junctions. Ann. N. Y. Acad. Sci. 137, 509–39.

Cachope, R., Mackie, K., Triller, A., O'Brien, J., Pereda, A.E., 2007. Potentiation of electrical and chemical synaptic transmission mediated by endocannabinoids. Neuron 56, 1034–47. doi:10.1016/j.neuron.2007.11.014

Cachope, R., Pereda, A.E., 2015. Opioids potentiate electrical transmission at mixed synapses on the Mauthner cell. J. Neurophysiol. 114, 689–697. doi:10.1016/j.brainres.2012.05.059

Calabrese, R.L., Norris, B.J., Wenning, A., Wright, T.M., 2011. Coping with variability in small neuronal networks. Integr. Comp. Biol. 51, 845–55. doi:10.1093/icb/icr074

Cooke, I.M., 2002. Reliable, responsive pacemaking and pattern generation with minimal cell numbers: the crustacean cardiac ganglion. Biol. Bull. 202, 108–36.

Correa, P. a., Gruninger, T., Garcia, L.R., 2015. DOP-2 D2-Like Receptor Regulates UNC-7 Innexins to Attenuate Recurrent Sensory Motor Neurons during C. elegans Copulation. J. Neurosci. 35, 9990–10004. doi:10.1523/JNEUROSCI.0940-15.2015

Cruz-Bermúdez, N.D., Marder, E., 2007. Multiple modulators act on the cardiac ganglion of the crab, Cancer borealis. J. Exp. Biol. 210, 2873–84. doi:10.1242/jeb.002949

Daur, N., Nadim, F., Bucher, D., 2016. The complexity of small circuits: the stomatogastric nervous system. Curr. Opin. Neurobiol. 41, 1–7. doi:10.1016/j.conb.2016.07.005

Dethier, J., Drion, G., Franci, A., Sepulchre, R., 2015. A Positive Feedback at the Cellular Level Promotes Robustness and Modulation at the Circuit Level. J. Neurophysiol. jn.00471.2015.

doi:10.1152/jn.00471.2015

Doloc-Mihu, A., Calabrese, R.L., 2016. Analysis of Family Structures Reveals Robustness or Sensitivity of Bursting Activity to Parameter Variations in a Half-Center Oscillator (HCO) Model. eNeuro 3, 1–22. doi:10.1523/ENEURO.0015-16.2016

Flamm, R., Harris-Warrick, R., 1986a. Aminergic modulation in lobster stomatogastric ganglion. II. Target Neurons of Dopamine, Octopamine, and Serotonin Within the Pyloric Circuit. J. Neurophysiol.

Flamm, R., Harris-Warrick, R., 1986b. Aminergic modulation in lobster stomatogastric ganglion. I. Effects on motor pattern and activity of neurons within the pyloric circuit. J. Neurophysiol.

Flamm, R.E., Harris-Warrick, R.M., 1986. Aminergic modulation in lobster stomatogastric ganglion. I. Effects on motor pattern and activity of neurons within the pyloric circuit. J. Neurophysiol. 55, 847–65.

Fort, T.J., Brezina, V., Miller, M.W., 2004. Modulation of an integrated central pattern generator-effector system: dopaminergic regulation of cardiac activity in the blue crab Callinectes sapidus. J. Neurophysiol. 92, 3455–70. doi:10.1152/jn.00550.2004

Goaillard, J., Taylor, A., Schulz, D., Marder, E., 2009. Functional consequences of animal-to-animal variation in circuit parameters. Nat. Neurosci. 12, 1424–1430. doi:10.1038/nn.2404.Functional

Goldman, M.S., Golowasch, J., Marder, E., Abbott, L.F., 2001. Global structure, robustness, and modulation of neuronal models. J. Neurosci. 21, 5229–38. doi:21/14/5229 [pii]

Grashow, R., Brookings, T., Marder, E., 2009. Reliable neuromodulation from circuits with variable underlying structure. Proc. Natl. Acad. Sci. U. S. A. 106, 11742–6. doi:10.1073/pnas.0905614106

Guirguis, M.S., Wilkens, J.L., 1995. The Role of the Cardioregulatory Nerves in Mediating Heart Rate Responses to Locomotion, Reduced Stroke Volume, and Neurohormones in Homarus

americanus. Biol. Bull. 188, 179. doi:10.2307/1542083

Gutierrez, G.J., Marder, E., 2013. Rectifying Electrical Synapses Can Affect the Influence of Synaptic Modulation on Output Pattern Robustness. J. Neurosci. 33, 13238–13248. doi:10.1523/JNEUROSCI.0937-13.2013

Gutierrez, G.J., O'Leary, T., Marder, E., 2013. Multiple Mechanisms Switch an Electrically Coupled, Synaptically Inhibited Neuron between Competing Rhythmic Oscillators. Neuron 77, 845–858. doi:10.1016/j.neuron.2013.01.016

Harris-Warrick, R.M., 2011. Neuromodulation and flexibility in Central Pattern Generator networks. Curr. Opin. Neurobiol. 21, 685–92. doi:10.1016/j.conb.2011.05.011

Harris-Warrick, R.M., Johnson, B.R., 2010. Checks and balances in neuromodulation. Front. Behav. Neurosci. 4, 1–9. doi:10.3389/fnbeh.2010.00047

He, S., Weiler, R., Vaney, D.I., 2000. Endogenous dopaminergic regulation of horizontal cell coupling in the mammalian retina. J. Comp. Neurol. 418, 33–40. doi:10.1002/(SICI)1096-9861(20000228)418:1<33::AID-CNE3>3.0.CO;2-J

Jin, N.G., Chuang, A.Z., Masson, P.J., Ribelayga, C.P., 2015. Rod electrical coupling is controlled by a circadian clock and dopamine in mouse retina. J. Physiol. 593, 1597–1631. doi:10.1113/jphysiol.2014.284919

Johnson, B., Harris-Warrick, R., 1990. Aminergic Modulation of Graded Synaptic Transmission in the Lobster Stomatogastric Ganglion. J. Neurosci.

Johnson, B., Peck, J., Harris-Warrick, R., 1994. Differential modulation of chemical and electrical components of mixed synapses in the lobster stomatogastric ganglion. J. Comp. ….

Johnson, B., Peck, J., Harris-Warrick, R., 1993. Amine modulation of electrical coupling in the pyloric network of the lobster stomatogastric ganglion. J. Comp. ….

Johnson, B.R., Peck, J.H., Harris-Warrick, R.M., 1995. Distributed amine modulation of graded chemical transmission in the pyloric network of the lobster stomatogastric ganglion. J.

Neurophysiol. 74, 437–52.

Johnson, B.R., Peck, J.H., Harris-Warrick, R.M., 1993. Amine modulation of electrical coupling in the pyloric network of the lobster stomatogastric ganglion. J. Comp. Physiol. A. 172, 715–32. doi:10.1007/BF00195397

Johnson, B.R., Schneider, L.R., Nadim, F., Harris-Warrick, R.M., 2005. Dopamine modulation of phasing of activity in a rhythmic motor network: contribution of synaptic and intrinsic modulatory actions. J. Neurophysiol. 94, 3101–3111. doi:10.1152/jn.00440.2005

Jury, S.H., Watson, W.H., 2000. Thermosensitivity of the lobster, Homarus americanus, as determined by cardiac assay. Biol. Bull. 199, 257–64.

Kepler, T.B., Marder, E., Abbott, L.F., 1990. The effect of electrical coupling on the frequency of model neuronal oscillators. Science 248, 83–5.

Kothmann, W.W., Massey, S.C., O'Brien, J., 2009. Dopamine-stimulated dephosphorylation of connexin 36 mediates AII amacrine cell uncoupling. J. Neurosci. 29, 14903–11. doi:10.1523/JNEUROSCI.3436-09.2009

Lane, B.J., Samarth, P., Ransdell, J.L., Nair, S.S., Schulz, D.J., 2016. Synergistic plasticity of intrinsic conductance and electrical coupling restores synchrony in an intact motor network. Elife 5. doi:10.7554/eLife.16879

Marder, E., 2012. Neuromodulation of neuronal circuits: back to the future. Neuron 76, 1–11. doi:10.1016/j.neuron.2012.09.010

Marder, E., 2011. Variability, compensation, and modulation in neurons and circuits. Proc. Natl. Acad. Sci. U. S. A. 108 Suppl , 15542–8. doi:10.1073/pnas.1010674108

Marder, E., Gutierrez, G.J., Nusbaum, M.P., 2016. Complicating connectomes Electrical coupling creates parallel pathways and degenerate circuit mechanisms. Dev. Neurobiol. doi:10.1002/dneu.

Marder, E., O'Leary, T., Shruti, S., 2014. Neuromodulation of circuits with variable parameters: single neurons and small circuits reveal principles of state-dependent and robust

neuromodulation. Annu. Rev. Neurosci. 37, 329–46. doi:10.1146/annurev-neuro-071013-013958

Maynard, D., 1953. Activity in a Crustacean Ganglion. I. Cardio-Inhibition and Acceleration in Panulirus Argus. Biol. Bull.

Miller, M.W., Sullivan, R.E., 1981. Some effects of proctolin on the cardiac ganglion of the Maine Lobster, Homarus americanus (Milne Edwards). J. Neurobiol. 12, 629–39. doi:10.1002/neu.480120611

Nadim, F., Brezina, V., Destexhe, A., Linster, C., 2008. State dependence of network output: modeling and experiments. J. Neurosci. 28, 11806–13. doi:10.1523/JNEUROSCI.3796-08.2008

Pereda, A., Triller, A., Korn, H., Faber, D.S., 1992. Dopamine enhances both electrotonic coupling and chemical excitatory postsynaptic potentials at mixed synapses. Proc. Natl. Acad. Sci. U. S. A. 89, 12088–92.

Piccolino, M., 1984. DECREASE OF GAP JUNCTION PERMEABILITY INDUCED AND CYCLIC ADENOSINE 3’:5'-MONOPHOSPHATE IN HORIZONTAL CELLS OF TURTLE RETINA. J. ….

Ransdell, J.L., Nair, S.S., Schulz, D.J., 2013a. Neurons within the Same Network Independently Achieve Conserved Output by Differentially Balancing Variable Conductance Magnitudes. J. Neurosci. 33, 9950–9956. doi:10.1523/JNEUROSCI.1095-13.2013

Ransdell, J.L., Nair, S.S., Schulz, D.J., 2013. Neurons within the Same Network Independently Achieve Conserved Output by Differentially Balancing Variable Conductance Magnitudes. J. Neurosci. 33, 9950–9956. doi:10.1523/JNEUROSCI.1095-13.2013

Ransdell, J.L., Nair, S.S., Schulz, D.J., 2012. Rapid homeostatic plasticity of intrinsic excitability in a central pattern generator network stabilizes functional neural network output. J. Neurosci. 32, 9649–58. doi:10.1523/JNEUROSCI.1945-12.2012

Ransdell, J.L., Temporal, S., West, N.L., Leyrer, M.L., Schulz, D.J., 2013b. Characterization of

inward currents and channels underlying burst activity in motor neurons of the crab cardiac ganglion. J. Neurophysiol. doi:10.1152/jn.00009.2013

Roffman, R.C., Norris, B.J., Calabrese, R.L., 2012. Animal-to-animal variability of connection strength in the leech heartbeat central pattern generator. J. Neurophysiol. 107, 1681–93. doi:10.1152/jn.00903.2011

Spitzer, N., Cymbalyuk, G., Zhang, H., Edwards, D.H., Baro, D.J., 2008. Serotonin transduction cascades mediate variable changes in pyloric network cycle frequency in response to the same modulatory challenge. J. … 99, 2844–63. doi:10.1152/jn.00986.2007

Städele, C., Heigele, S., Stein, W., 2015. Neuromodulation to the Rescue: Compensation of Temperature-Induced Breakdown of Rhythmic Motor Patterns via Extrinsic Neuromodulatory Input. PLOS Biol. 13, e1002265. doi:10.1371/journal.pbio.1002265

Sullivan, R.E., Miller, M.W., 1984. Dual effects of proctolin on the rhythmic burst activity of the cardiac ganglion. J. Neurobiol. 15, 173–196.

Williams, A.H., Calkins, A., O'Leary, T., Symonds, R., Marder, E., Dickinson, P.S., 2013. The neuromuscular transform of the lobster cardiac system explains the opposing effects of a neuromodulator on muscle output. J. Neurosci. 33, 16565–75. doi:10.1523/JNEUROSCI.2903-13.2013

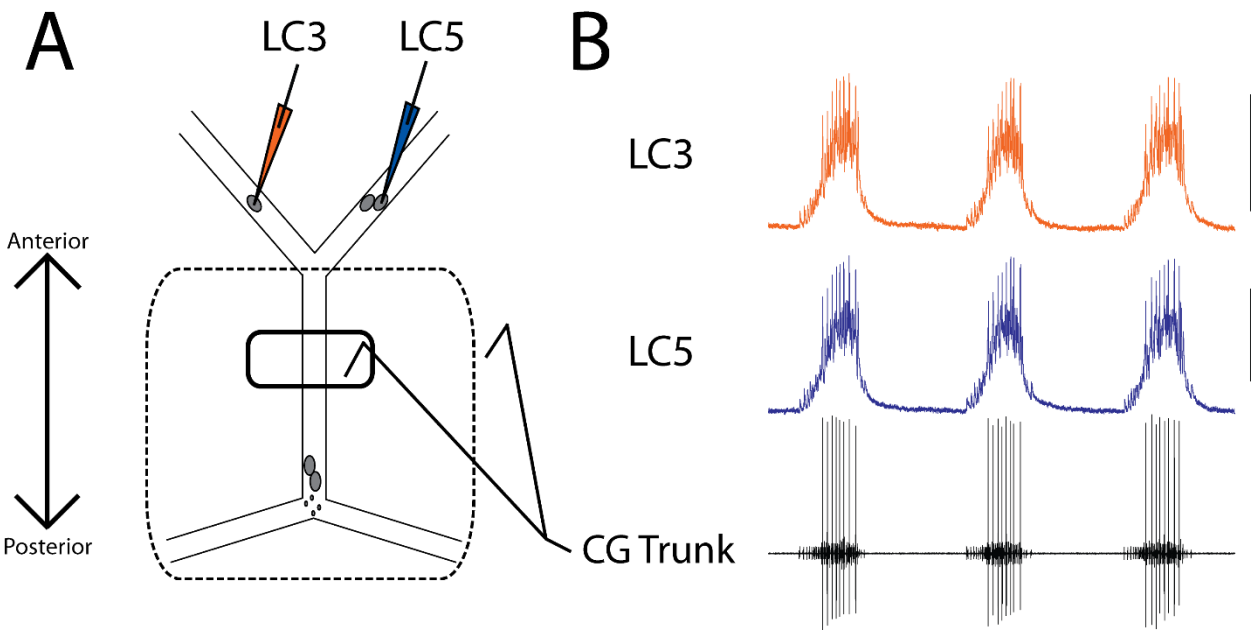

FIGURE 2.1: *Experimental setup and typical activity in the CG.* A) Intracellular electrodes recorded simultaneously from LC3 and either LC4 or LC5. Extracellular recordings were taken from a petroleum jelly well on the CG trunk (solid line). For experiments which applied modulators or TEA exclusively to anterior LCs, the extracellular recording was taken from a single large well allowing anterior LCs to be exposed to the perfusate while protecting the remainder of the ganglion (dashed line). B) Representative control activity showing the rhythmic synchronized bursting of LCs. (Scale bars = 10mV, recording length = 14 sec)

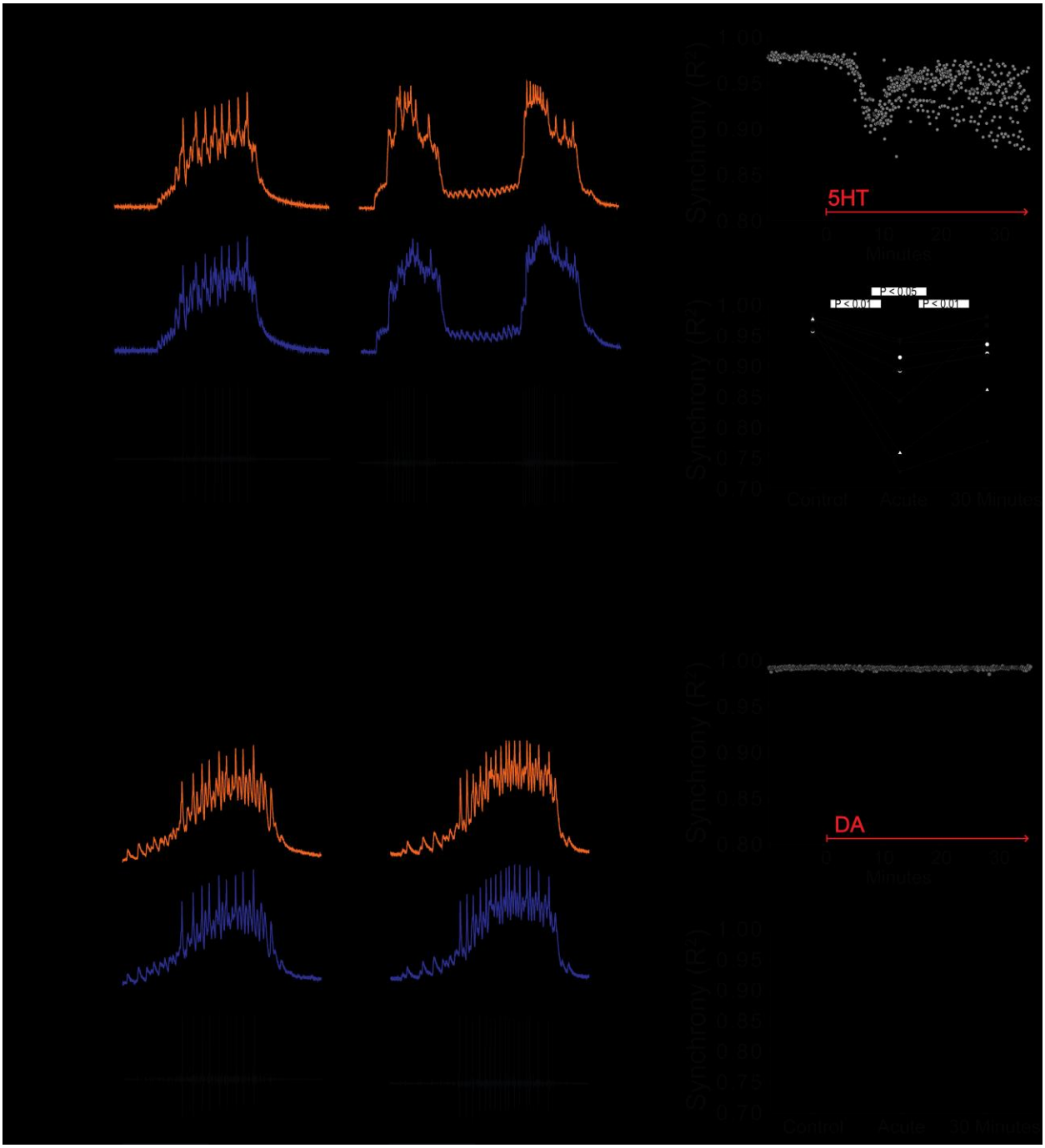

FIGURE 2.2: *Effects of 5HT and DA on synchrony of LC voltage waveforms* A) Representative traces show that LCs with virtually identical control activity produce different burst waveforms after application of 5HT. Bursts in 5HT occurred in doublets in most preparations (6 of 8).

Scale bars = 10 mV and 1 second. B) Waveform synchrony (R^2) was calculated for every burst across a full experiment. Scatterplot shows consistent synchronized bursting across 10 minutes of control activity followed by 30 minutes of continuous perfusion of 5HT. An acute loss of synchrony accompanies the onset of modulation. Doublet bursting results in two distinct bands of R^2 values during 30 minutes of 5HT perfusion. C) R^2 was averaged for 10 consecutive bursts at each of 3 time points: control (5 minutes prior to perfusion), Acute (at the point R^2 reached a minimum), and after 30 minutes of modulation. A significant decrease occurred from control to acute (Signed Rank test, $p<0.01$), and a significant increase between acute and 30 minutes (Signed Rank test, $p<0.05$). Synchrony was not restored to control levels after 30 minutes (paired t-test, $p< 0.05$). N=8 preparations. D) Representative traces show that excitability and network output are affected by DA, but LCs remain synchronized. Scale bars = 10 mV and 1 second. E) R^2 was calculated for every burst across a full experiment. Scatterplot shows this for 10 minutes of control activity followed by 30 minutes in DA. R^2 values are largely unaffected by changes in activity caused by DA. F) R^2 was averaged for 10 consecutive bursts at each of 3 time points: control (5 minutes prior to perfusion), Acute (sampled from the same time-point as 5HT), and after 30 minutes of modulation. There were no significant differences between any two groups (paired t-tests). N=6 preparations.

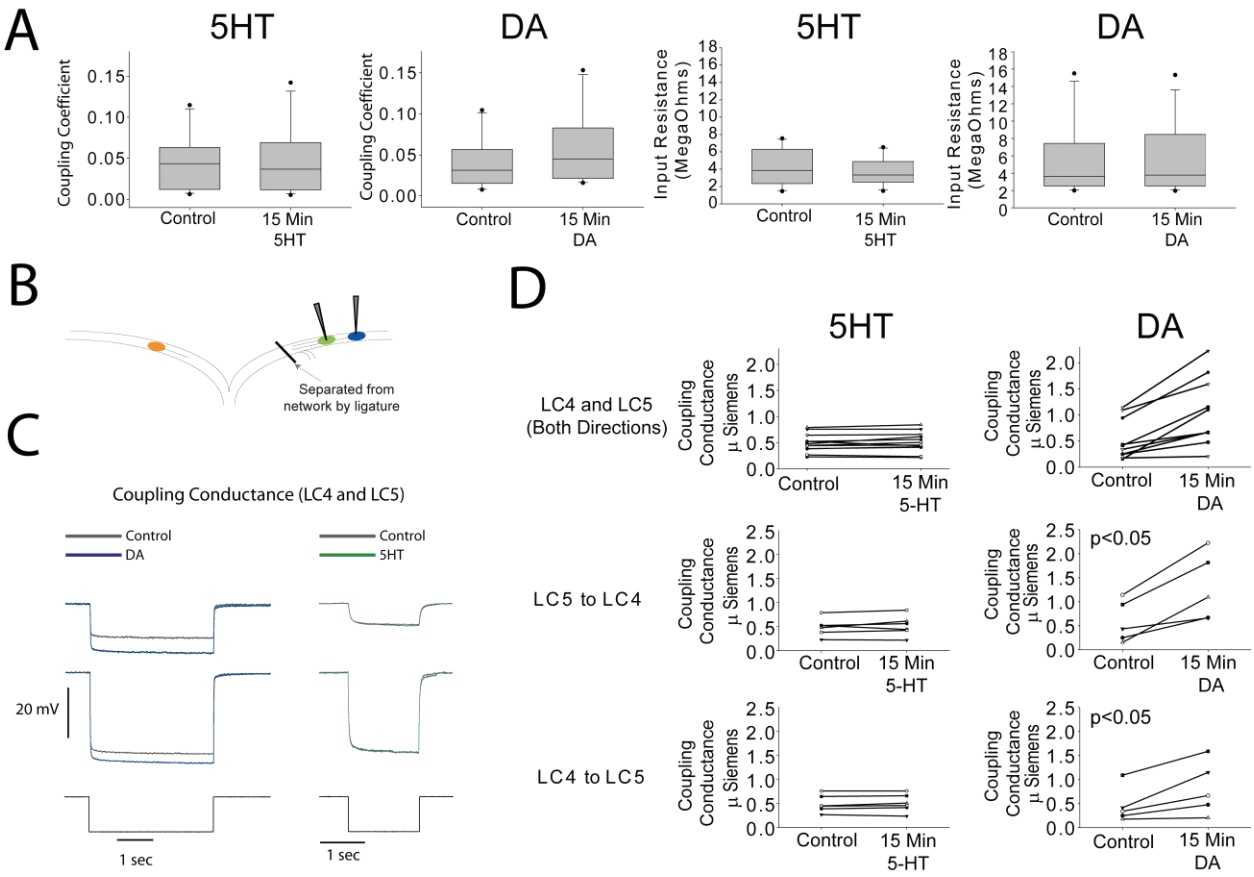

FIGURE 2.3: *Effects of 5HT and DA on Electrical Coupling*. A) Coupling coefficients for LC3-LC4 or LC3-LC5 in the active network were not significantly changed by 5HT. Mean coupling coefficient increased by 41% in DA ($p<0.01$). B) Diagram of reduced preparation used to test the effect of 5HT and DA on coupling conductance. LC4 and LC5 somata were physically isolated by thread ligature. C) Coupling conductance between LC4 and LC5 was unchanged by 5HT, and increased by DA. Top row in C shows coupling conductance in both directions for N=6 preparations before and after modulation. These data are then separated by directionality. Coupling Conductance was significantly increased in DA in both directions ($p<0.05$ for each, mean increase 149%, N=5). D) Representative traces of current injections used to calculate coupling conductance before and after DA exposure (left) and 5HT exposure (right). Traces in

grey show voltage responses of LC4 (top) and LC5 (middle) to a -8 nA hyperpolarizing current injection (bottom). Overlaid traces show the voltage response to the same current injection after DA (left, blue) and 5HT (right, green).

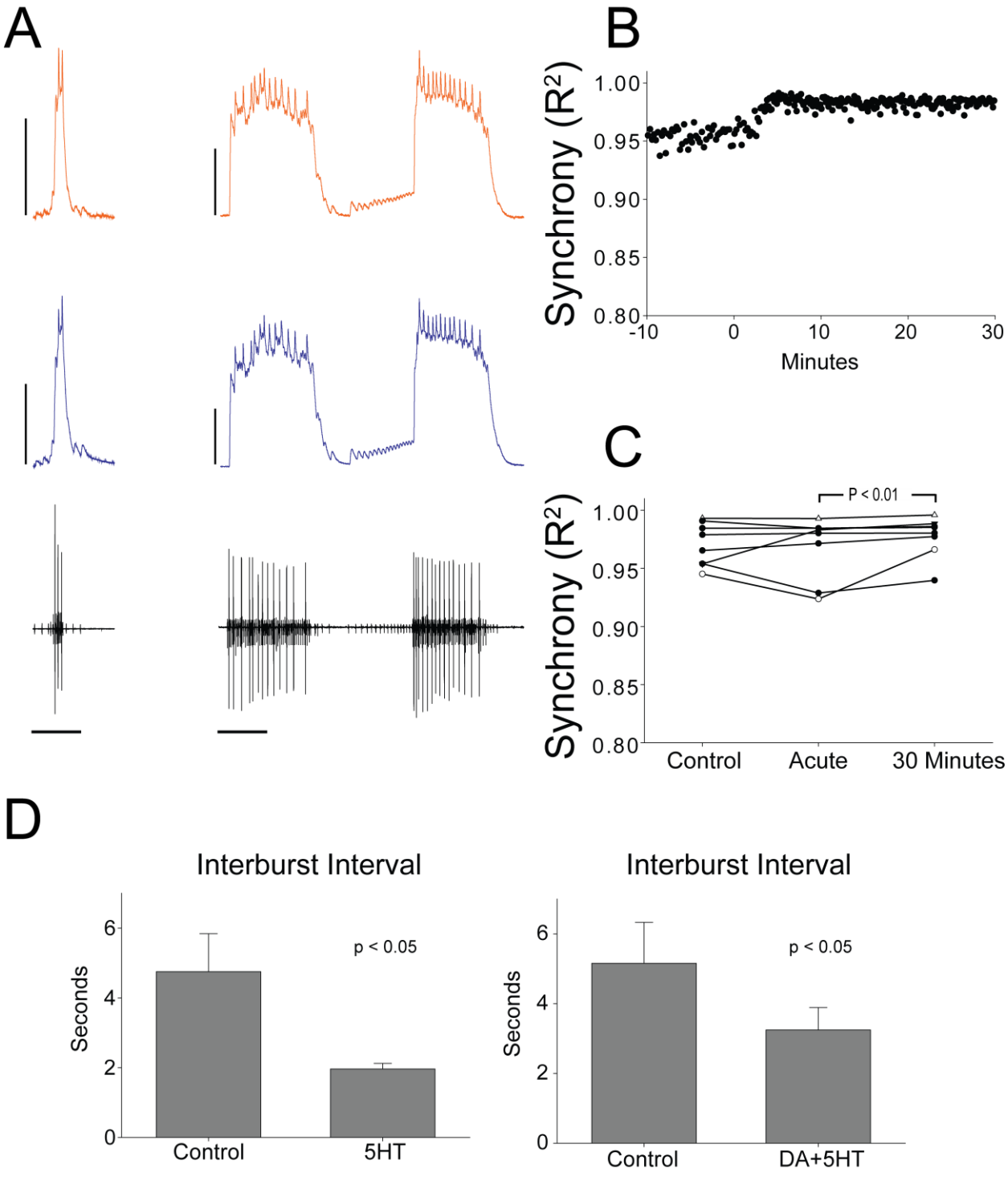

Figure 2.4: *During simultaneous co-application of 5HT and DA, network output resembles effects of 5HT, but burst waveforms remain synchronized*. A) Representative traces show LCs maintain synchronized voltage waveforms during co-application of DA and 5HT. 5 out

of 8 preparations transitioned to bursting in doublets, and network output shows increased number of spikes per burst, spike frequency in each burst, burst duration and LC duty cycle. Scale bars = 10 mV and 1 second. B) R^2 was calculated for every burst across a full experiment. Scatterplot shows this for 10 minutes of control activity followed by 30 minutes of perfusion with both modulators. C) R^2 was averaged for 10 consecutive bursts at each of 3 time points: control (5 minutes prior to perfusion), Acute, and after 30 minutes of modulation. There was no significant difference between control and acute conditions, but a significant increase from acute to 30 minutes (paired t-test, $p<0.01$). N=8. D) Interburst Interval decreases sharply in 5HT alone, and in 5HT+DA ($p<0.05$ for each).

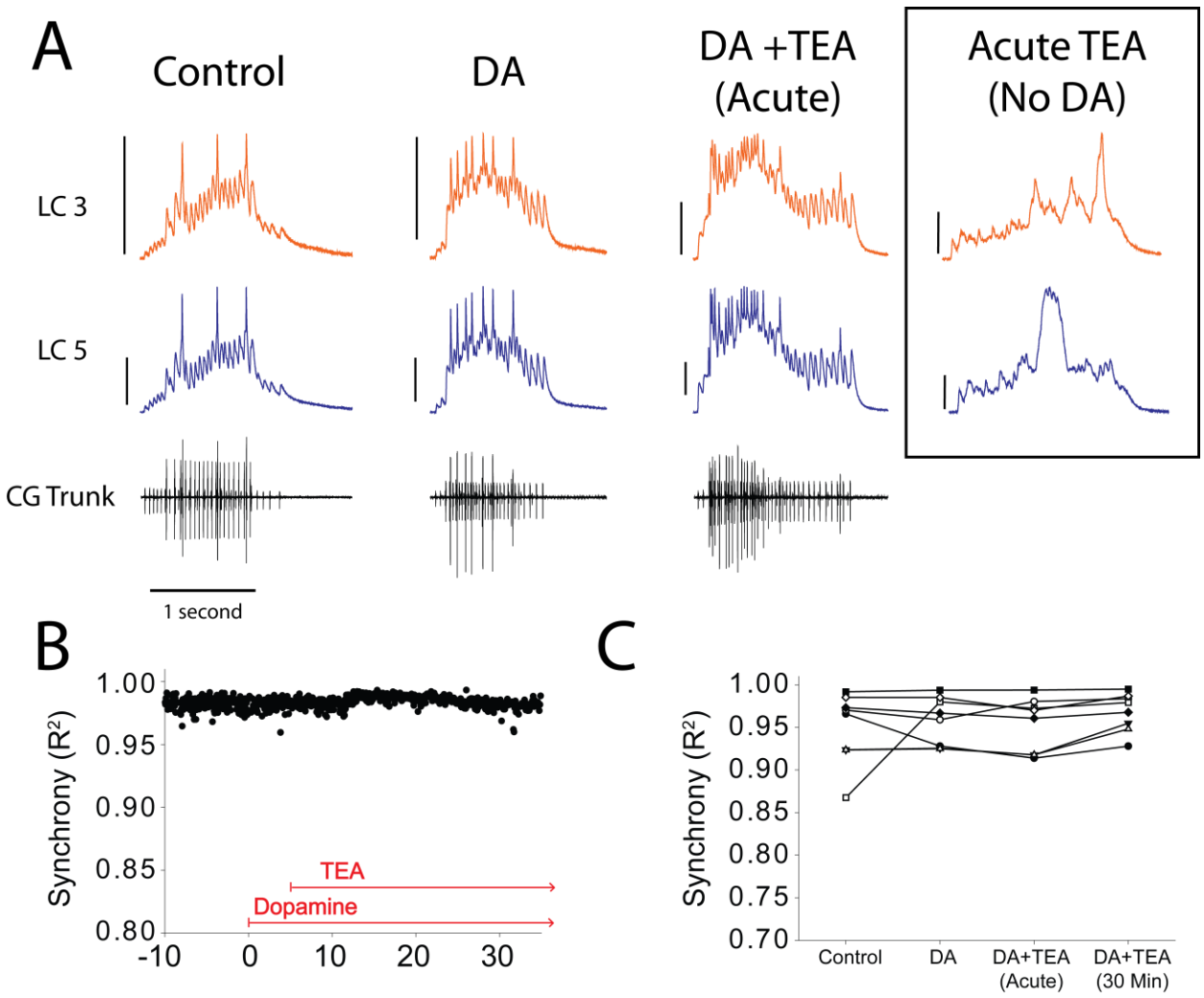

FIGURE 2.5: *DA prevents desynchronization with TEA.* A) TEA normally desynchronizes voltage waveforms, but application of DA prevents desynchronization. LCs maintain synchronized voltage waveforms throughout these experiments despite undergoing substantial changes in voltage activity. Application of DA significantly increased burst duration, the number of spikes per burst, and the LC duty cycle. Addition of TEA further increased excitability. N=8 preparations. Representative traces are shown at control, acute DA, DA and Acute TEA. Traces in the box at the far right illustrate acute desynchronization in TEA in the absence of DA (separate experiment). Scale bars = 10 mV and 1 second. B) R^2 was calculated for every burst across a full experiment. Scatterplot shows throughout 10

minutes of control activity followed by 5 minutes of DA exposure, followed by 30 minutes in DA and TEA. C) R^2 was averaged for 10 consecutive bursts at each of 4 time points: control (5 minutes prior to perfusion), after 5 minutes in DA, at the mean time point for desynchronization in TEA observed previously, and after 30 minutes exposure to the DA/TEA saline. No significant differences were detected across groups. N=8 preparations.

	# LC Spikes per Burst	LC Spike Frequency (Hz)	Burst Duration	Interburst Interval	Cycle Period	LC Duty Cycle
CONTROL	5.850 ±2.722	6.239 ±3.184	0.642 ± 0.367	3.177 ±0.683	3.768 ±0.960	0.183 ±0.0587
5HT (Anterior)	10.850 ± 2.961 (P = <0.001)	11.533 ± 3.391 (P = 0.001)	0.739 ± 0.411 (P = 0.016)	2.702 ±0.658 (P = <0.001)	3.441 ±0.983 (P = 0.091)	0.232 ±0.0633 (P = 0.002)
CONTROL	4.450 ± 3.415	5.849 ± 4.945	0.614 ± 0.295	4.555 ± 4.131	5.119 ± 4.547	0.0974 ± 0.0455
DA (Anterior)	10.200 ± 6.414 (P = 0.022)	10.382 ±10.159 (P = 0.036)	0.756 ± 0.138 (P = 0.321)	4.117 ±3.955 (P = 0.084)	4.894 ± 4.198 (P = 0.187)	0.157 ± 0.0551 (P = 0.062)
CONTROL	6.250±1.883	5.640±3.995	0.749±0.580	4.149±3.069	5.149±3.086	0.161±0.0799
5HT (Whole Network)	9.625±2.789 (P = 0.008)	16.133±3.417 (P = <0.001)	0.610±0.161 (P = 0.179)	2.035±0.456 (P = 0.042)	2.607± 0.563 (P = 0.034)	0.241±0.0530 (P = 0.050)
CONTROL	8.850±3.978	8.854±4.878	0.715±0.280	3.882±2.009	4.654±2.022	0.164±0.0744
DA (Whole Network)	11.225±5.337 (p=.014)	11.268±7.434 (p=0.048)	0.806±0.281 (P = 0.016)	2.952±0.729 (P = 0.078)	3.638±0.951 (P = 0.148)	0.211±0.0411 (P = 0.039)
CONTROL	2.600±4.034	4.840±3.818	0.403±0.361	3.829±3.321	4.141±3.614	0.0953±0.0425
DA+5HT	11.525 ±3.578 (P = <0.001)	10.345±3.144 (P = 0.050)	1.074±0.447 (P = 0.020)	2.779±1.816 (P = 0.037)	3.997±2.014 (P = 0.195)	0.275±0.0831 (P = 0.003)
CONTROL	3.367±2.353	5.792±3.128	0.549±0.176	3.036±2.137	3.312±2.259	0.119±0.0311
DA (5 Min)	7.890±5.344 (P = 0.008).	8.248±7.954 (P = 0.055)	0.895±0.250 (P = 0.036)	2.560±0.609 (P = 0.156)	3.344±0.768 (P = 0.742)	0.247±0.0465 (P = <0.001)
DA+TEA (Acute)	16.387±7.653 (P = 0.008)	15.193±8.062 (P = 0.008)	0.860±0.574 (P = 0.378)	2.937±0.883 (P = 0.051)	3.968±1.055 (P = 0.004)	0.231±0.101 (P = 0.871)

Table 2.1: *Effects of each manipulation on LC bursting output*

Statistics for each are shown as median ± SD. For all modulator applications, effects that are significantly different from control are marked with grey boxes. For DA+TEA, p-values listed are a comparison with DA. All 6 measurements in DA+TEA are significantly different from control ($p<0.01$).

CHAPTER 3

Animal-to-Animal Variability in the Activity of the Isolated Cardiac Ganglion of *C. borealis*

ABSTRACT

Central pattern generator networks underlying a particular behavior can vary substantially across animals in their synaptic and intrinsic conductances, yet still generate stable network output across the lifetime of the animal. How much variability can exist across animals and which cellular and network-level parameters are regulated in order to achieve stable network output? Studies of the same network across a large number of animals have only been performed using a few invertebrate central pattern generator networks. These studies have yielded interesting insights, but it remains unclear what principles can be generalized across neural networks, which may only apply under certain conditions, or which may simply be an idiosyncratic feature of the network chosen for experimentation. Analyzing variability of additional networks from different species can help to clarify these uncertainties. To this end, we have analyzed the temporal patterns of 3 distinct classes of bursts in the crab cardiac ganglion using networks from 131 animals over the course of 5 years. We find that in the CG, output features such as burst duration, duty cycle, and relative phasing have a great deal more variability than described for other CPGs. We also find differences in network activity between winter and summer that correlate with temperature-independent seasonal changes in crustacean cardiovascular output. We discuss the functional implications, and how future studies

could use these findings to develop a more detailed understanding of network variability and homeostatic processes.

INTRODUCTION

CPG networks continuously produce robust and reliable rhythmic output throughout the lifetime of an animal and tend to be responsible for basic motor functions essential for survival. The study of invertebrate CPGs has been invaluable in advancing our understanding of neural and network output because of their relatively small number of cells which can be unambiguously identified across animals. A surprising conclusion from investigations in the crustacean stomatogastric ganglion (STG) and leech heartbeat CPG is that networks are able to accomplish highly conserved output from neurons and networks with variable underlying properties; intrinsic and synaptic conductances can vary 2- to 5-fold in magnitude across animals while still producing conserved output (Calabrese et al., 2011; Marder and Goaillard, 2006; Marder, 2011). Further, mRNA levels of a given ion channel can also vary as much as 2- to 9-fold across animals (Schulz et al., 2007, 2006; Tobin et al., 2009).

Despite this variability, network output must be homeostatically regulated in order to continuously produce activity that meets the needs of the animal. However, it is not clear exactly how these cellular and network-level parameters are regulated to achieve stable output. Examining a large number of networks may provide clues as to which properties are regulated by discovering network properties that co-vary (Bucher et al., 2005; Goaillard et al., 2009). Alternatively, such examination may identify certain features where greater variability is tolerated (Bucher et al., 2005; Goaillard et al., 2009).

Analysis of CPG activity across a large number of animals has been used successfully in several invertebrate networks to reveal general principles of network

activity, especially the crustacean STG and leech heartbeat CPG (Bucher et al., 2005; Goaillard et al., 2009; Lamb and Calabrese, 2013; Norris et al., 2011; Roffman et al., 2012). Examining multiple distinct networks with this approach may help to reveal additional important principles that transfer across networks, or help to clarify which findings may be idiosyncratic to a particular network. Phase relationships of pyloric neurons of the stomatogastric ganglion (STG) are maintained as a fairly constant function of frequency (Goaillard et al., 2009; Greenberg and Manor, 2005; Hooper, 1997; Manor et al., 2003), including during the animal's growth (Bucher et al., 2005; Mouser et al., 2008) and during acute temperature change both *in vitro* and *in vivo* (Soofi et al., 2014; Tang et al., 2010). How conserved must burst durations and phasing be in rhythmic networks? Is strict phase maintenance is a general principle of network function that applies to all rhythmic networks? A recent study using the cardiac ganglion of the lobster *H. americanus* found that the OFF phase of pacemaker interneurons could be significantly more variable than those reported in the STG (Williams et al., 2013). In the lobster, this network has several basic features that are different from what is observed in crabs. Both the pacemaker interneurons and the LC motor neurons begin firing at approximately the same time, and therefore the "ON" phase for each neuron is fairly constrained (Williams et al., 2013). This is not the case in *C. borealis*, where pacemaker cells and LCs do not begin firing at the same time. Unlike LCs in *H. americanus* (Williams et al., 2013), the LCs of *C. borealis* are not endogenous oscillators, but rather are silent in the absence of pacemaker activity and require ongoing pacemaker drive to sustain bursting (Lane et al., 2016). Additionally, our recordings of *C. borealis* indicate the presence of multiple types of pacemaker spikes. These distinctions indicate that phase

relationships in *C. borealis* are unlike those in *H. americanus*. As with the lobster CG, we hypothesize that in *C. borealis*, pacemaker burst durations do not need to be scaled with cycle period in all rhythmic motor networks. Further, we hypothesize that this variability can apply to both types of pacemaker spikes as well as the ON phase of the different bursts.

To investigate this, we characterize burst activity in the *C. borealis* cardiac ganglion across 131 animals. The cardiac ganglion (CG) is a 9-cell central pattern generator network (CPG) responsible for the rhythmic contraction of the heart of the crab *C. borealis* (Cooke, 2002; Welsh and Maynard, 1951). While each individual CG is remarkably consistent in its activity from cycle-to-cycle, many basic characteristics in the steady-state output of the CG vary considerably across animals. A great deal is known about the variability of intrinsic properties of LCs (Lane et al., 2016; Ransdell et al., 2013a, 2013b, 2012), but far less has been characterized regarding the variability of pacemaker activity across animals (Williams et al., 2013). LCs display complex burst waveforms that ultimately arise from the dynamic interactions between excitatory inputs from SCs and the intrinsic properties of LCs. To understand how LCs produce the output of the CG network, it is necessary to recognize the complex role of pacemaker cells, and the variability of network activity observed across animals. To study this population-level variability, we have analyzed pacemaker and LC bursting of the CG across 131 animals recorded over a period of approximately 5 years. Extracellular recordings show two overlapping but distinct amplitudes of pacemaker spikes that have distinct postsynaptic effects in *C. borealis*. We conduct the first thorough characterization of the

bursting for these two distinct classes of pacemaker spikes across a large number of animals together with LC bursting. These data are analyzed in order to reveal trends in activity features that are strongly correlated over a broad range in order to make inferences about the homeostatic regulation of CG output. We found that relative phasing of pacemaker and motor neuron activity is not strictly maintained in relation to cycle period in the cardiac ganglion, and that LCs across animals receive different temporal patterns of excitatory drive from physiologically distinct pacemaker cells. We found that both classes of pacemaker have variable ON and OFF phasing and that each correlates with motor neuron output. We also find seasonal differences in the steady-state activity of the CG that could explain *in vivo* observations of cardiovascular activity (Jury and Watson, 2000), and also indicating that temperature-independent seasonal changes are likely to be a source of variance in our data.

METHODS:

Animals:

Adult male crabs were shipped from The Fresh Lobster Company (Gloucester, MA) and maintained in artificial seawater tanks at 12°C for 1 day to several weeks before use. Animals were anaesthetized on ice for 30 minutes prior to dissection. Animals were then dissected, and the heart removed from the animal and placed in physiological saline. Hearts were pinned down, and the ventral wall of the heart removed to expose the CG. The CG was then isolated and pinned in a Sylgard-lined Petri dish prior to experimentation. Saline solution during dissection and physiological recordings were kept at approximately 12°C throughout the year.

Electrophysiology:

After dissection, a petroleum jelly well was constructed on the ganglionic trunk, and preparations were placed on electrophysiology rigs for recording. The temperature of the stage was adjusted to maintain saline at 12°C. Preparations were monitored for normal activity and allowed at least 30 minutes to equilibrate before proceeding with recordings. Extracellular recordings were taken from the trunk using stainless steel pin electrodes and a differential AC amplifier (A-M Systems, Carlsborg, WA). All data were acquired using pClamp 9 or pClamp 10 software (Molecular Devices). Two-electrode voltage clamp for EPSCs was performed using an AxoClamp 2B amplifier or an AxoClamp 900A amplifier (Molecular Devices). *C. borealis* physiological saline consisted of

440mM NaCl, 26mM $MgCl_2$, 13mM $CaCl_2$, 11mM KCl, and 10mM HEPES, pH adjusted to 7.4-7.5.

Data Analysis:

Extracellular recordings used for each analysis lasted 2-5 minutes. All extracellular activity was analyzed using Spike 2 version 7. Action potentials were identified by relative amplitudes and grouped into bursts for analysis. Each characteristic measured is an average from the entire recording. R-values are obtained by a Pearson correlation.

Exclusion criteria:

Preparations that produced bursts that were not rhythmic or consistent in their level of output were not included. Preparations were also not used if they displayed abnormal activity or which appeared damaged. Preparations were excluded when LC activity produced tonic spikes that were not correlated with pacemaker drive, and were likely damaged during dissection. Finally, preparations which did not fire at least 2 LC spikes during each pacemaker burst were not included.

RESULTS

Range of variability and correlations in burst characteristics

The bursting from any individual CG is remarkably internally consistent in its burst-to-burst activity. However, across animals there is a great deal of variability in the length of each of 3 burst types, the interburst interval, and the cycle period (marked on extracellular traces in Figure 1A for reference). There are 4 small pacemaker cells in the network, and all pacemaker cells make synaptic contact with all LCs within the ganglionic trunk and do not propagate beyond the trunk (Fort et al., 2004; Hartline, 1967; Hawkins and Howse, 1978; Mirolli et al., 1987). Pacemaker firing in the CG has largely been treated as a homogenous burst of action potentials, with no distinctions made among different types of input to LCs. Figure 1A illustrates that there are clearly two distinct amplitudes of pacemaker spikes visible in extracellular recordings. However, the cell(s) responsible for each distinct type have not been identified. In discussing the bursting characteristics of each, we will maintain a convention of referring to the "small amplitude pacemaker" (SP) and "medium amplitude pacemaker" (MP) bursts. The largest amplitude spikes correspond to the Large Cell motor neurons (LCs), and this designation therefore does imply the cellular origins and represents the synchronized output of the network directly responsible for muscle contraction (Cooke, 2002). In this network, the phasing of the three burst types are nested: The small amplitude pacemaker burst (SP) precedes the other two and outlasts them. The MP spikes are contained within the SP burst, and LC spikes are contained within the MP burst. These relationships are illustrated in the phase plot in Figure 1B. A full cycle ranges from 0 to 1, and the start of

each cycle is defined by the first SP spike in a burst, and ends with the first spike of the next SP burst. The "ON" and "OFF" phase for each burst type is the fraction of the cycle at which that burst begins and ends, expressed as mean ± SD. The SP OFF phase was 0.365±0.097, the MP ON phase was 0.0961± 0.066, the MP OFF phase was 0.322 ± 0.088, the LC ON phase was 0.131 ± 0.073, and LC OFF phase was 0.297±0.088.

To characterize the animal-to-animal variability in the *C. borealis* CG, we first examined the range and distribution of basic descriptive features for each of the three burst types, beginning with the burst duration and duty cycle (burst duration / cycle period). We first examined the distribution of these two characteristics individually, shown in the histograms in Figure 2. Small amplitude pacemaker (SP) burst duration (2.055±1.642) medium amplitude pacemaker (MP) burst duration (1.168±0.627) and Large Cell motor neurons (LC) burst duration (0.887±0.589) were distributed across a wide range, and were not normally distributed (Figure 2). We interpret that there may be a lower boundary below which reliable bursting does not occur, but no clear upper boundary on this range, with a small number of preparations displaying prolonged bursts. SP duty cycle (0.371±0.111), MP duty cycle (0.224±0.067), and LC duty cycle (0.165±0.0615) fit a normal distribution that is approximately symmetrical.

We examined the relationships between the burst duration for each distinct burst type in a pairwise fashion (Figure 3). Data from all preparations are shown in the left column (Figure3A). The strongest correlation was between the MP burst duration and LC burst duration (R=0.9443). The SC burst duration was correlated with MP burst

duration (R= 0.6960) and LC burst duration (R=0.6943), but to a lesser extent. However, a small number of preparations with very long burst durations appeared to be obscuring relationships between SP burst and the other two. These 5 preparations with the longest SC burst and cycle period were removed to examine relationships among the remaining data (Figure 3B). After removing these, the correlation between MC duty cycle and LC duty cycle was not greatly affected by the removal of outlying data, and remained the most strongly correlated pair (R=0.9207). However, linear regression now revealed much stronger correlations between SP and MP bursts (R=0.8675), and also between SP and LC bursts (R=0.8025). The 5 preparations removed were also found to obscure relationships among the remaining 126 preparations in subsequent analyses as well (Figure 5A, 5C).

We next examined burst duty cycles in the same manner. Pairwise correlations among burst types for all preparations is shown at left, and again at right after removal of the same 5 preparations (Figure 4). The R-values between MP and LC duty cycles was highest (R= 0.8192 at left, R= 0.7974 at right). SP duty cycle and MP duty cycle were weakly correlated, but showed a substantially higher correlation after removal of the outlying preparations (0.5254 at left, R= 0.6854 at right). The relationship between SP and LC duty cycle were also weakly correlated (R= 0.4325 at left, R= 0.5229 at right).

Phase Relationships in the CG

Work with other central pattern generators, particularly the crustacean STG has found that while the burst durations of each cell type are variable, their relative phasing remains fairly constant. To test whether this was the case in the cardiac ganglion, the cycle period was plotted against the "ON" and "OFF" phase for each burst type (Figure 5A). Due to the overlap in the data sets, this was split into two plots in Figure 5A for visualization, and each fit by linear regression. R-values were as follows: R= 0.4348 for MP ON phase, R= 0.2107 for MP OFF phase, R= 0.3496 for LC ON phase, R= 0.2786 for LC OFF phase, and R= 0.1079 for SP OFF phase. Again, the same 5 preparations removed earlier (seen to the right of the dashed line with cycle periods >11 seconds) appeared to disrupt the trends shown in the rest of the data. These preparations were removed from the dataset for subsequent analyses, as they tended to obscure trends among the majority of our dataset. Data were re-plotted with the remaining 126 preparations (Figure 5B) and fit by linear regression. R-values after removing the outliers were as follows: R= 0.1829 for MP ON phase, R= 0.0941 for MP OFF phase, R= 0.0333 for LC ON phase, R= 0.0111 for LC OFF phase, and R= 0.1376 for SP OFF phase.

Across a nearly 6-fold range of cycle periods, the slopes of these regression lines remained relatively flat, ranging from -0.01 to 0.001. The revealed that the *relative* phase does not vary greatly as a function of cycle period. One way that relative phase could be maintained across this range is if the latency from the beginning of the cycle scales linearly with cycle period. To determine whether this was the case, we plotted the latency to each phase against the cycle period, and fit each by linear regression. R-values

were as follows: R= 0.5654 for MP ON phase, R= 0.7046 for MP OFF phase, R= 0.7022 for LC ON phase, R= 0.6892 for LC OFF phase, and R= 0.6892 for SP OFF phase. This indicated that phasing does roughly scale with cycle period, but not with the strict phase maintenance observed in other CPG networks.

Given the strong relationship between burst durations for MP and LC, we considered the possibility that MP bursts should be considered the "true" pacemaker for the network. For this alternative hypothesis, the latency is now normalized to the beginning of the MP burst. We again plotted each phase as a function of cycle period (Figure 5C). R-values were as follows: R= 0.2223 for MP OFF phase, R= 0.2774 for LC ON phase, R= 0.1680 for LC OFF phase. After removing outliers, R-values were as follows: R= 0.2137 for LC ON phase, R= 0.1560 for LC OFF phase, and R= 0.3066 for MP OFF phase (Figure 5D). We plotted the phase latency versus cycle period as before. R-values were 0.1075 for the LC ON phase, 0.6208 for the LC OFF phase, and 0.6223 for the MP OFF phase. The MP burst was therefore less predictive of phasing than the initial process normalizing to SP spikes (Figure 5D).

We had primarily focused on burst durations until this point, but the full cycle period is a combination of the burst duration and the interburst interval (the silent period between the end of one burst and the beginning of the next). The lack of predictive power of the cycle period could be explained if the burst duration and interburst interval do not have a linear relationship. Additionally, the stronger relationship between burst durations as compared to duty cycles suggests this as well. We therefore hypothesized

that these two components of the cycle period do not co-vary. The burst duration was plotted versus the interburst interval (Figure 6). This revealed that SP burst duration (R=0.4205), MP burst duration (R=0.3147), and LC burst duration (R=0.3431) are only weakly related to the length of the interburst interval (Figure 6). These results indicate that the two components of the cycle period do not co-vary, and that the parameters regulating the duration of each heart contraction are likely regulated independently from those that regulate the contraction frequency.

Correlated features of LC spiking

Next, we focused on the LC firing, which alone represent the output of the network (Figure 7). Longer burst durations are correlated with a greater number of spikes per burst (R=0.6874) and a greater duty cycle (R=0.7002). The number of spikes per burst was also related to the spike frequency within each burst (R=0.5625)(Figure 7). Other characteristics were less strongly correlated: duty cycle and the number of spikes (R=0.4993), duty cycle and spike frequency (R=0.977) burst duration and spike frequency (R=0.1435) (Figure7).

Seasonal variation

The cardiovascular activity of lobsters displays temperature-independent seasonal adjustments in heart rate (Jury and Watson, 2000). This could be explained by seasonal changes in the activity of the CG. The animals used in this study were wild-caught animals, and arrived fresh throughout the year. We separated our data by the date of each recording, and separated those in winter months (December through February) from those

collected in summer months (June through August). The cycle frequency of cardiac ganglia in the winter was significantly slower in the winter months than in summer months (Figure 8, *t-test*, $p<0.01$). The small cell burst duration was also much longer in winter months (*t-test*, $p<0.01$). Although the bursts occurred less frequently in winter, the number of LC spikes within each burst was significantly higher (*t-test*, $p<0.05$). Not all aspects of network output appear to change across seasons. For instance, the spike frequency within each burst was the same across these groups (Figure 8). Seasonal effects may therefore explain some of the variance in our data.

Firing properties of two distinct classes of pacemaker inputs

Figure 8 illustrates several examples of the range of variability described in the analyses above. These recordings all consistently show two distinct amplitudes of action potentials from pacemaker cells. Sample traces showing bursts from several networks and the corresponding burst waveforms recorded intracellularly from LCs. The identities of the cells involved and the functional significance of their different temporal patterns of firing are still unclear (Cooke, 2002). To begin investigating this, we hypothesized that these cells might vary in their synaptic strength. Figure 1B shows distinct amplitudes of EPSCs from the small and medium spikes in two preparations. Using two-electrode voltage clamp, cells were held at -80mV (left) and -90mV (right) to record EPSCs while also preventing action potentials in the other LCs. SP spikes appear to correlated with smaller EPSCs, while MP spikes appear to correlate in larger amplitude EPSCs. These excitatory potentials appear imposed over a slow wave of electrotonic feed-forward excitation from the electrical coupling between pacemaker cells and LCs (García-

Crescioni and Miller, 2011). This is in agreement with general differences seen in EPSPs, but at this stage the investigation of the differences between these spikes, their cellular origins, and their synaptic effects are preliminary. Further studies manipulating these cells and examining their activity will be necessary for a full understanding of variability in CG activity across animals.

DISCUSSION

Range of variability and correlations in burst characteristics

Our results indicate that the MP bursts are most strongly correlated with LC bursts. We therefore considered the possibility that MP bursts should be considered the "true" pacemaker for the network. However, this is problematic for several reasons: MP bursts are not more predictive of the phasing of motor neurons, MP bursting does not seem to occur without SP spiking activity (which may indicate they are dependent on SP spiking). Finally, SP bursting also correlates with LC bursts, and we interpret that the difference in correlation is more likely attributable to a difference in synaptic strength to LCs rather than pacemaking activity. A number of features of LC bursting output appear correlated and ranged from R=0.0977 to R=0.7002. The strongest relationship is between burst duration and duty cycle. In this case, we determined that a great deal of variability exists due to variation in interburst interval (discussed below). We interpret that the strengths of these correlations do not necessarily indicate a strict co-regulation of these features. However, we must acknowledge that the activity observed *in vitro* is measured after the removal of other regulated physiological parameters that influence CG activity

such as sensory feedback, modulation, and hemolymph oxygenation (Cooke, 1988; Dickinson, 2006; García-Crescioni et al., 2010; Taketeru, 2003; Wilkens, 1993; Wilkens and McMahon, 1992). It is unknown how the removal of these factors may influence the output of the isolated CG.

Phasing and Cycle Period

In the *H. americanus* CG, computational analysis suggests that the duration of LC bursting after the LC burst has terminated may have effects on cycle period and response to perturbation (Williams et al., 2013). The measurements here indicate a similar variability in the OFF phasing for both types of pacemaker burst, but the predictions about how this affects response to perturbation have not yet been biologically tested. The relationship between LC bursts and cycle period has been examined in other contexts for multiple decapod species to demonstrate and describe how voltage activity in LCs feeds back to and alters pacemaker activity in individual animals (Benson, 1980; Berlind, 1989; Mayeri, 1973). These studies did not examine co-variation of these properties across a large number of animals, and it is difficult to infer from the data presented (Benson, 1980; Berlind, 1989; Mayeri, 1973). The most thorough examinations of phasing and cycle period across animals have been performed in the STG, and thus provide the most data for direct comparison across networks (Bucher et al., 2005; Goaillard et al., 2009; Hooper, 1997; Tang et al., 2010). An analysis of the pyloric rhythm across 99 animals plotted phase latency and phase against cycle period similar to those shown in Figure 5B (Bucher et al., 2005). Latency showed a linear correlation, increasing with cycle period.

The R^2 value was used to explain the fraction of the variance explained by the variance in cycle period. For the three cell types used in this study, R^2 values ranged from 0.63 to 0.97. The equivalent data for the three burst types in our study (squaring the R-values in Figure 5) ranged from 0.29 to 0.47. A similar analysis for the phasing of three pyloric cells was done for the *C. borealis* STG using 69 crabs (Goaillard et al., 2009). Of the 3 cells, the ON phase for the PY cell displayed the most variability in its phasing and had a standard deviation of 0.050 cycles (Goaillard et al., 2009). By contrast, the standard deviation for all ON and OFF phases measured in this study were larger, ranging from 0.066-0.097. These comparisons indicate that phasing in the CG can be far more variable than in the STG.

Burst durations in the CG were much more strongly correlated than were duty cycles, and little relationship was found across animals between burst duration and interburst interval. Together, we interpret that the parameters controlling appropriate heart contraction (bursting) may be regulated independently of the frequency of heart contraction (cycle period).

Our data also raise another interesting possibility about the phasing of interneurons. In the STG studies used for comparison, the pyloric cells examined are themselves motor neurons directly responsible for the phasic series of muscle contractions, and their strict maintenance of phase preserves the fictive motor output *in vitro* (Bucher et al., 2005; Goaillard et al., 2009; Hooper, 1997; Tang et al., 2010), and corresponds to motor patterns retained *in vivo* (Soofi et al., 2014). In the cardiac ganglion, only the LCs are responsible for muscle contraction (Cooke, 2002, 1988). They receive excitatory input for variable lengths of time before summation of

pacemaker inputs initiates the LC burst, and continue to receive inputs for variable lengths of time after the LC burst. It is possible that due to the additional layer of neuronal processing between interneurons and muscle contraction that a greater amount of variability can be tolerated in their phasing (Williams et al., 2013).

Utility of the CG in the study of variability across animals

The ability to examine covariance of output features, or distributions with relatively small standard deviation could potentially point towards the conserved parameters important for homeostatic regulation. By studying many distinct networks that differ in their architecture and function, we can benefit from the advantages of each by gaining different insights into the regulation of network output. Similar collections of recordings have been useful in advancing the utility of other invertebrate CPGs, particularly the crustacean stomatogastric ganglion and the leech heartbeat CPG (Bucher et al., 2005; Goaillard et al., 2009; Lamb and Calabrese, 2013; Norris et al., 2011; Roffman et al., 2012). Unlike the STG, the CG generates rhythmicity through the use of excitatory synapses and is not dependent on extrinsic modulation for rhythmic network activity (Marder and Bucher, 2007)(Cooke, 2002). Although they perform analogous function, the CPGs networks controlling the heartbeat of the leech *H. medicinalis* and of the crab *C. borealis* function quite differently. The leech heartbeat CPG has a segmental organization, relies on inhibitory synaptic connections and post-inhibitory rebound bursting, and displays complex asymmetric patterns in its bilaterally symmetrical networks (Calabrese et al., 2016)(Kristan et al., 2005). By contrast, the crab CG has only

excitatory synapses and no equivalent of the bilaterally asymmetric activity (Cooke, 2002).

Seasonal Variation

The origins of variability in cellular and synaptic properties are difficult to identify; the animals used for these studies are wild-caught adult males, with little known about their genetic variability, developmental processes, or life history. These and other factors may all play a role in the generation of animal-to-animal variability. Despite these uncertainties, we interpret that at least some of the variability can be attributed to seasonal changes in the basal activity of the CG. It should be noted that the length of time each crab was allowed to acclimate in our tanks prior to dissection was not standardized and ranged from less than a day to several weeks. Although this factor was not controlled, there were no procedural changes in protocols across seasons, and thus we would expect any effect of acclimation time to influence our data uniformly. Interestingly, our data on cycle frequency are in agreement with *in vivo* observations of lobsters by Jury and Watson (2000). Lobsters caught in the winter and summer months were acclimated for 4 weeks in tanks maintained at 15°C, after which their cardiovascular activity was compared. It was found that lobsters in the winter had a significantly lower baseline heart rate than those in summer. These data provide evidence for temperature-independent seasonal adjustments in the crustacean cardiovascular system. This argues that our data are not an artifact from lack of standardized acclimation time, but rather reflect seasonal adjustments in the basal state of cardiac ganglion activity that may underlie the differences in cardiovascular output described by Jury and Watson (2000).

Additionally, responses to acute temperature change were tested in lobsters of both seasons, and both revealed similar responses that were dependent on the cardioregulatory nerves (Jury and Watson, 2000). However, the cardiovascular responses of lobsters in winter months was of shorter duration, and may be due to altered expression of modulatory receptors (Jury and Watson, 2000; Wood et al., 1995).

Multiple types of variable synaptic input and LC activity

The burst waveforms of LCs are quite variable across animals, and ultimately result from a complex interaction of pacemaker inputs and LC intrinsic properties. Differences in LC waveforms across animals appear to arise at least in part from different patterns of excitatory drive. In the features we have examined here, MC spikes are most strongly correlated with the network output of the motor neurons, and appear to play the most important role in influencing LC output. SC spikes and MC spikes both produce EPSCs in LC motor neurons, and therefore both of these unique inputs are influencing their activity. SC and MC bursts do not appear to maintain strict relationships in the timing and duration of their bursts, but rather are quite variable across animals. It seems clear, albeit from a small number of trials, that the EPSCs from these two cells are not equivalent, and produce EPSCs with distinct amplitudes. Experiments using a sucrose gap to stop spike mediated pacemaker-LC synaptic transmission in the blue crab *C. sapidus* revealed the electrotonic feed-forward effect of pacemaker cells, which is likely the cause of the slow excitatory current underlying the spike-mediated EPSCs (García-Crescioni and Miller, 2011). These data all suggest that LCs across animals do not receive equivalent temporal patterns of excitatory drive. Further investigation will be

necessary to characterize these synapses further: Do they display frequency-dependent facilitation or depression? Are the relative weights of these inputs is preserved across animals? Do they provide the same net excitation across animals?

A more detailed characterization could help to address broader questions: are LC intrinsic conductances variable across animals because they are specifically tuned to the pacemaker inputs they receive (Goaillard et al., 2009; Norris et al., 2011; Roffman et al., 2012)? Does having these parallel pathways of excitation confer robustness to the rhythmic output of the CG (Marder et al., 2016, 2015)? Are different patterns of pacemaker activity related to differential responses to modulation (Marder et al., 2014)? Future studies of pacemaker variability in the CG help to address the factors that determine cellular variability, network robustness, and differential responses to modulation.

The physiological underpinnings of two distinct spike amplitudes still require explanation. Detailed studies using microscopy and physiology in other crustacean species may provide clues that could guide further investigation. Differences across decapod species certainly exist, but there is evidence that 3 of the pacemaker cells are similar to one another, while the fourth has unique properties. In the crab *P. sanguinolentus*, three of the four "small cells" appear to be electrically coupled at multiple sites along their axons, which is believed to provide highpass filtering to synchronize their action potentials (Cooke, 2002; Mirolli et al., 1987). This microscopy study further concluded that the fourth small cell axon was morphologically distinct from the other 3, and was likely to be functionally distinct as well (Mirolli et al., 1987). Although they encountered difficulties tracing the fourth SC axon to each of its contacts,

the pioneering work of J. Alexandrowicz on the innervation of decapod hearts, and microscopy studies of *C. sapidus* indicates that it too extends to the anterior portion of the trunk (Alexandrowicz, 1934; Hawkins and Howse, 1978). Electrical coupling among 3 pacemaker axons may help to explain why we observe two distinct forms of pacemaker firing, but due to differences across species, we cannot be certain. In the lobsters *P. interruptus* and *H. americanus*, all 4 pacemaker cells can fire independently (Friesen, 1975a, 1975b, 1975c; Hartline, 1967). Still, three of the cells in *P. interruptus* appear similar and do not show frequency-dependent synaptic changes, but the remaining cell shows strong frequency-dependent antifacilitation (Friesen, 1975c)(Friesen, 1975b). Investigations of the *H. americanus* CG found that one particular small cell was responsible for beginning each burst (Hartline, 1967), but this cell's EPSP amplitude relative to the others has not been determined (Hartline, 1979). The neurotransmitter(s) used by CG pacemaker cells has been somewhat controversial (Cooke, 2002). Examination of synaptic vesicles by microscopy suggests that more than one transmitter may be used by SCs (Mirolli et al., 1987). Based on LC responses to various neurotransmitters, it is generally agreed that glutamate is used by SCs (Delgado et al., 2000; Hashemzadeh-Gargari and Freschi, 1992), and possible acetylcholine as well (Cooke, 2002; Freschi and Livengood, 1989; Sullivan and Miller, 1990).

REFERENCES

Alexandrowicz, J., 1934. The innervation of the heart of Crustacea. i. Decapoda. Stomatopoda. QJ Microsc. Sci.

Benson, J.A., 1980. Burst reset and frequency control of the neuronal oscillators in the cardiac ganglion of the crab, Portunus sanguinolentus. J. Exp. Biol. 87, 285–313.

Berlind, A., 1989. Feedback from motor neurones to pacemaker neurones in lobster cardiac ganglion contributes to regulation of burst frequency. J. Exp. Biol. 294, 277–294.

Bucher, D., Prinz, A.A., Marder, E., 2005. Animal-to-animal variability in motor pattern production in adults and during growth. J. Neurosci. 25, 1611–9.

Calabrese, R.L., Norris, B.J., Wenning, A., 2016. The neural control of heartbeat in invertebrates. Curr. Opin. Neurobiol. 41, 68–77.

Calabrese, R.L., Norris, B.J., Wenning, A., Wright, T.M., 2011. Coping with variability

in small neuronal networks. Integr. Comp. Biol. 51, 845–55.

Cooke, I.M., 2002. Reliable, responsive pacemaking and pattern generation with minimal cell numbers: the crustacean cardiac ganglion. Biol. Bull. 202, 108–36.

Cooke, I.M., 1988. Studies on the crustacean cardiac ganglion. Comp. Biochem. Physiol. C. 91, 205–18.

Delgado, J.Y., Oyola, E., Miller, M.W., 2000. Localization of GABA- and glutamate-like immunoreactivity in the cardiac ganglion of the lobster Panulirus argus. J. Neurocytol. 29, 605–19.

Dickinson, P.S., 2006. Neuromodulation of central pattern generators in invertebrates and vertebrates. Curr. Opin. Neurobiol. 16, 604–14.

Fort, T.J., Brezina, V., Miller, M.W., 2004. Modulation of an integrated central pattern generator-effector system: dopaminergic regulation of cardiac activity in the blue crab Callinectes sapidus. J. Neurophysiol. 92, 3455–70.

Freschi, J.E., Livengood, D.R., 1989. Membrane current underlying muscarinic cholinergic excitation of motoneurons in lobster cardiac ganglion. J. Neurophysiol. 984–995.

Friesen, W., 1975a. Physiological anatomy and burst pattern in the cardiac ganglion of the spiny lobsterPanulirus interruptus. J. Comp. Physiol. 173–189.

Friesen, W., 1975b. Synaptic interactions in the cardiac ganglion of the spiny lobsterPanulirus interruptus. J. Comp. Physiol. 191–205.

Friesen, W., 1975c. Antifacilitation and facilitation in the cardiac ganglion of the spiny lobsterPanulirus interruptus. J. Comp. Physiol. 207–224.

García-Crescioni, K., Fort, T.J., Stern, E., Brezina, V., Miller, M.W., 2010. Feedback

from peripheral musculature to central pattern generator in the neurogenic heart of the crab Callinectes sapidus: role of mechanosensitive dendrites. J. Neurophysiol. 103, 83–96.

García-Crescioni, K., Miller, M.W., 2011. Revisiting the reticulum: feedforward and feedback contributions to motor program parameters in the crab cardiac ganglion microcircuit. J. Neurophysiol. 106, 2065–77.

Goaillard, J.-M., Taylor, A.L., Schulz, D.J., Marder, E., 2009. Functional consequences of animal-to-animal variation in circuit parameters. Nat. Neurosci. 12, 1424–30.

Greenberg, I., Manor, Y., 2005. Synaptic depression in conjunction with A-current channels promote phase constancy in a rhythmic network. J. Neurophysiol. 93, 656–77.

Hartline, D.K., 1979. Integrative neurophysiology of the lobster cardiac ganglion. Integr. Comp. Biol. 19, 53–65.

Hartline, D.K., 1967. Impulse identification and axon mapping of the nine neurons in the cardiac ganglion of the lobster Homarus americanus. J. Exp. Biol. 47, 327–40.

Hashemzadeh-Gargari, H., Freschi, J., 1992. The Effects of Glutamate Agonists on Voltage-Clamped Motoneurons of the Lobster Cardiac Ganglion. J. Exp. … 63, 53–63.

Hawkins, W.E., Howse, H.D., 1978. A Light and Electron Microscopic Study of the Cardiac Ganglion of the Blue Crab Callinectes sapidus Rathbun. Trans. Am. Microsc. Soc. 97, 363.

Hooper, S.L., 1997. Phase maintenance in the pyloric pattern of the lobster (Panulirus interruptus) stomatogastric ganglion. J. Comput. Neurosci. 4, 191–205.

Jury, S.H., Watson, W.H., 2000. Thermosensitivity of the lobster, Homarus americanus, as determined by cardiac assay. Biol. Bull. 199, 257–264.

Kristan, W.B., Calabrese, R.L., Friesen, W.O., 2005. Neuronal control of leech behavior. Prog. Neurobiol. 76, 279–327.

Lamb, D.G., Calabrese, R.L., 2013. Correlated Conductance Parameters in Leech Heart Motor Neurons Contribute to Motor Pattern Formation. PLoS One 8, e79267.

Lane, B.J., Samarth, P., Ransdell, J.L., Nair, S.S., Schulz, D.J., 2016. Synergistic plasticity of intrinsic conductance and electrical coupling restores synchrony in an intact motor network. Elife 5.

Manor, Y., Bose, A., Booth, V., Nadim, F., 2003. Contribution of synaptic depression to phase maintenance in a model rhythmic network. J. Neurophysiol. 90, 3513–28.

Marder, E., 2011. Variability, compensation, and modulation in neurons and circuits. Proc. Natl. Acad. Sci. U. S. A. 108 Suppl , 15542–8.

Marder, E., Bucher, D., 2007. Understanding circuit dynamics using the stomatogastric nervous system of lobsters and crabs. Annu. Rev. Physiol. 69, 291–316.

Marder, E., Goaillard, J.-M., 2006. Variability, compensation and homeostasis in neuron and network function. Nat. Rev. Neurosci. 7, 563–74.

Marder, E., Goeritz, M.L., Otopalik, A.G., 2015. Robust circuit rhythms in small circuits arise from variable circuit components and mechanisms. Curr. Opin. Neurobiol. 31, 156–163.

Marder, E., Gutierrez, G.J., Nusbaum, M.P., 2016. Complicating connectomes Electrical coupling creates parallel pathways and degenerate circuit mechanisms. Dev. Neurobiol.

Marder, E., O'Leary, T., Shruti, S., 2014. Neuromodulation of circuits with variable parameters: single neurons and small circuits reveal principles of state-dependent and robust neuromodulation. Annu. Rev. Neurosci. 37, 329–46.

Mayeri, E., 1973. A Relaxation Oscillator Description of the Burst-Generating Mechanism in the Cardiac Ganglion of the Lobster, Homarus americanus. J. Gen. Physiol. 62, 473–488.

Mirolli, M., Cooke, I.M., Talbott, S.R., Miller, M.W., 1987. Structure and localization of synaptic complexes in the cardiac ganglion of a portunid crab. J. Neurocytol. 16, 115–30.

Mouser, C., Nadim, F., Bose, A., 2008. Maintaining phase of the crustacean tri-phasic pyloric rhythm. J. Math. Biol. 57, 161–181.

Norris, B.J., Wenning, A., Wright, T.M., Calabrese, R.L., 2011. Constancy and variability in the output of a central pattern generator. J. Neurosci. 31, 4663–74.

Ransdell, J.L., Nair, S.S., Schulz, D.J., 2013a. Neurons within the Same Network Independently Achieve Conserved Output by Differentially Balancing Variable Conductance Magnitudes. J. Neurosci. 33, 9950–9956.

Ransdell, J.L., Nair, S.S., Schulz, D.J., 2012. Rapid homeostatic plasticity of intrinsic excitability in a central pattern generator network stabilizes functional neural network output. J. Neurosci. 32, 9649–58.

Ransdell, J.L., Temporal, S., West, N.L., Leyrer, M.L., Schulz, D.J., 2013b. Characterization of inward currents and channels underlying burst activity in motoneurons of crab cardiac ganglion. J. Neurophysiol. 110, 42–54.

Roffman, R.C., Norris, B.J., Calabrese, R.L., 2012. Animal-to-animal variability of

connection strength in the leech heartbeat central pattern generator. J. Neurophysiol. 107, 1681–93.

Schulz, D.J., Goaillard, J.-M., Marder, E., 2006. Variable channel expression in identified single and electrically coupled neurons in different animals. Nat. Neurosci. 9, 356–62.

Schulz, D.J., Goaillard, J.-M., Marder, E.E., 2007. Quantitative expression profiling of identified neurons reveals cell-specific constraints on highly variable levels of gene expression. Proc. Natl. Acad. Sci. U. S. A. 104, 13187–91.

Soofi, W., Goeritz, M.L., Kispersky, T.J., Prinz, A. a, Marder, E., Stein, W., 2014. Phase maintenance in a rhythmic motor pattern during temperature changes in vivo. J. Neurophysiol. 111, 2603–13.

Sullivan, R.E., Miller, M.W., 1990. Cholinergic activation of the lobster cardiac ganglion. J. Neurobiol. 21, 639–650.

Taketeru, K., 2003. 5.3. Mechanosensing in the lobster cardiac ganglion . Comp.Biochem.Physiol., A 134 , S16.

Tang, L.S., Goeritz, M.L., Caplan, J.S., Taylor, A.L., Fisek, M., Marder, E., 2010. Precise temperature compensation of phase in a rhythmic motor pattern. PLoS Biol. 8, e1000469.

Tobin, A.-E., Cruz-Bermúdez, N.D., Marder, E., Schulz, D.J., 2009. Correlations in ion channel mRNA in rhythmically active neurons. PLoS One 4, e6742.

Welsh, J., Maynard, D., 1951. Electrical activity of a simple ganglion. Fed. ….

Wilkens, J., 1993. Re-evaluation of the stretch sensitivity hypothesis of crustacean hearts: hypoxia, not lack of stretch, causes reduction in heart rate of isolated hearts. J. Exp.

Biol. 232, 223–232.

Wilkens, J.L., McMahon, B.R., 1992. Intrinsic properties and extrinsic neurohormonal control of crab cardiac hemodynamics. Experientia.

Williams, A.H., Kwiatkowski, M. a, Mortimer, A.L., Marder, E., Zeeman, M. Lou, Dickinson, P.S., 2013. Animal-to-animal variability in the phasing of the crustacean cardiac motor pattern: an experimental and computational analysis. J. Neurophysiol. 109, 2451–65.

Wood, D.E., Gleeson, R.A., Derby, C.D., 1995. Modulation of behavior by biogenic amines and peptides in the blue crab, Callinectes sapidus. J. Comp. Physiol. A. 177, 321–33.

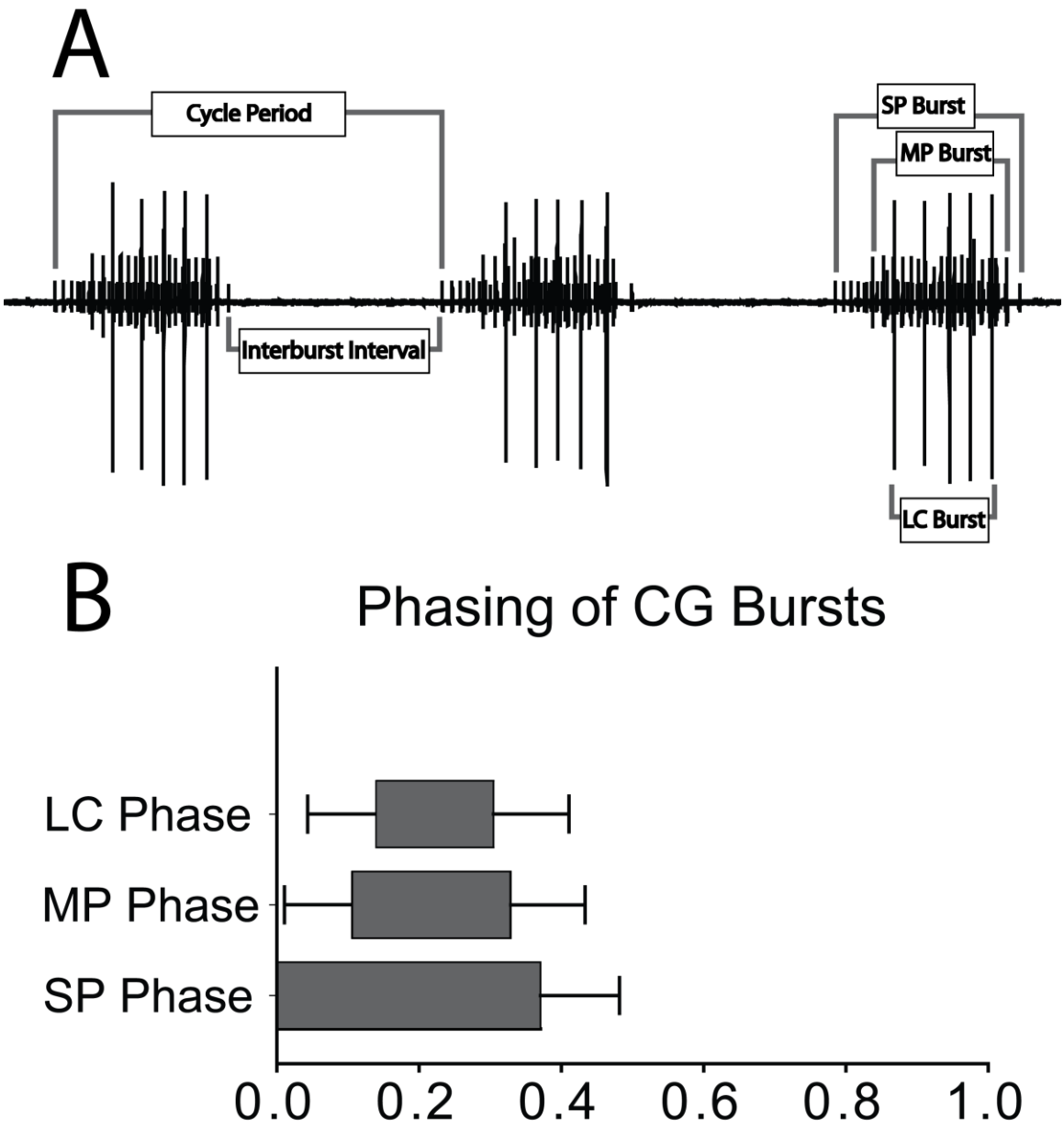

FIGURE 3.1: *Representative extracellular activity and phasing in the CG*. A) Sample extracellular recording from the ganglionic trunk of the CG shows three consecutive bursts to illustrate the consistent and rhythmic nature of network output. Features of bursting that vary across animals important for our analyses are labeled for clarity: cycle period, interburst interval, small-amplitude pacemaker burst (SP burst), medium-amplitude pacemaker burst (MP burst), and Large cell motor neuron bursts (LC burst).

Duration of recording = 7.5 seconds. B) Phase plots for each burst type are shown based on an average across 131 animals. Cycle period is defined by the start of the SP burst, which by definition occurs at zero. The phase (fraction of the cycle period) in which each burst turns “ON” and “OFF” are shown as mean ± SD.

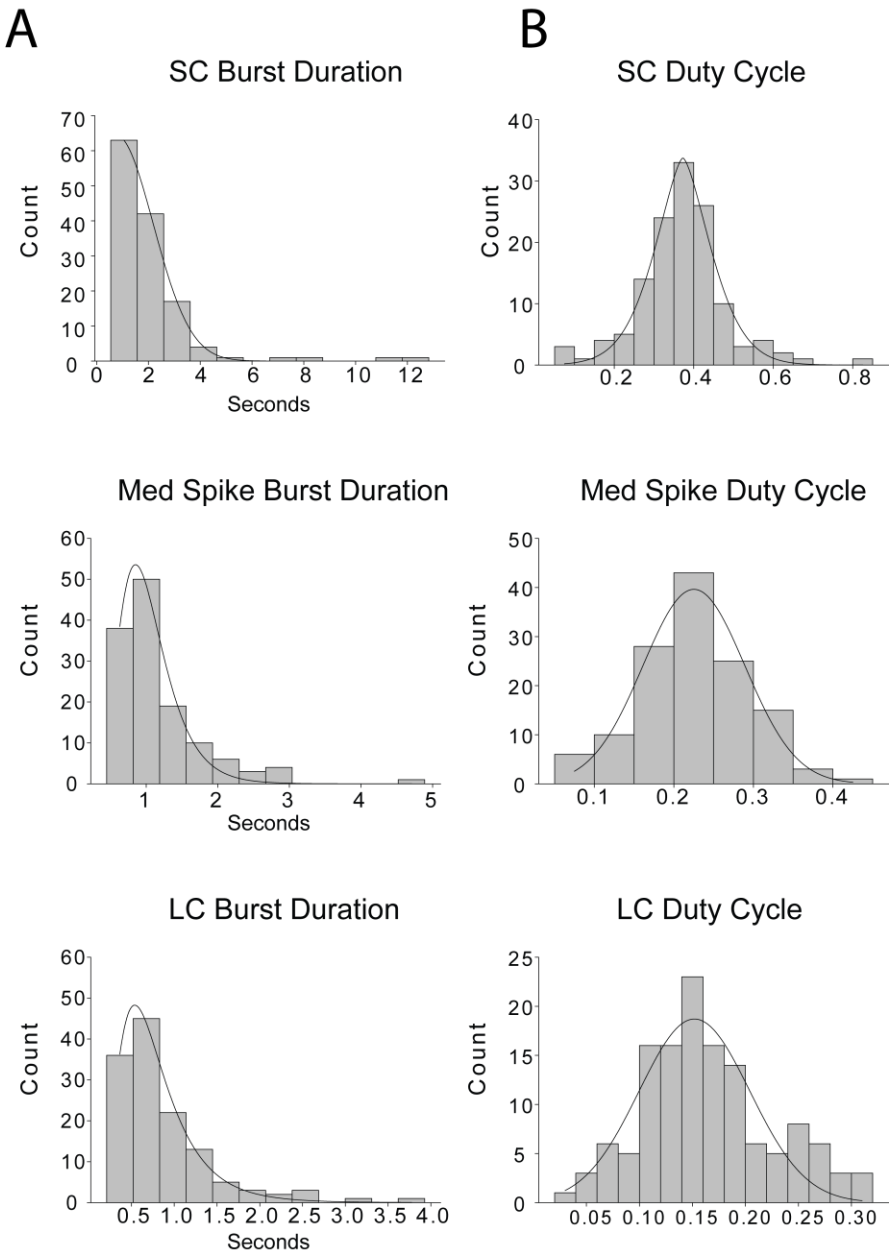

FIGURE 3.2: *Distributions of duration and duty cycle for each burst type in the CG***.** A) The burst duration was calculated for each of the three burst types in all networks, and plotted as histograms. These values must be positive and appear to have a lower boundary but no clear upper boundary, leading to a longer-tailed distribution for longer burst durations. Expressed as median±SD, SP burst duration was 1.576±0.844 seconds, MP burst duration was 0.985±0.505 seconds, and LC burst duration was 0.738±0.481

seconds. B) Duty cycle for each of the three burst types was calculated for all networks. Duty cycles for all three burst types show a normal distribution that is approximately symmetrical. Expressed as median±SD, SP burst duty cycle was 0.368±0.097, MP burst duty cycle was 0.218±0.065, and LC burst duty cycle was 0.155±0.0612.

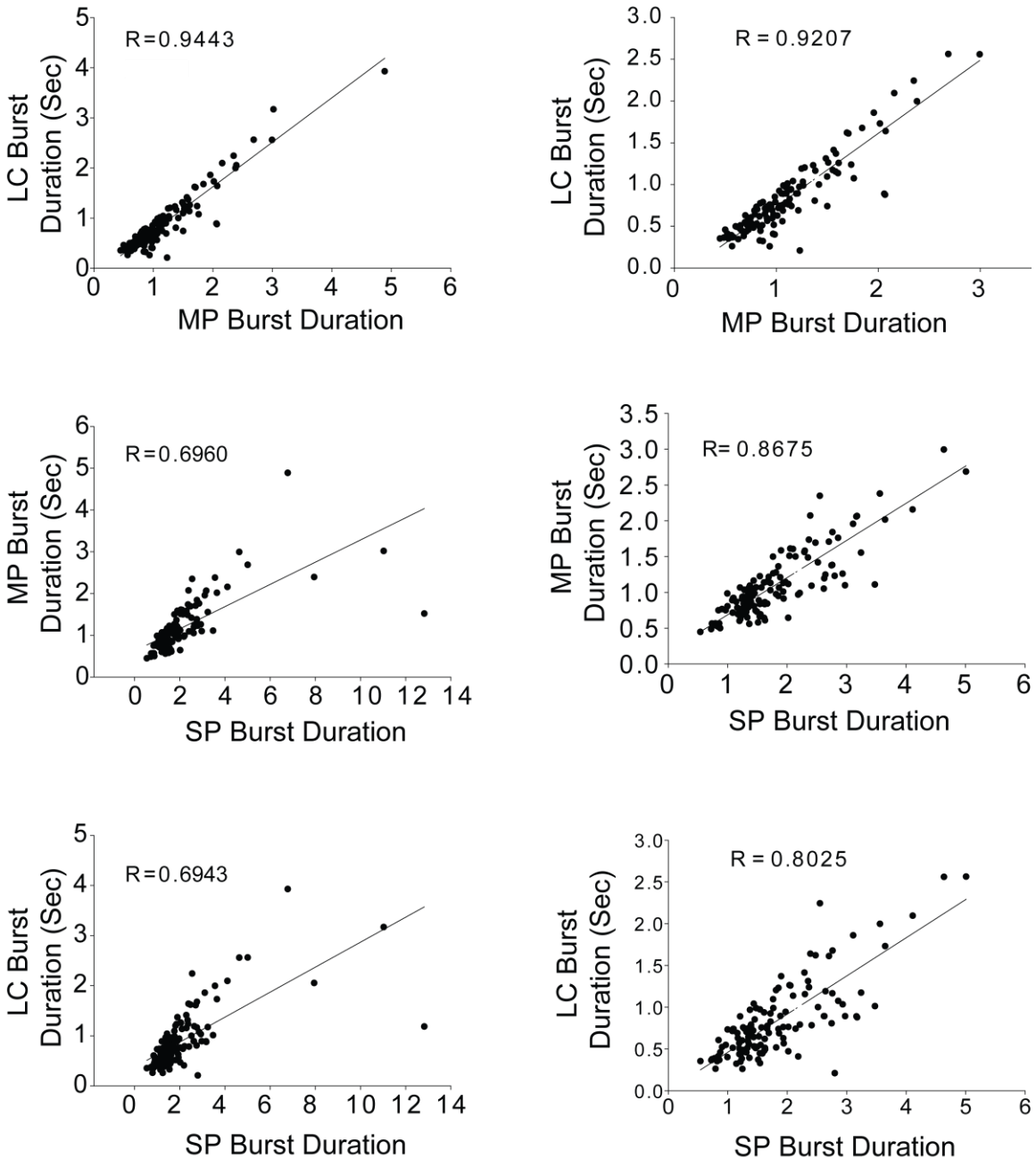

FIGURE 3.3: *Correlations among burst types in the CG*. A) Pairwise correlations of burst durations show a strong relationship between MP and LC burst duration both before and after removal of outlying data (R=0.9943 before; R=0.9207 after). SP burst duration is correlated with MC burst duration, a relationship that was revealed among the majority of preparations after outlying data was removed (R=0.6960 before; R=0.8675 after). SP

burst duration is correlated with LC burst duration, likewise revealed among the majority of preparations after outlying data was removed (R=0.6943 before; R=0.8025 after).

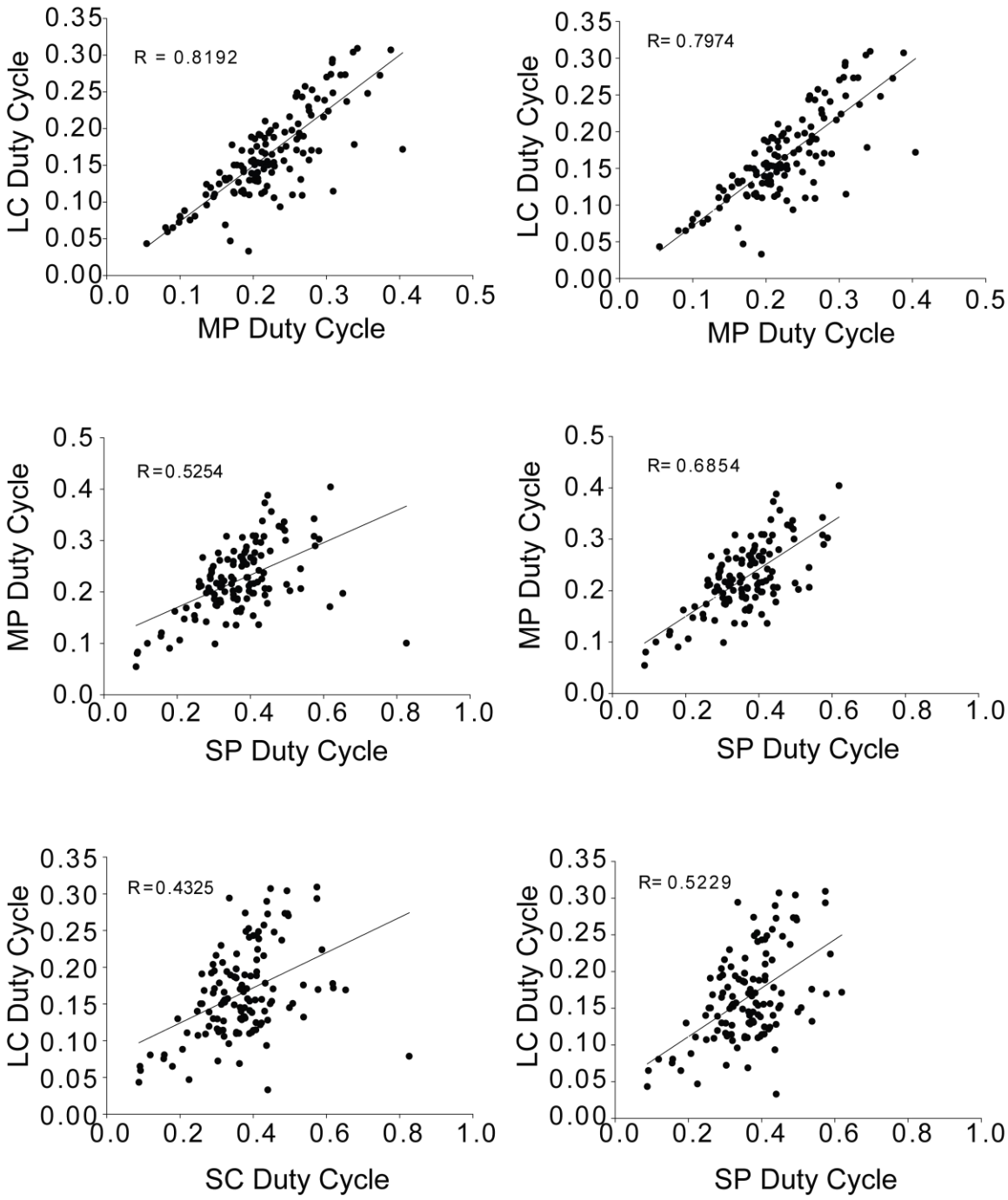

FIGURE 3.4: *Correlation strength among burst duty cycles*. Pairwise correlations of burst duty cycles show a strong relationship between MP and LC duty cycles both before and after removal of outlying data (R=0.8192 before; R=0.7974 after). SP duty cycle is more weakly correlated with MC duty cycle, but a stronger relationship is revealed

among the majority of preparations after outlying data was removed (R=0.5254 before; R=0.6854 after). Correlation strength between SP duty cycle and LC duty cycle again revealed a stronger relationship among the majority of preparations after outlying data was removed (R=0.4325 before; R=0.5229 after).

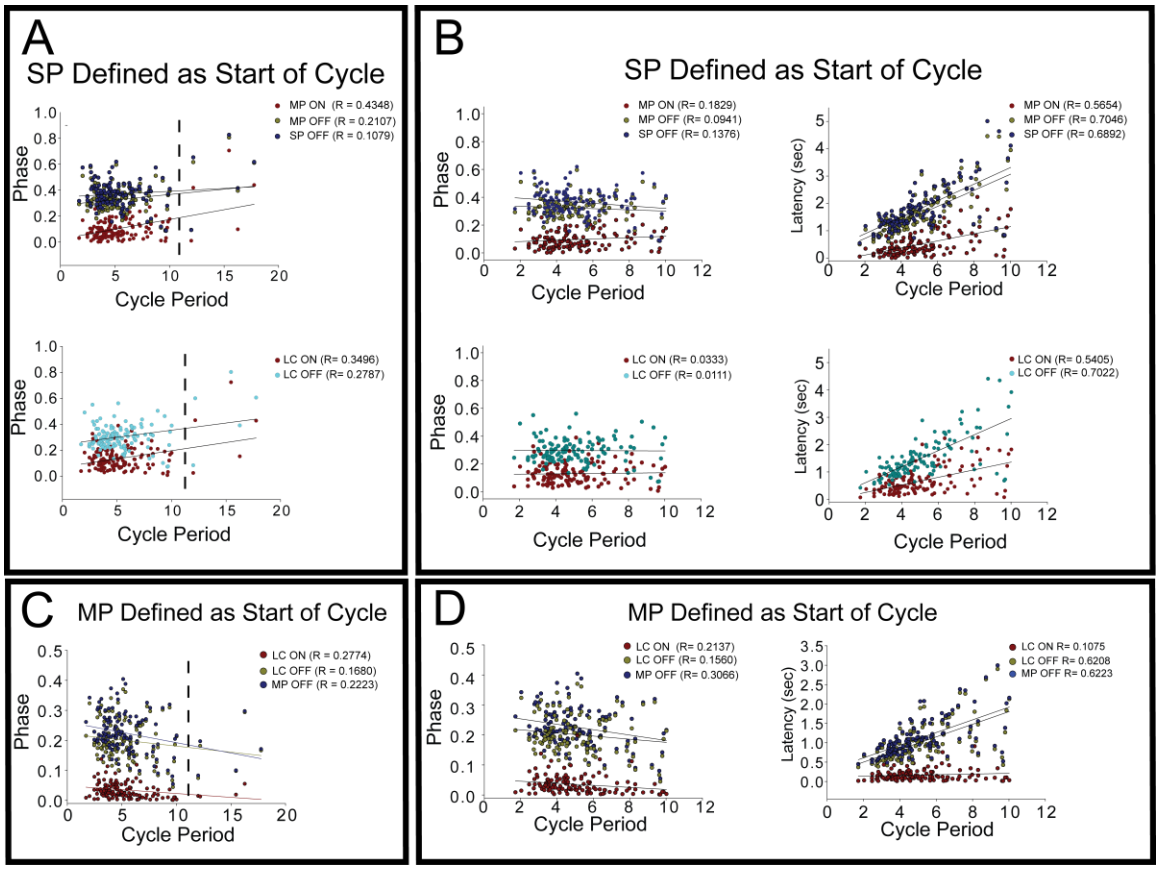

FIGURE 3.5: *Phasing and latency to burst ON and OFF times as a function of cycle period*. A) ON and OFF phase for each burst type was plotted against cycle period and fit with a linear regression. The overlap of phasing data visually obscured these data, and SP and MP phasing (A,top) is plotted separately from LC data (A, bottom). R-values for each phase were: R= 0.4348 for MP ON phase, R= 0.2107 for MP OFF phase, R= 0.3496 for LC ON phase, R= 0.2786 for LC OFF phase, and R= 0.1079 for SP OFF phase. Data to the right of the vertical dashed line was removed for the reanalysis in B. B) Data are replotted after removal of the 5 preparations as in Figure 3 and Figure 4. R-values after removing the outliers were as follows: R= 0.1829 for MP ON phase, R= 0.0941 for MP OFF phase, R= 0.0333 for LC

ON phase, R= 0.0111 for LC OFF phase, and R= 0.1376 for SP OFF phase. These data with outliers removed were then used to test whether the latency to burst ON and OFF phase scaled linearly with cycle period. R-values were as follows: R= 0.5654 for MP ON phase, R= 0.7046 for MP OFF phase, R= 0.5405 for LC ON phase, R= 0.7022 for LC OFF phase, and R= 0.6892 for SP OFF phase. C) Data were re-examined by the same methods in A, this time defining MP as the start of each cycle to test its predictive power for motor output. R-values for each phase were: R= 0.2774 for LC OFF phase, R= 0.1680 for LC OFF phase, R= 0.2223 for MP OFF phase. Data to the right of the vertical dashed line was removed for reanalysis in D. D) Data were re-examined as in (B), defining MP as the start of each cycle. R-values after removing the outliers were as follows: R= 0.3066 for MP OFF phase, R= 0.2137 for LC ON phase, R= 0.1560 for LC OFF phase. These data with outliers removed were then used to test whether the latency to burst ON and OFF phase scaled linearly with cycle period when cycles were defined by MP bursts. R-values were as follows: R= 0.6223 for MP OFF phase, R= 0.1075 for LC ON phase, and R= 0.6208 for LC OFF phase.

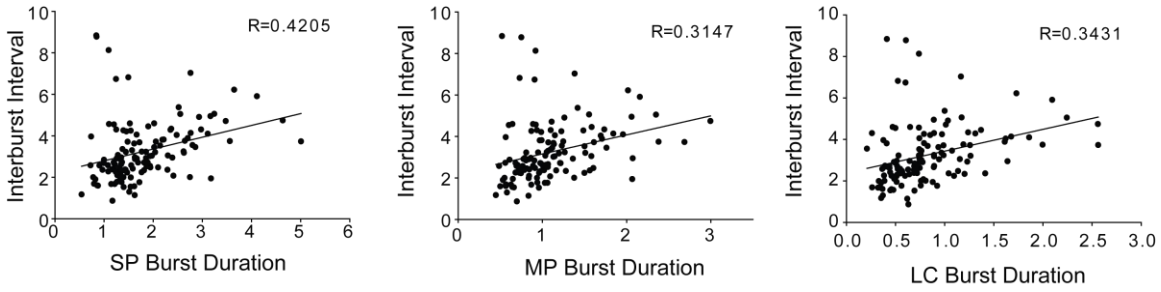

FIGURE 3.6: *Burst durations are not strongly correlated with interburst interval*. Each burst duration was plotted against the interburst interval and fit with regression lines. R-values for each of the three bursts were: R=0.4205 for SP Burst duration, R=0.3147 for MP bursts, and 0.3431 for LC bursts.

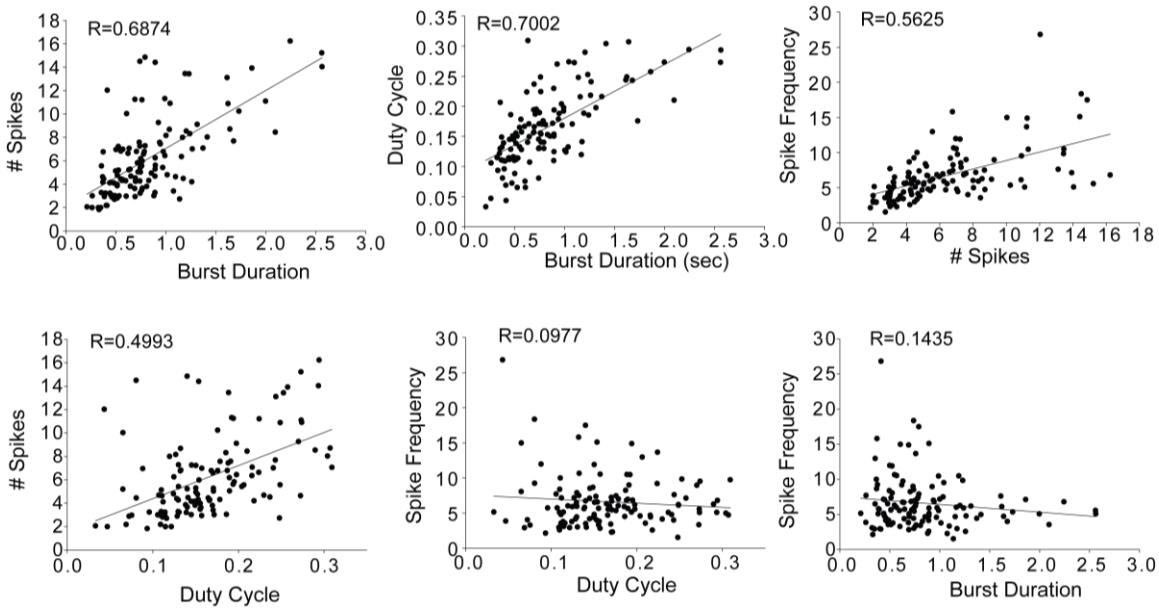

FIGURE 3.7: *Relationships among LC burst characteristics*. Various features of LC firing output were plotted against one another to examine whether there was any covariance in these features. R-values were as follows: R=0.5625 for number of spikes vs spike frequency; R=0.7002 for burst duration vs duty cycle; R=0.6874 for burst duration vs number of spikes per burst; R=0.1435 for burst duration vs spike frequency; R=0.4993 for duty cycle vs number of spikes per burst; R=0.0977 for duty cycle vs spike frequency.

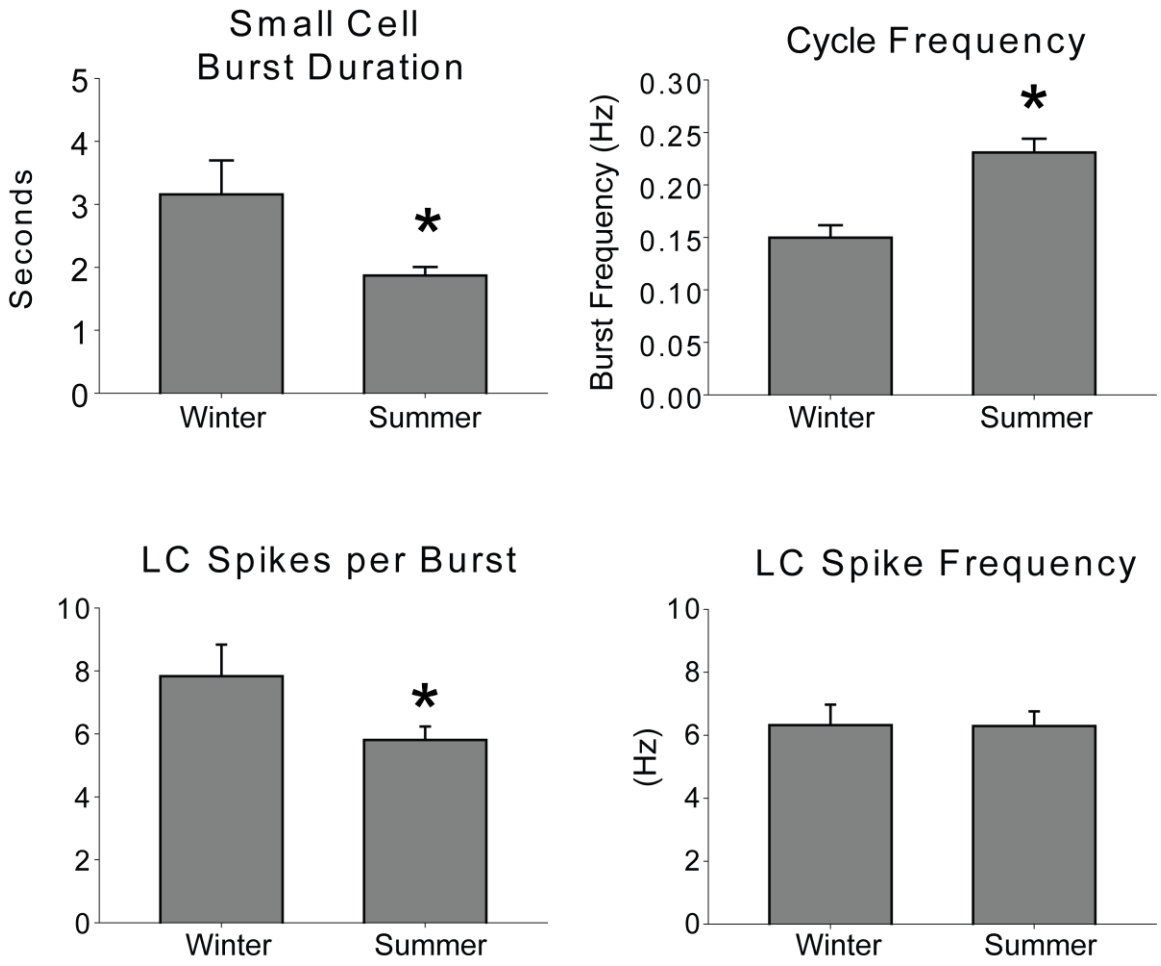

FIGURE 3.8: *Seasonal Differences in CG activity*. In winter months (Dec-Feb), pacemaker burst duration is significantly longer than in summer months (Jun-Aug), but they occur less frequently (t-tests, $p<0.01$ for both). In the winter, significantly more spikes are present in LC bursts ($p<0.05$). However, the lack of difference in LC spike frequency shows that not all characteristics of CG output change.

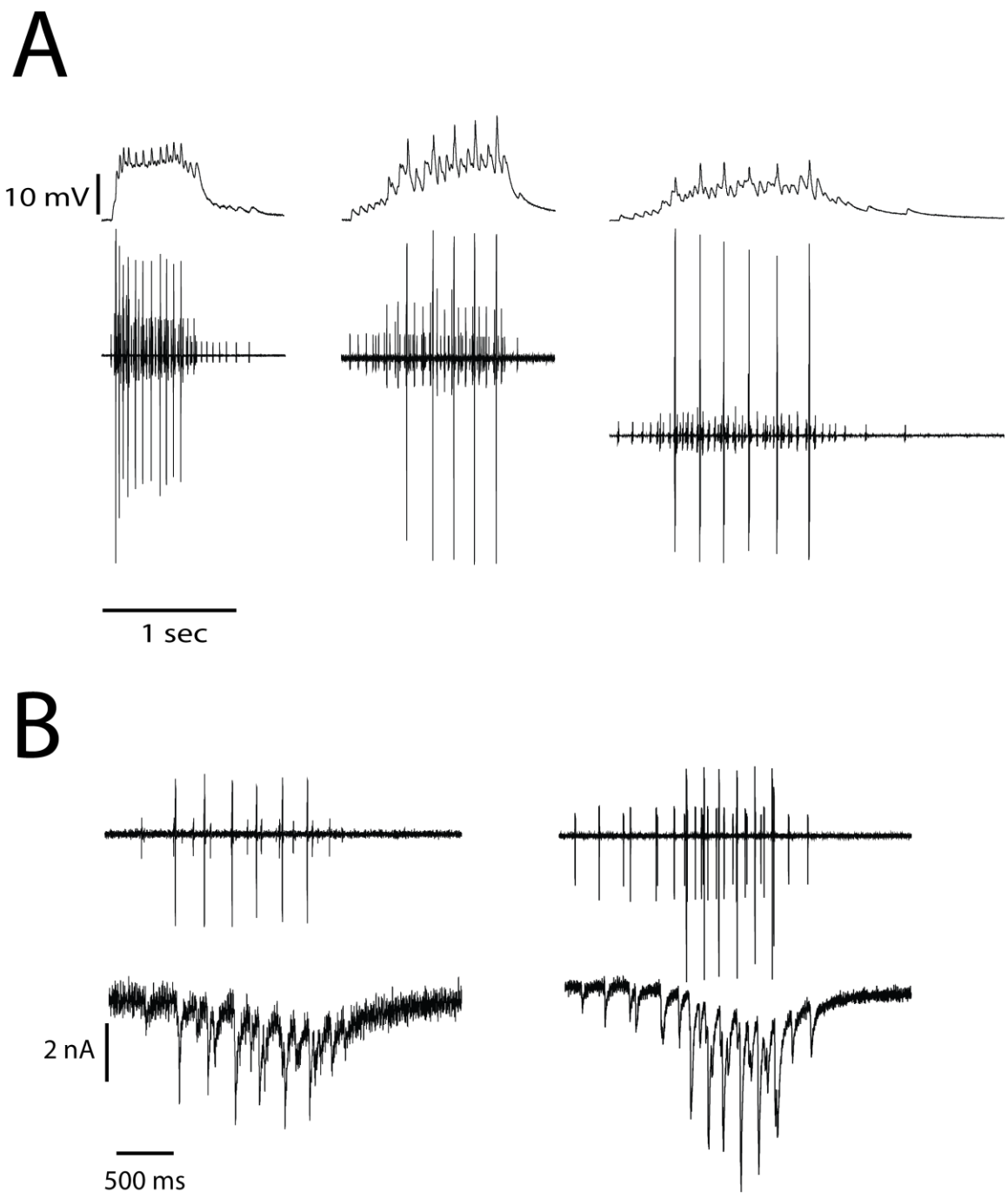

FIGURE 3.9: *Representative traces of distinct patterns of pacemaker activity and pacemaker EPSCs* A) Paired intracellular and extracellular traces from 3 networks illustrates some of the diversity of firing patterns described in previous figures. Left: 1 small spike followed by 1 medium spike are sufficient to elicit the beginning of LC Burst.

Middle: (from same preparation as Figure 1) show approximately 10 SP spikes over and 3 MP spikes before the first LC spike. Right: Longer burst than at left and middle, but SP spiking continues much longer after MP and LC bursts have ceased. Pacemaker firing continues for hundreds of milliseconds before terminating. B) LCs in the intact network were voltage clamped at -80 mV (left) and -90 mV (right), revealing distinct magnitudes of EPSCs corresponding to the small and medium pacemaker spikes. Extracellular traces show SC and MC spikes aligned with their corresponding EPSC.

DISCUSSION

Even on a moment-to-moment basis, neuronal activity involves nonlinear interactions among many intrinsic membrane properties and many different complex forms of interaction between neurons, which can be highly variable while still achieving functionally appropriate output (Marder and Goaillard, 2006; Goaillard et al., 2009a; Calabrese et al., 2011; Marder et al., 2014). Understanding how these processes generate appropriate network function across the lifetime of an animal represents a fundamental and important goal of neuroscience research (Drion et al., 2015; Marder et al., 2015; Gjorgjieva et al., 2016; Schulz and Lane, 2017). The data presented here have highlighted that each of these characteristics can be highly variable both within and across animals, and that they are subject to multiple layers of regulation including activity-dependent homeostatic changes in conductances as well as flexibility conferred by physiological factors such as neuromodulation.

From the data in the preceding chapters, I draw 6 main conclusions:

1) Across synchronized LCs within a network, variability of intrinsic properties makes network synchrony vulnerable to perturbations that differentially affect conductances.
2) Gap-junctional coupling conductance between LCs is not set at a static value, but can be modified by homeostatic compensation to restore network synchrony.

3) Increased I_A after TEA application demonstrates that intrinsic compensation of LCs can contribute to the restoration of synchrony.
4) Neuromodulation can both cause and prevent desynchronization of LCs, depending on their conductance targets.
5) Co-modulation may represent a mechanism by which network properties can be altered in response to changing environmental conditions while maintaining core aspects of network function such as synchrony or phasing.
6) The basal state of activity of the CG is highly variable across animals, and different patterns of synaptic drive may be important in understanding variability across LCs.

Some of the greatest advantages of the CG are the ability to study and bring cellular and network-level processes into an integrative understanding of neuronal function. Ultimately, a systems view of neuroscience incorporates levels of organization and timescales beyond what was examined here: everything from molecules to behavior, and from developmental timescales to the lifetime of the animal. The cardiac ganglion offers a tractable and experimentally accessible system in which to explore homeostatic regulation across multiple layers of biological organization and timescales. These include activity-dependent and modulation-dependent regulation of excitability through correlated patterns ion channel mRNA expression (Tobin et al., 2009), to examination of the CG as part of an integrated CPG-effector system (Stern et al., 2007, 2009, 2010), to integrative physiological approach at an organismal level (Wilkens and McMahon, 1992; Wilkens, 1999).

The possibilities are extremely rich, and below I have outlined several areas where I believe future studies with the cardiac ganglion can build on the data presented in the previous chapters to further our understanding of stable cellular and network properties.

Variability of intrinsic properties and variability of electrical coupling:

The experiments in Chapter 1 demonstrating homeostatic compensation illustrate that intrinsic properties and electrical coupling are not set at static values within a network, and that magnitudes of both can change to restore activity after perturbation. Networks have both the ability to tune intrinsic cellular properties such that synchrony is an emergent property of their activity, and they also have the ability to force cells with disparate output into synchronized behavior through changes in electrical coupling. The distinction between these two mechanisms used to restore synchrony in Chapter 1 can be helpful in framing the following questions. How is the regulation of appropriate cellular conductances influenced by electrical coupling, and vice versa? Are they co-regulated? Do neurons rely primarily on regulation of intrinsic conductances to achieve synchrony and rely on electrical coupling as a "back-up"? Is there an optimal balance achieved by relying on both simultaneously? Are both of these properties fluid over the lifetime of an animal, or do they return to a "set-point"?

The use of electrical coupling to promote synchrony is observed across animal phyla, and the above questions highlight areas of homeostatic regulation of neuronal activity that represent important gaps in our knowledge. At present, we are unable to provide complete answers these questions and do not fully understand what sensing mechanisms and molecular pathways are involved in the regulation of electrical coupling. The cardiac ganglion offers an excellent model system to advance our understanding of these questions.

The most thoroughly understood pathways for regulation of intrinsic properties are tied to calcium influx resulting from the voltage activity of individual cells (Barish, 1998; Liu et al., 1998; O'Leary et al., 2013). Variability of intrinsic conductances in LCs within a network has been most thoroughly examined for the K^+ currents I_{HTK} and I_A, but is thought to extend to other intrinsic currents (Ransdell et al., 2012a, 2013a, 2013c; Lane et al., 2016). This makes the question of whether calcium currents vary across LCs within a network of particular interest for future studies of variability and homeostatic regulation. In the context of electrically coupled neurons, voltage changes are effectively "averaged" across the cells as increased electrical coupling makes the cells more isopotential. Theoretically, if calcium conductance magnitudes vary within a network, each cell could receive a different "readout" of its own activity even if the activity of those cells is identical. This potential impact on calcium-sensing mechanisms would be expected to affect feedback to the molecular pathways that regulate membrane conductances. It remains unknown whether this feedback should also be expected to influence the long-term regulation of electrical coupling.

The data presented in the previous chapters in conjunction with previous work from the Schulz lab has noted interesting relationships between the strength of electrical coupling and variability and intrinsic properties that may help to shed light on these questions and offer several avenues for future pursuits. The parameter space of intrinsic properties observed in LC3 appears to be confined to a narrower range than the intrinsic properties of LC4 and LC5 (Ransdell et al., 2013b). Based solely on knowledge of intrinsic variability, one might predict LC4 and LC5 could be desynchronized more easily. Interestingly, the desynchronization described in Chapters 1 and 2 is observed between LC3, but was never observed between LC4 and LC5. We believe this is because LC4 and LC5 are much more strongly coupled to one another than either of these cells is to LC3. These data suggest the tantalizing possibility that weaker electrical coupling leads to more constraints on intrinsic variability, or conversely that stronger electrical coupling might remove constraints on intrinsic variability.

Variability of intrinsic properties and variability of synaptic inputs:

Does variability in synaptic drive influence the regulation of intrinsic properties? The data in chapter 3 suggest that LCs across networks receive different patterns of synaptic drive. This data set can be analyzed further to find differences in spike frequency and other properties of pacemaker drive that may differ across animals. Ultimately, the output of LCs is influenced by its synaptic connections and its intrinsic excitability. The timing of and strength of each pacemaker spike throughout the burst

influence the burst waveforms in LCs, and activate voltage-gated ion channels. This ultimately produces burst waveforms which can be quite variable from one animal to the next. Are synaptic inputs calibrated in such a way that LCs do not need to be differentially tuned to accommodate them? Or does the variability of synaptic inputs to LCs drive them to have differentially tuned intrinsic conductances?

Motor neurons can receive inputs from multiple other neurons, and the relative strengths of these synapses can vary. In the crab stomatogastric ganglion, LP receives nearly synchronized inhibitory input from both PD and AB cells (Marder and Eisen, 1984). These cells use different neurotransmitters and the synapses have different reversal potentials (Marder and Eisen, 1984), and these synapses are differentially weighted across animals (Goaillard et al., 2009b). Thus the inputs they receive are a composite IPSP, with a reversal potential that can vary from one animal to the next (Goaillard et al., 2009b). Interestingly, the total combined conductance of these synapses appears to be conserved (Goaillard et al., 2009b). Motor neurons of the leech heartbeat CPG each have 4 inputs, and it was found that both their absolute and relative strengths are not maintained across animals, suggesting that each individual cell finds its own unique solution to balancing synaptic inputs (Norris et al., 2011)(Roffman et al., 2012).

Computational modeling of network variability and robustness

The bidirectional interactions between the computational modeling and biological investigation have great promise for advancing theoretical and experimental

understanding of the CG system. Many computational models, including those used in Chapter 1 have moved beyond a single "ideal" model of a network to more accurately reflect biological variability and to test the sensitivity of systems to changes in individual parameters (Prinz et al., 2004; O'Leary et al., 2013, 2014; Doloc-Mihu and Calabrese, 2014, 2016; Lane et al., 2016). Singular ideal models often rely on mean values from measurement of various parameters, which fails to reflect the variability seen across biological populations, and can even fail to describe any member of that neuronal population (Golowasch et al., 2002). Studies that embrace modeling of variability have been useful for understanding network robustness and neuromodulation, and have helped advance theoretical understanding as well as guide experimentation (O'Leary et al., 2013, 2014; Marder et al., 2016). An important and recurring theme in the study of neural networks is that the degeneracy, functional overlap, and parallel pathways observed in complex biological systems confers robust function (Marder and Goaillard, 2006; Beverly et al., 2011; Whitacre, 2012; Drion et al., 2015; Marder et al., 2015, 2016).

Computational modeling in Chapter 1 was used to explore variability and compensation of LCs within a network. Computational models of the cardiac ganglion have explored intrinsic excitability of model LCs, and then further advanced by biological data to inform our studies of synchrony across LCs (Ball et al., 2010; Ransdell et al., 2012b, 2013b, 2013d; Lane et al., 2016). In these studies, pacemaker activity was not changed across networks and was not responsive to LC activity. Chapter 3 begins to acknowledge variability across animals in the range of pacemaker activity across networks, and discusses the implications. Advancing models of the CG toward a more

comprehensive exploration of variability of pacemaker activity across populations and their dynamic interactions with LC activity could be a useful pathway forward for a comprehensive understanding of network function. A large dataset such as the set of recordings in Chapter 3 could help to provide a biological basis for moving such studies forward in a realistic way. This potential future direction could help to advance our understanding of network robustness and neuromodulation.

Activity-dependent regulation of ion channel and innexin mRNA abundance

Molecular regulation of gene expression ultimately underlies membrane excitability. Individual cell types display particular steady-state patterns of ion channel gene expression (Schulz et al., 2006, 2007; Tobin et al., 2009). Expression of genes encoding for ion channels can be influenced by many factors, including neuronal activity and neuromodulators (Barish, 1998; Rodgers et al., 2011, 2013; Zhang and Golowasch, 2011; Temporal et al., 2012, 2014). These two factors can be difficult to disentangle because neuromodulation influences activity. The CG is capable of maintaining endogenous rhythmicity without any extrinsic modulation, and artificial manipulations of activity can be easily performed to ask how molecular profiles change as a consequence. Individual LCs can be isolated for single-cell qPCR or RNA-seq. This, together with the recently published neural transcriptome of *C. borealis,* leaves the CG well-poised as a powerful model system for a comprehensive examination of the activity-dependent regulation of mRNA abundance.

REFERENCES

Ball JM, Franklin CC, Tobin A-E, Schulz DJ, Nair SS (2010) Coregulation of ion channel conductances preserves output in a computational model of a crustacean cardiac motor neuron. J Neurosci 30:8637–8649 Available at: http://www.ncbi.nlm.nih.gov/pubmed/20573909 [Accessed November 23, 2012].

Barish ME (1998) Intracellular calcium regulation of channel and receptor expression in the plasmalemma: Potential sites of sensitivity along the pathways linking transcription, translation, and insertion. J Neurobiol 37:146–157.

Beverly M, Anbil S, Sengupta P (2011) Degeneracy and neuromodulation among thermosensory neurons contribute to robust thermosensory behaviors in Caenorhabditis elegans. J Neurosci 31:11718–11727 Available at: http://www.pubmedcentral.nih.gov/articlerender.fcgi?artid=3167209&tool=pmcentrez&rendertype=abstract [Accessed February 28, 2013].

Calabrese RL, Norris BJ, Wenning A, Wright TM (2011) Coping with variability in small neuronal networks. Integr Comp Biol 51:845–855 Available at: http://www.pubmedcentral.nih.gov/articlerender.fcgi?artid=3223479&tool=pmcentrez&rendertype=abstract [Accessed June 5, 2013].

Doloc-Mihu A, Calabrese RL (2014) Identifying crucial parameter correlations maintaining bursting activity. PLoS Comput Biol 10:e1003678 Available at: http://www.pubmedcentral.nih.gov/articlerender.fcgi?artid=4063674&tool=pmcentrez&rendertype=abstract [Accessed September 19, 2014].

Doloc-Mihu A, Calabrese RL (2016) Analysis of Family Structures Reveals Robustness or Sensitivity of Bursting Activity to Parameter Variations in a Half-Center Oscillator (HCO) Model. eNeuro 3 Available at: http://eneuro.sfn.org/cgi/doi/10.1523/ENEURO.0015-16.2016.

Drion G, O'Leary T, Marder E (2015) Ion channel degeneracy enables robust and tunable neuronal firing rates. Proc Natl Acad Sci U S A 112:E5361–E5370 Available at: http://www.pnas.org/content/112/38/E5361.abstract.

Gjorgjieva J, Drion G, Marder E (2016) ScienceDirect Computational implications of biophysical diversity and multiple timescales in neurons and synapses for circuit performance. Curr Opin Neurobiol 37:44–52 Available at: http://dx.doi.org/10.1016/j.conb.2015.12.008.

Goaillard J, Taylor A, Schulz D, Marder E (2009a) Functional consequences of animal-to-animal variation in circuit parameters. Nat Neurosci 12:1424–1430 Available at: http://www.nature.com/neuro/journal/vaop/ncurrent/full/nn.2404.html [Accessed January 9, 2013].

Goaillard J-M, Taylor AL, Schulz DJ, Marder E (2009b) Functional consequences of animal-to-animal variation in circuit parameters. Nat Neurosci 12:1424–1430 Available at: http://www.pubmedcentral.nih.gov/articlerender.fcgi?artid=2826985&tool=pmcentrez&rendertype=abstract [Accessed March 25, 2014].

Golowasch J, Goldman MS, Abbott LF, Marder E (2002) Failure of averaging in the construction of a conductance-based neuron model. J Neurophysiol 87:1129–1131.

Lane BJ, Samarth P, Ransdell JL, Nair SS, Schulz DJ (2016) Synergistic plasticity of

intrinsic conductance and electrical coupling restores synchrony in an intact motor network. Elife 5 Available at: http://elifesciences.org/lookup/doi/10.7554/eLife.16879.

Liu Z, Golowasch J, Marder E, Abbott LF (1998) A model neuron with activity-dependent conductances regulated by multiple calcium sensors. J Neurosci 18:2309–2320 Available at: http://www.ncbi.nlm.nih.gov/pubmed/9502792.

Marder E, Eisen JS (1984) Transmitter identification of pyloric neurons: electrically coupled neurons use different transmitters. J Neurophysiol 51:1345–1361.

Marder E, Goaillard J-M (2006) Variability, compensation and homeostasis in neuron and network function. Nat Rev Neurosci 7:563–574 Available at: http://www.ncbi.nlm.nih.gov/pubmed/16791145 [Accessed May 21, 2013].

Marder E, Goeritz ML, Otopalik AG (2015) Robust circuit rhythms in small circuits arise from variable circuit components and mechanisms. Curr Opin Neurobiol 31:156–163 Available at: http://dx.doi.org/10.1016/j.conb.2014.10.012.

Marder E, Gutierrez GJ, Nusbaum MP (2016) Complicating connectomes Electrical coupling creates parallel pathways and degenerate circuit mechanisms. Dev Neurobiol.

Marder E, O'Leary T, Shruti S (2014) Neuromodulation of circuits with variable parameters: single neurons and small circuits reveal principles of state-dependent and robust neuromodulation. Annu Rev Neurosci 37:329–346 Available at: http://www.ncbi.nlm.nih.gov/pubmed/25032499.

Norris BJ, Wenning A, Wright TM, Calabrese RL (2011) Constancy and variability in the output of a central pattern generator. J Neurosci 31:4663–4674 Available at:

http://www.pubmedcentral.nih.gov/articlerender.fcgi?artid=3071692&tool=pmcentrez&rendertype=abstract [Accessed June 5, 2013].

O'Leary T, Williams AH, Caplan JS, Marder E (2013) Correlations in ion channel expression emerge from homeostatic tuning rules. Proc Natl Acad Sci U S A 110:E2645–E2654 Available at: http://www.ncbi.nlm.nih.gov/pubmed/23798391 [Accessed June 28, 2013].

O'Leary T, Williams AH, Franci A, Marder E (2014) Cell types, network homeostasis, and pathological compensation from a biologically plausible ion channel expression model. Neuron 82:809–821 Available at: http://www.ncbi.nlm.nih.gov/pubmed/24853940 [Accessed July 22, 2014].

Prinz A a, Bucher D, Marder E (2004) Similar network activity from disparate circuit parameters. Nat Neurosci 7:1345–1352 Available at: http://www.ncbi.nlm.nih.gov/pubmed/15558066 [Accessed September 24, 2013].

Ransdell JL, Nair SS, Schulz DJ (2012a) Rapid homeostatic plasticity of intrinsic excitability in a central pattern generator network stabilizes functional neural network output. J Neurosci 32:9649–9658 Available at: http://www.ncbi.nlm.nih.gov/pubmed/22787050 [Accessed October 24, 2014].

Ransdell JL, Nair SS, Schulz DJ (2012b) Rapid homeostatic plasticity of intrinsic excitability in a central pattern generator network stabilizes functional neural network output. J Neurosci 32:9649–9658 Available at: http://www.ncbi.nlm.nih.gov/pubmed/22787050 [Accessed November 14, 2012].

Ransdell JL, Nair SS, Schulz DJ (2013a) Neurons within the Same Network Independently Achieve Conserved Output by Differentially Balancing Variable

Conductance Magnitudes. J Neurosci 33:9950–9956 Available at: http://www.jneurosci.org/cgi/doi/10.1523/JNEUROSCI.1095-13.2013 [Accessed June 12, 2013].

Ransdell JL, Nair SS, Schulz DJ (2013b) Neurons within the Same Network Independently Achieve Conserved Output by Differentially Balancing Variable Conductance Magnitudes. J Neurosci 33:9950–9956 Available at: http://www.jneurosci.org/cgi/doi/10.1523/JNEUROSCI.1095-13.2013.

Ransdell JL, Temporal S, West NL, Leyrer ML, Schulz DJ (2013c) Characterization of inward currents and channels underlying burst activity in motoneurons of crab cardiac ganglion. J Neurophysiol 110:42–54 Available at: http://www.ncbi.nlm.nih.gov/pubmed/23576706 [Accessed August 1, 2013].

Ransdell JL, Temporal S, West NL, Leyrer ML, Schulz DJ (2013d) Characterization of inward currents and channels underlying burst activity in motoneurons of crab cardiac ganglion. J Neurophysiol 110:42–54 Available at: http://www.ncbi.nlm.nih.gov/pubmed/23576706.

Rodgers EW, Krenz W-D, Jiang X, Li L, Baro DJ (2013) Dopaminergic tone regulates transient potassium current maximal conductance through a translational mechanism requiring D1Rs, cAMP/PKA, Erk and mTOR. BMC Neurosci 14:143 Available at: http://www.pubmedcentral.nih.gov/articlerender.fcgi?artid=3840709&tool=pmcentrez&rendertype=abstract.

Rodgers EW, Krenz W-DC, Baro DJ (2011) Tonic dopamine induces persistent changes in the transient potassium current through translational regulation. J Neurosci 31:13046–13056 Available at:

http://www.pubmedcentral.nih.gov/articlerender.fcgi?artid=3544522&tool=pmcentrez&rendertype=abstract [Accessed May 7, 2013].

Roffman RC, Norris BJ, Calabrese RL (2012) Animal-to-animal variability of connection strength in the leech heartbeat central pattern generator. J Neurophysiol 107:1681–1693 Available at: http://www.ncbi.nlm.nih.gov/pubmed/22190622 [Accessed December 19, 2012].

Schulz DJ, Goaillard J-M, Marder E (2006) Variable channel expression in identified single and electrically coupled neurons in different animals. Nat Neurosci 9:356–362 Available at: http://www.ncbi.nlm.nih.gov/pubmed/16444270 [Accessed January 29, 2013].

Schulz DJ, Goaillard J-M, Marder EE (2007) Quantitative expression profiling of identified neurons reveals cell-specific constraints on highly variable levels of gene expression. Proc Natl Acad Sci U S A 104:13187–13191 Available at: http://www.pubmedcentral.nih.gov/articlerender.fcgi?artid=1933263&tool=pmcentrez&rendertype=abstract.

Schulz DJ, Lane BJ (2017) Homeostatic plasticity of excitability in crustacean central pattern generator networks. Curr Opin Neurobiol 43:7–14 Available at: http://linkinghub.elsevier.com/retrieve/pii/S0959438816301714.

Stern E, Fort T, Miller M, Peskin C, Brezina V (2007) Decoding modulation of the neuromuscular transform. Neurocomputing 70:1753–1758 Available at: http://www.sciencedirect.com/science/article/pii/S0925231206003894 [Accessed August 4, 2013].

Stern E, García-crescioni K, Miller MW, Peskin CS (2010) A method for decoding the

neurophysiological spike-response transform. 184:212–241.

Stern E, García-Crescioni K, Miller MW, Peskin CS, Brezina V (2009) Modeling the complete cardiac ganglion – heart muscle network of the crab Callinectes sapidus. BMC Neurosci 10:P295.

Temporal S, Desai M, Khorkova O, Varghese G, Dai A, Schulz DJ, Golowasch J (2012) Neuromodulation independently determines correlated channel expression and conductance levels in motor neurons of the stomatogastric ganglion. J Neurophysiol 107:718–727 Available at: http://www.pubmedcentral.nih.gov/articlerender.fcgi?artid=3349629&tool=pmcentrez&rendertype=abstract [Accessed January 27, 2013].

Temporal S, Lett KM, Schulz DJ (2014) Activity-dependent feedback regulates correlated ion channel mRNA levels in single identified motor neurons. Curr Biol 24:1899–1904 Available at: http://www.ncbi.nlm.nih.gov/pubmed/25088555 [Accessed September 16, 2014].

Tobin A-E, Cruz-Bermúdez ND, Marder E, Schulz DJ (2009) Correlations in ion channel mRNA in rhythmically active neurons. PLoS One 4:e6742 Available at: http://www.pubmedcentral.nih.gov/articlerender.fcgi?artid=2727049&tool=pmcentrez&rendertype=abstract [Accessed November 23, 2012].

Whitacre JM (2012) Biological robustness: paradigms, mechanisms, and systems principles. Front Genet 3:67 Available at: http://www.pubmedcentral.nih.gov/articlerender.fcgi?artid=3350086&tool=pmcentrez&rendertype=abstract [Accessed October 17, 2013].

Wilkens JL (1999) The control of cardiac rhythmicity and of blood distribution in

crustaceans. Comp Biochem Physiol Part A Mol Integr Physiol 124:531–538 Available at: http://linkinghub.elsevier.com/retrieve/pii/S1095643399001464.

Wilkens JL, McMahon BR (1992) Intrinsic properties and extrinsic neurohormonal control of crab cardiac hemodynamics. Experientia 48:827–834.

Zhang Y, Golowasch J (2011) Recovery of rhythmic activity in a central pattern generator: analysis of the role of neuromodulator and activity-dependent mechanisms. J Comput Neurosci 31:685–699 Available at: http://www.ncbi.nlm.nih.gov/pubmed/21573963 [Accessed May 13, 2013].

VITA

I was born in St. Louis, Missouri to parents Paul and Deborah Lane, and grew up with my two brothers Michael and Kevin. I attended De Smet Jesuit High School in St. Louis, and received my undergraduate degree from the University of Notre Dame, where I majored in science pre-professional studies. As an undergraduate, I gained experience in the scientific process in the lab of Dr. Rick Samson at Saint Louis University. Until this point, my formal classroom experience of the sciences had primarily emphasized facts and what we already known as a result of scientific studies. This opportunity to see research in action made me far more aware of how we move forward through the unknown to gain new understanding. During my senior year at Notre Dame, I taught courses through Kaplan Test Preparation centers to help other students prepare for the entrance exams to medical and dental school. This was my first experience teaching, and found quite by accident that it was something I truly enjoyed.

I taught Biology and Environmental Science at Marquette High School in Chesterfield, Missouri. As part of this job, I was continually looking at science news articles that I could relate to the curriculum and demonstrate to my students that science was an exciting enterprise that continues to uncover new and fascinating insights into ourselves and the world around us. I was continually drawn to neuroscience, where it was clear that a great deal of mystery remains but also that we are equipped with the tools to make satisfying progress in answering "big-picture" questions. While teaching, my own enthusiasm for this grew and I decided not to simply appreciate biological sciences from the sidelines but to become actively engaged in the process.

I interviewed with neuroscience labs at the University of Missouri and was very impressed with the faculty and graduate students. After a few short rotations, I joined the Schulz

lab. It was ideal mixture of addressing captivating concepts and questions, achieving mechanistically satisfying answers through the combined approaches of molecular biology and electrophysiology, and has been a fantastic group of people to work with. I have accepted a postdoctoral position in the lab of Dr. Gina Turrigiano at Brandeis University, where I will continue to study the regulation of neuronal excitability in the mammalian cortex, and plan to pursue a career in neuroscience research.